

External Coil for MR Imaging of the Prostate

A Major Qualifying Project
submitted to the faculty of
WORCESTER POLYTECHNIC INSTITUTE
in partial fulfillment of the
requirements for the Degree of Bachelor of Science

by
Nathan Climer
Ben Holmes
Deepa Krishnaswamy

March 6, 2010

Submitted

Report submitted to

Professor Ludwig
Professor McNeill
Professor Mendelson

This report represents the work of one or more WPI undergraduate students submitted to the faculty as evidence of completion of a degree requirement. WPI routinely publishes these reports on its website without editorial or peer review.

Acknowledgements

The group members would like to extend our deepest thanks to those that helped with our project. We would first like to thank our main advisor, Professor Reinhold Ludwig for continuously providing us with feedback, resources, and contacts that made this project possible. Next, we would like to thank our secondary advisors, Professor Mendelson and Professor McNeill, whose feedback throughout the project was most appreciated.

We would also like to thank Neil Whitehouse for his help in manufacturing the copper tubing for our coil and the acrylic casing that contains our project. Without his expertise in manufacturing, the project would have never come off the paper. In addition, thanks to Tom Angelotti, for dedicating time to helping us solder the coil.

Another person who was invaluable to creating our project was Peter Serano. Pete devoted his personal time to helping us understand and create RF simulations for the coil. His time and devotion allowed us to succeed in one of the most complicated parts of this project.

Finally, we would like to thank all the employees of Insight MRI, whose expertise in the design of MRI receive coils provided us with a backbone with which to build our project. We would specifically like to thank Rostislav Lemdiasov, without whom we would never have gotten the coil working. He spent many hours helping us debug our coil, as well as being a constant mentor on MRI technologies.

Authorship

	Abstract	Ben Holmes
1	Introduction	Deepa Krishnaswamy
2	Literature Review	
2.1	Prostate Cancer and MRI	Deepa Krishnaswamy Nathan Climer/Deepa Krishnaswamy
2.2	Existing imaging systems	
3	Project Strategy	
3.1	Initial Client Statement	Nathan Climer
3.2	Objectives and Constraints	Nathan Climer Deepa Krishnaswamy/Nathan Climer
3.3	Revised Client Statement	
3.4	Project Approach	Nathan Climer
4	Design Alternatives	
4.1	Design and Simulation	
4.1.1	Alternative Designs	Nathan Climer
4.1.2	Feasibility testing through DC Simulation	Nathan Climer
4.1.3	Optimization	Nathan Climer
4.1.4	Conceptual Designs	Deepa Krishnaswamy
4.1.5	RF Modeling	Ben Holmes
4.1.6	Further Design Calculations	Deepa Krishnaswamy
5	Design Verification	
5.1	Decisions and Construction	Deepa Krishnaswamy
5.1.1	Choice of copper medium	Deepa Krishnaswamy
5.1.2	Coil shaping	Deepa Krishnaswamy
5.1.3	Attachment to surface mount boards	Deepa Krishnaswamy
5.1.4	Casing	Nathan Climer
5.2	Tuning and Matching the Coil	Nathan Climer
5.2.1	Procedure for tuning and matching the coil	Nathan Climer
	Verifying Tuning and Matching using Variable Volume Phantom	Nathan Climer Deepa Krishnaswamy/Nathan Climer
5.2.3	Verifying Tuning and Matching using Biological Loads	
5.3	SNR Uniformity Testing	Nathan Climer
6	Discussion	
6.1	Coil Testing Behavior	Ben Holmes
6.2	Safety features	Deepa Krishnaswamy
6.3	Economics and social issues	Deepa Krishnaswamy
6.4	Manufacturability	Deepa Krishnaswamy
7	Final Design and Validation	Deepa Krishnaswamy

8	Conclusions and Recommendations	Ben Holmes/Nathan Climer
Appendix A	MATLAB DC Simulation of Helmholtz Coil	Nathan Climer
Appendix B	Port numbers used in HFSS and AnalyzerS	Ben Holmes
Appendix C	AnalyzerS MATLAB script	Ben Holmes
Appendix D	MATLAB Lumped Elements Definition	Ben Holmes
Appendix E	Raw Data for Phantom Load Testing	Nathan Climer
Appendix F	IRB Approval Documentation	Nathan Climer
Appendix G	Biological Load Test of Tuning and Matching	Nathan Climer
Appendix H	Raw Data for Magnetic Field Uniformity Testing	Nathan Climer

In addition, Nathan Climer created the DC simulations for this project, outlined in Appendix A of this report. Ben Holmes performed the RF simulations, outlined in Appendixes B-D of this report. Deepa Krishnaswamy created the copper tubing coil, outlined in Sections 5.1.1-5.1.3. Nathan Climer created the acrylic casing for this project, outlined in 5.1.4. All group members worked together to collect data for biological load testing on the coil, outlined in Appendix F-G. Nathan Climer and Deepa Krishnaswamy performed testing on Phantom Load Testing (Appendix E), and magnetic field uniformity testing (Appendix H).

Table of Contents

Abstract	1
1 Introduction	2
2 Literature Review	4
2.1 <i>Prostate Cancer and MRI</i>	4
2.2 <i>Existing imaging systems</i>	6
3 Project Strategy	11
3.1 <i>Initial Client Statement</i>	11
3.2 <i>Objectives and Constraints</i>	12
3.3 <i>Revised Client Statement</i>	15
3.4 <i>Project Approach</i>	15
4 Design Alternatives	17
4.1 <i>Design and Simulation</i>	17
4.1.1 <i>Alternative Designs</i>	17
4.1.2 <i>Feasibility testing through DC Simulation</i>	20
4.1.3 <i>Optimization</i>	27
4.1.4 <i>Conceptual Designs</i>	28
4.1.5 <i>RF Modeling</i>	32
4.1.6 <i>Further Design Calculations</i>	33
5 Design Verification	34
5.1 <i>Decisions and Construction</i>	34
5.1.1 <i>Choice of copper medium</i>	34
5.1.2 <i>Coil shaping</i>	36
5.1.3 <i>Attachment to surface mount boards</i>	38
5.1.4 <i>Casing</i>	39

5.2	<i>Tuning and Matching the Coil</i>	40
5.2.1	Procedure for tuning and matching the coil	42
5.2.2	Verifying Tuning and Matching using Variable Volume Phantom	44
5.2.3	Verifying Tuning and Matching using Biological Loads	46
5.3	<i>SNR Uniformity Testing</i>	49
6	Discussion	52
6.1	<i>Coil Bench Testing Behavior</i>	52
6.2	<i>Safety features</i>	53
6.3	<i>Economics and social issues</i>	53
6.4	<i>Manufacturability</i>	54
7	Final Design and Validation	56
7.1	<i>Specific Aims</i>	56
7.2	<i>Repetition of Work</i>	56
7.3	<i>Experimental Methods</i>	57
7.4	<i>Data Analysis</i>	58
8	Conclusions and Recommendations	59
	References	60
	Glossary of Terms and Acronyms	63
Appendix A	MATLAB DC Simulation of Helmholtz Coil	i
Appendix B	Port numbers used in HFSS and AnalyzerS	xx
Appendix C	AnalyzerS MATLAB script	xxi
Appendix D	MATLAB Lumped Elements Definition	xxvii
Appendix E	Raw Data for Phantom Load Testing	xxix
Appendix F	IRB Approval Documentation	xliv

Appendix G	Biological Load Test of Tuning and Matching	liv
Appendix H	Raw Data for Magnetic Field Uniformity Testing	lxvi

Table of Figures

Figure 2-1: Endorectal Coil [13].....	8
Figure 2-2: Comparison of Phased Array and Endorectal Coil Images[9]	10
Figure 3-1: Helmholtz Coil Example Construction	12
Figure 3-2: Anatomical Constrains of Pelvic Region	13
Figure 3-3: Siemens Bore Cross-section.....	14
Figure 4-1: Coil Design 1 Placement.....	18
Figure 4-2: Coil Design 2 Placement.....	19
Figure 4-4: Helmholtz Coil 1D Magnetic Field Distribution.....	22
Figure 4-5: Helmholtz Coil 3D Magnetic Field Distribution (Cross section along central axis)	24
Figure 4-6: Helmholtz Coil 3D Magnetic Field Distribution (Cross section perpendicular to central axis)	25
Figure 4-7: Non-Ideal Helmholtz Coil Example.....	26
Figure 4-8: Example SNR Drop-off.....	27
Figure 4-9: SNR Proportionality Constant (arbitrary units) at point of Prostate with Different Radii	28
Figure 4-10: SNR Drop-off off coil design 1 (-3 dB Cutoffs Shown) (White circle is point of prostate)..	29
Figure 4-11: SNR Drop-off off coil design 2 (White circle represents point of Prostate).....	30
Figure 4-12: SNR Drop-off of coil design 3 (White circle is point of prostate).....	31
Figure 4-13: Port between Coil Segments	32
Figure 5-1: Skin depth vs. frequency	35
Figure 5-2: Magnetic Field Distribution inside and outside of a hollow conductor [3].....	36
Figure 5-3: End of tubing after cut and sanded.....	37
Figure 5-4: Bent copper tubing	37
Figure 5-5: Flattened end of the copper tubing.....	38
Figure 5-6: Soldering of copper tubing to the surface mount board	38
Figure 5-7: Capacitor soldered to the surface mount board.....	39
Figure 5-8: MRI Casing	40
Figure 5-9: 2D Original Layout of capacitors.....	41
Figure 5-10: Layout with 2 additional breaks	43
Figure 5-12: Example S11 parameter graph from a student	47
Figure 5-13: Example Smith chart from a student.....	48
Figure 5-14: Magnetic Field Test Arrangement to Investigate Helmholtz Receive Coil Sensitivity	49
Figure 5-15: Magnetic Field Distribution in Vertical Direction	50

Figure 5-16: Front to Back Magnetic Field Strength Distribution..... 51

Abstract

The goal of this project was to show that the Helmholtz coil architecture is viable for use in MRI systems. Based on DC simulations, we have determined the coil dimensions to accommodate the largest range of patients, fit in an MRI scanner, and have the best possible SNR. Through exhaustive bench testing, we verified that our coil was able to be tuned to human loads and exhibited expected behavior, supporting that this product should be pursued in the future.

1 Introduction

Prostate cancer is the second most common cancer to affect men in the United States [1]. A common factor to this disease is age, as close to 70% of men diagnosed with the disease are over 65 years. In 2008 in the United States alone, over 180,000 men were diagnosed with prostate cancer, causing approximately 30,000 fatalities [1].

Using Magnetic Resonance Imaging (MRI) as a successful soft tissue imaging approach can significantly help with the detection of prostate cancer. Most importantly, it can be used to avoid unnecessary treatments such as surgery and radiation therapy, if the growth is benign and not malignant. It is possible to get different opinions from multiple doctors if desired. MRI provides a full image of the prostate to show where the cancer is located. MRI is also one of the best imaging techniques to target problems associated with soft tissues, such as those of the prostate and surrounding region [2]. Cancerous prostate tissue has significant structural differences which can be seen in MR images. When imaged, prostate cancer itself has a lower signal intensity than the surrounding tissue. Even with this, MRI provides good soft tissue contrast. Endorectal coils as well as phased array coil MRI systems have been shown to have a higher accuracy than other methods in determining certain prostate cancer conditions. For instance, compared to Transrectal ultrasound (TRUS), endorectal MRI has much higher accuracies which are between 75% and 90% [2].

One of the most active areas of development in MR instrumentation centers on RF coil technology. This technology has been applied primarily for disease specific receive coils. The receive coil picks up the signal from the body stimulated by the MRI system. In order to generate an accurate image, these coils need to be able to pick up the MRI signal with a very high signal to noise ratio (SNR) over a wide field of view (FOV). The higher the SNR, the higher the contrast of the image at high resolutions can be. The reconstructed images for prostate imaging need to be high enough in both quality and resolution to allow oncologists to diagnose and stage the different types of prostate cancer and conditions [2].

Another important factor in determining the effectiveness of a receive coil is the FOV. An extensive FOV allows for a larger area of the body that can be effectively viewed when imaged. This larger area allows radiologists to use the coil for screening nearby organs and tissues for metastasized prostate cancer. A thorough examination of the region is important to understand and observe whether the cancer has spread [2].

The endorectal coil is often considered by researchers as the best coil for prostate imaging due to producing images, which can find cancer from 87% to 98% of the time [3]. The endorectal coil system

consists of one surface coil that can be placed within centimeters of the prostate utilizing a catheter inserted in the rectum. The coil is placed in a small balloon at the end of the catheter. After being inserted, the balloon is inflated, expanding the coil. [4]

One of the biggest benefits of using the endorectal coil is that the close proximity to the prostate allows the receive coil to pick up a much stronger signal. Thus, it will have a larger SNR than coils placed farther away [5-8].

Despite the clinical accuracy of this coil system, the system contains inherent flaws. First, setting the coil up is time consuming and very expensive. Specialized electronics are needed to tune and match the coil through a catheter. In addition, set up of the coil needs to be done by a trained professional to prevent injury to the patient. These tests are also very hard on the patient. Patients are required to have the coil in their anuses for the entire MRI scan, which can take up to an hour. Finally, this type of coil also presses against the prostate during imaging. This distorts the prostate in the image, which can obfuscate the staging process [4].

Testing using the endorectal coil also has a high failure rate because the coil is not placed on the patient. Patients rectal cavities may be compressed by large tumors or swelling of the prostate [9]. Pain due to the endorectal coil can also cause failure for the study to be carried out. Finally, the coil may be too difficult to place in some patients, again causing a failure to image [10]. Because of the high costs of running MRI imaging, these failures to image can be extremely expensive.

Because of these limitations, there is a demand for a system that can deliver similar imaging results of an endorectal coil, but non-invasively. This project will investigate the Helmholtz architecture as a possible solution to this problem.

2 Literature Review

2.1 Prostate Cancer and MRI

Prostate cancer is the second most common cancer to affect men in the United States [1]. A common factor to this disease is age, as close to 70% of men diagnosed with the disease are over 65 years. In 2008 in the United States alone, over 180,000 men were diagnosed with prostate cancer, causing approximately 30,000 fatalities [1].

There are a number of distinct methods that are used for screening for prostate cancer. Screening is needed as a patient should not have to undergo unnecessary treatment. Magnetic Resonance Imaging (MRI) is used to gather more information about the cancer and its location. The first screening method is the Digital Rectal Exam (DRE), in which the doctor inserts a lubricated gloved finger into the rectum [1]. Through the rectal wall, rough spots and bumps are felt on the prostate gland. The advantage of this examination is that it can catch cancer at an early stage which in turn affects the treatment prognosis. The test lasts a number of minutes with minimal side effects. Unfortunately there are a number of disadvantages to performing the DRE. It easily makes patients nervous, uncomfortable and embarrassed. If the cancer is detected early, in some cases it can lead to treatments that are not necessary that in turn come with longer lasting side effects [1]. Only in 15%-25% of cases do abnormal findings in a DRE (with performing a biopsy) actually lead to prostate cancer [11]. The way the doctor performs the test also makes a difference, as it depends on the patient's position and the doctor's expertise. If the patient is obese, it can make the examination more difficult, as the doctor may not be able to feel the prostate completely.

Another method for detecting prostate cancer is the Prostate – Specific Antigen (PSA) Test. PSA is a protein that is produced by the prostate gland. It is normal to have a low level, but prostate cancer and other prostate conditions may increase the level [1]. This can include prostatitis, the inflammation of the prostate, or benign prostatic hyperplasia (BHP), which is an enlargement of the prostate [1]. Currently it has not been shown that these conditions cause cancer, but many men have these conditions along with cancer.

There are a number of limitations to the test, as there are many cases of false-positives (high PSA level but no cancer) and false-negatives (normal PSA level but cancer is present) that occur each year [1]. The false positives make up a large portion of the test's outcomes, at about 70% [12]. The test can also only detect small tumors that may or may not critically affect the man's quality of life. The test cannot differentiate between benign prostate conditions and cancer, which is a major drawback. There is a large

controversy over the PSA test, as the benefits of the test may outweigh the unnecessary treatments. It could result in surgery or radiation therapy, both which have lasting side effects [1].

Transrectal ultrasound is another method that is currently used for prostate cancer screening [11]. The ultrasound is used as an imaging modality for a variety of prostate conditions, including enlargement of the prostate, abnormal growth, and detecting certain disorders of the prostate. It involves an ultrasound probe that is inserted into the rectum of the patient. The advantage of this technique is that images can be easily obtained from different angles. One disadvantage is that there is some patient discomfort from inserting the ultrasound probe, along with mild side effects.

Using MRI as a successful soft tissue imaging approach can significantly help with the detection of prostate cancer. Most importantly, it can be used to avoid unnecessary treatments such as surgery and radiation therapy, if the growth is benign and not malignant. It is possible to get different opinions from multiple doctors if desired. MRI provides a full image of the prostate to show where the cancer is located. This should be compared to the DRE, as the position and size of the patient can reduce the ability for the doctor to detect bumps and rough spots. MRI is also one of the best imaging techniques to target problems associated with soft tissues, such as those of the prostate and surrounding region [2]. Cancerous prostate tissue has significant structural differences which can be seen in MR images. Prostate cancer itself has a lower signal intensity than the surrounding tissue. Even with this, MRI provides good soft tissue contrast. Endorectal coils as well as phased array coil MRI systems have been shown to have a higher accuracy than other methods in determining certain prostate cancer conditions. For instance, compared to Transrectal ultrasound (TRUS), endorectal MRI has much higher accuracies which are between 75% and 90% [2]. This is also due to improved MRI technology and better interpretation of the images.

Though there are a number of advantages to using MRI as opposed to other methods, there are still a number of disadvantages and limitations. The current MRI systems have relatively high sensitivity, but are inadequate in terms of finding the specific tumor location. According to one study the sensitivity was at 75% but had a low specificity of 55% in determining a prostate tumor location [2]. Factors such as BHP and prostatitis affect MRI results, and may show up as false positives. These have the same low signal intensity as prostate cancer.

Another disadvantage of MRI is the appearance of calcium. Since bones have no hydrogen atoms, it is difficult to see them when an MRI scan is performed [13]. In some cases not seeing calcium provides an advantage. In other cases, it hinders the ability to find pathological calcification in tumors and soft tissues. The acquisition time of images is relatively long in MRI, and patient breathing and the beating of the

heart may result in distortion of the images. In order to complete the scan itself, it takes about 30 minutes, and comparing to a CT scan which takes around five minutes to complete [14].

The cost of an MRI scan is also a major deterrent for many customers. According to Remake Health Inc., the average cost an MRI scan in the Boston, MA area is approximately \$650. This varies depending on the facility location and size, the number and type of doctors involved with the screening, etc. The cost usually ranges from \$1200 to \$4000, depending on what part of the body is being imaged [2]. For instance brain scans are highly priced compared to a scan of the knee. The type of contrast agent used in the MRI scan also makes a difference in the cost. CT scans on the other hand are usually cheaper, in a range of \$1200 to \$3200.

Because of these limitations, there is a strong pressure to develop MRI systems that can better overcome these obstacles. The existing state of the art is continuously updated to match these needs. Despite these problems, MRI is well suited for diagnostics of prostate cancer. It provides clear images of soft tissue, and can differentiate between malignant and benign tumors and is especially useful for detecting where the cancer is specifically located.

2.2 Existing imaging systems

One of the most active areas of development in MR instrumentation centers around RF coil technology. This technology has been applied primarily for disease specific receive coils. The receive coil picks up the signal from the body stimulated by the MRI system. In order to generate an accurate image, these coils need to be able to pick up the MRI signal with a very high signal to noise ratio (SNR) over a wide field of view (FOV). The higher the SNR, the higher the contrast of the image at high resolutions can be. This increase in performance with SNR is especially important in the imaging of small organs such as the prostate, and the cancers that lie within them. The reconstructed images for prostate imaging need to be high enough in both quality and resolution to allow for oncologists to diagnose and stage the different types of prostate cancer and conditions [2].

Another important factor in determining the effectiveness of a receive coil is the FOV. An extensive FOV allows for a larger area of the body that can be effectively viewed when imaged. This larger area allows radiologists to use the coil for screening nearby organs and tissues for metastasized prostate cancer. The larger effective FOV can thus increase a coil's versatility. A large FOV in prostate cancer imaging can allow for the oncologists to view the entire prostate, as well as surrounding regions. A thorough examination of the region is important to understand and observe whether or not the cancer has spread [2].

Because many factors contribute to the effectiveness of a coil, clinicians look at how well the receive coil can identify specific diseases. Clinicians refer to this as the sensitivity of the coil, and is reported in percent if cancer has been found. This is different than the coil sensitivity, which is a physical property of the coil, discussed later on. This paper will refer to the ability of the coil to detect specific diseases as clinical sensitivity. This method of grading is unfortunately not solely dependent on the coil. The images created by the MRI are only as good as the person interpreting them. Thus, the sensitivity is heavily dependent on the experience of those evaluating the images. People that test the imaging modalities are trained for the specific image modality. The human interpretation of these images has often resulted in significantly varying results from study to study [15].

The endorectal coil (example shown in Figure 2-1) is often considered by researchers as the best coil for prostate imaging due to having a large sensitivity, with a rating of 87% to 98% [3], which is much higher than the prostate cancer sensitivity of 59%-62% of the pelvic phased array coil [5]. The endorectal coil system consists of one surface coil that can be placed within centimeters of the prostate utilizing a catheter inserted in the rectum. The coil is placed in a small balloon at the end of the catheter. After being inserted, the balloon is inflated, expanding the coil. The tuning and matching are done through an external circuit, and the transmission of signals is done through the catheter [4].

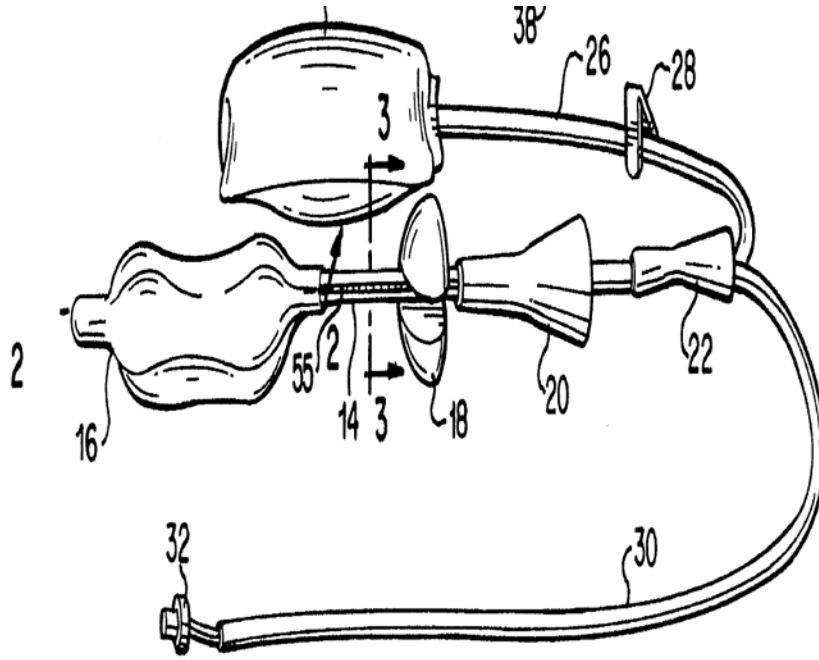


Figure 2-1: Endorectal Coil [13]

The endorectal coil works because it is a flexible coil. These flexible coils can be collapsed down into small sizes for insertion. After the catheter is put in place, saline solution or air is used to fill up a small balloon, which extends this coil to its full size [4, 8].

One of the biggest benefits of using the endorectal coil is that the close proximity to the prostate allows the receive coil to pick up a much stronger signal. Thus, it will have a larger SNR than coils placed farther away [5-8]. A higher SNR allows the reconstructed images to exhibit relatively high resolution. This allows the endorectal coil to achieve a larger resolution than other coil systems, up to around 0.24 to 0.7 cm [16].

Despite the clinical accuracy of this coil system, the system contains inherent flaws. First, setting up the coil is time consuming and very expensive. Specialized electronics are needed to tune and match the coil through a catheter. In addition, set up of the coil needs to be done by a trained professional to prevent injury to the patient. These tests are also very hard on the patient. Patients are required to have the coil in their anuses for the entire MRI scan, which can take up to an hour. Finally, this type of coil also presses against the prostate during imaging. This distorts the prostate in the image, which can obfuscate the staging process [4].

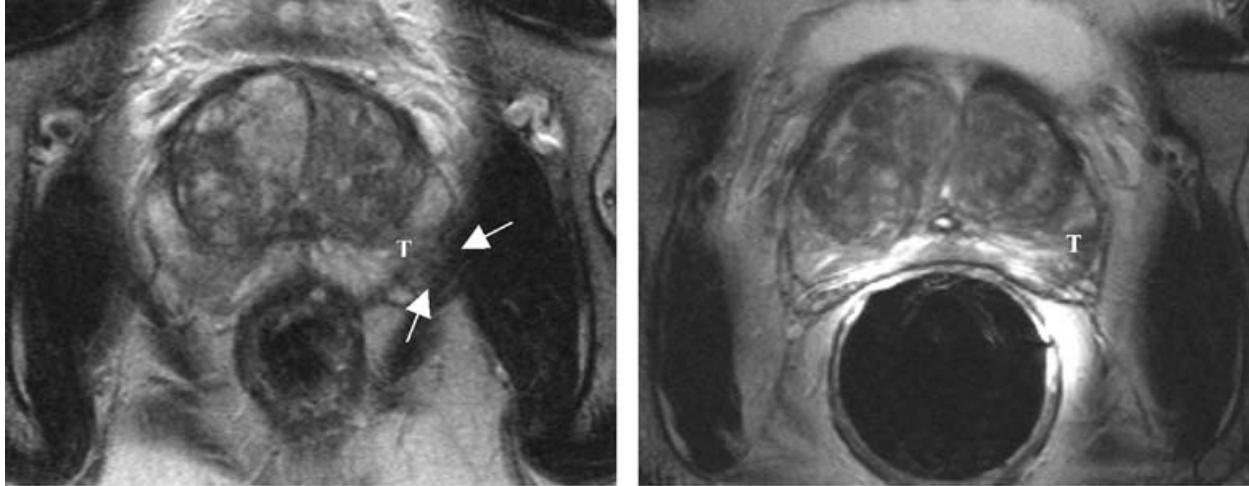
Testing using the endorectal coil also has a high failure rate because the coil is not placed on the patient. Patients' rectal cavities may be compressed by large tumors or swelling of the prostate [9]. Pain due to the study can also cause failure for the study to be carried out. Finally, the coil may be too difficult to place on some patients, again causing a failure to image [10]. Because of the high costs of running MR imaging, these failures to image can be extremely expensive.

Because of these limitations, there is a demand for a system that can deliver similar imaging results of an endorectal coil, but non-invasively. Obviously, one alternative to the endorectal coil is the phased array coil. This system is a set of multiple coils placed around a region of the body. Almost like a phased array antenna system, it can collect significant data to image a target region. The voltage signals are picked up by these separate coils through separate channels, and the data is subsequently combined within the MR scanner. The combination of the signals from these coils allows for a higher SNR than the coils could deliver individually [17].

One type of phased array coil typically used in MR imaging of the prostate is the pelvic phased array coil. This type of array coil is specifically designed for the pelvic regions. However, the applications of phased-array coils can go beyond imaging the pelvic region. Recently, there has been a lot of development by Siemens Corp. resulting in the so called "Total Imaging Matrix" (TIM) concept. The TIM system is an imaging matrix whose coverage is that of the entire body.

In imaging prostate cancer, phased array coils have many benefits to other imaging methods. First, the combination of coils increases the SNR of the system significantly [17]. In addition, this method is completely non-invasive. Phased array coils cause very little discomfort and pain while imaging, and do not press on the prostate. The phased array coil also has the benefit of providing a more uniform FOV.

In Figure 2.3, you can see the comparison between an endorectal coil and a phased array coil. Figure A contains an image taken with a phased array coil, while Figure B has an image recorded with an endorectal coil. Figure A has a relatively uniform amplitude over the area of the image. The arrows point to an area that may be diagnosed as a tumor [9]. However in Figure B, the area near the rectum is much brighter than regions farther away. The coil is so sensitive in these regions that it must be set to the maximum value shown. This means areas farther away from the rectum will have a much lower dynamic range in signal intensities, which can lower the effectiveness of the coil at picking up cancer in these regions.



A)

B)

Figure 2-2: Comparison of Phased Array and Endorectal Coil Images[9]

Despite these benefits, the SNR of the phased array coil is still too small to compete with the endorectal coil. Whether or not this drop in resolution affects the clinical equivalence of the two methods is of heated debate. Clinical study results range from equivalent to the endorectal coil, to missing half the results the endorectal coil picks up [5, 6, 9, 17].

One method of increasing the SNR of these phased array coils is by designing phased array coils for 3T MRI scanners. Because of the higher B_0 field strength, these systems have almost twice the SNR than the standard 1.5T MRI Scanners [18].

While running an external phased array coil at 3T does increase the clinical accuracy of the systems, it still does not have the image quality of the endorectal coil in 1.5T in the vicinity of the prostate. The endorectal coil in a 3T clinical scanner still shows the same benefits as the phased array coil in this system as well, making the endorectal coil still the best choice for the best picture possible [18]. Though a 3T scanner delivers much better results, 3T imaging is very expensive.

While these systems are the latest developments in the field, they fail to reach conclusive clinical accuracy that would allow them to compete with the endorectal coil design.[5, 6, 9, 18-20] Alternatives to the pre-mentioned architectures are rare in the literature. In order to develop a competitive coil, this project will explore the use of an alternative coil design, and evaluate its performance at the bench.

3 Project Strategy

3.1 Initial Client Statement

One essential part of the MRI is the receive coil. This receive coil is vital for picking up the MR signal from the body. This received signal is used for reconstructing the image. Receive coils can be customized for specific disease and anatomical applications. Various coil architectures are used to view different anatomical regions, depending on what part of the body is to be imaged. A simple planar coil is one example of a commonly used surface coil. It can be used as a small FOV coil [21]. The advantages are that it is small in size and relatively easy to construct [21]. One of the drawbacks is that there is field non-uniformity [21]. Only near the wire frame does the field increase greatly. Outside the coil, the field is prone to changes depending on the position and direction of coil [21].

A planar coil is not an ideal choice for our application, as the project requires high field uniformity as well as a high SNR. We therefore researched a particular coil architecture known as a Helmholtz Coil.

The Helmholtz design is a pair of two identical coils that are parallel to each other [22]. Since the coils are wired in series, the current in each coil flows in the same direction [22]. The coils are placed on either side of the patient. The distance of loop separation is equal to the radius of the coils for best possible performance [22]. Distance between the coils is kept as small as possible to maximize coil sensitivity [23].

The Helmholtz coil based is designed to create a uniform magnetic field [22]. It has a very uniform magnetic field in the center of the coils. This occurs because field components that are parallel to the two coil axes are added together. Field components that are perpendicular to each other are subtracted [24]. The strength of the field drops by 50% at the edges of the coil. An example of the coil can be seen below in Figure 3.1 [24].



Figure 3-1: Helmholtz Coil Example Construction

The strength of the field is proportional to the number of turns, the radius of the coil, and the current applied. The main advantage of the Helmholtz coil configuration is that it creates a uniform magnetic field in the center of the coil. Increasing the separation between the coils improves the uniformity of the field [22]. The SNR is very high, which is needed for obtaining clear and undistorted images of the body. Compared to an endorectal coil, the use of this coil architecture will hopefully eliminate patient discomfort as well.

One drawback of using the Helmholtz coil design is image degradation. The loss of signal amplitude occurs because of the distance between the two loops is relatively large [23]. The spacing of the coil is also extremely vital, because if it is too small, distortion will occur [25]. If the coils are far apart because of the size of the patient, then the image may not be as clear compared to someone of a smaller size. This is because the farther apart the two coils, the lower the coil sensitivity.

3.2 Objectives and Constraints

The goal of our project is to create a coil architecture to be used in an MRI that can image the prostate. The main design goal of our project is to have a high SNR. As the name suggests, SNR is a measure of how much more signal the system has compared to the noise, so therefore for a high SNR, the signal must be large and the amount of noise must be small. SNR depends on many factors, some not actually dependent on the RF coil. Most importantly, SNR depends on the B1 field strength, as well as the resistance of the coil. These details will be addressed later on in the report.

The second goal of our project is ease of use. For the coil to be successful and used in an MR scanner, it must be easily implemented within the system, and simple to operate by technicians. Another consideration is comfort for the patient. This design must have clear advantages to the endorectal coil and other methods, and comfort is a large issue to be considered. Therefore the method of attachment of the coil to the bed of the MRI machine is vital.

Many different factors limit our design. The first limitation is the size of the human body. We determined the absolutes of this limitation through collections of anatomical data. This data was received from two sources. The measurement from the pelvic bone to pelvic bone was obtained from The Handbook of Anatomical Measurements. This has a value of 27 +/- 4 cm. This data was used as a scale for the Atlas of the Visual Human Male. [26]Using a z-chart, we determined the value for which 90% of the population would fit in the coil. This data was used to generate the physical constraints shown below in Figure 3.2.

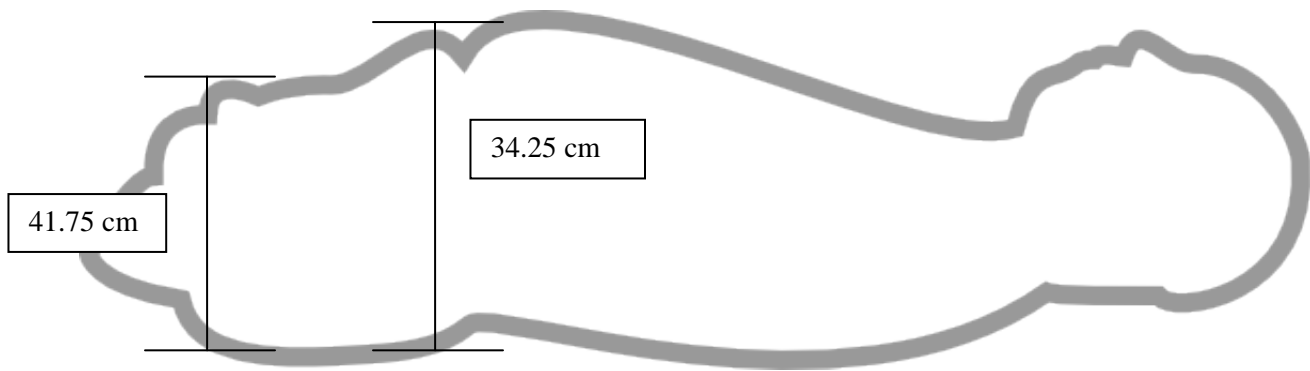


Figure 3-2: Anatomical Constrains of Pelvic Region

Another physical constraint on the coil is the layout of the Siemens system, as shown in Figure 3-3. The bore that our coil must fit inside is only 60 cm in diameter. In addition, there is a bed in the Siemens' system that further limits out layout.

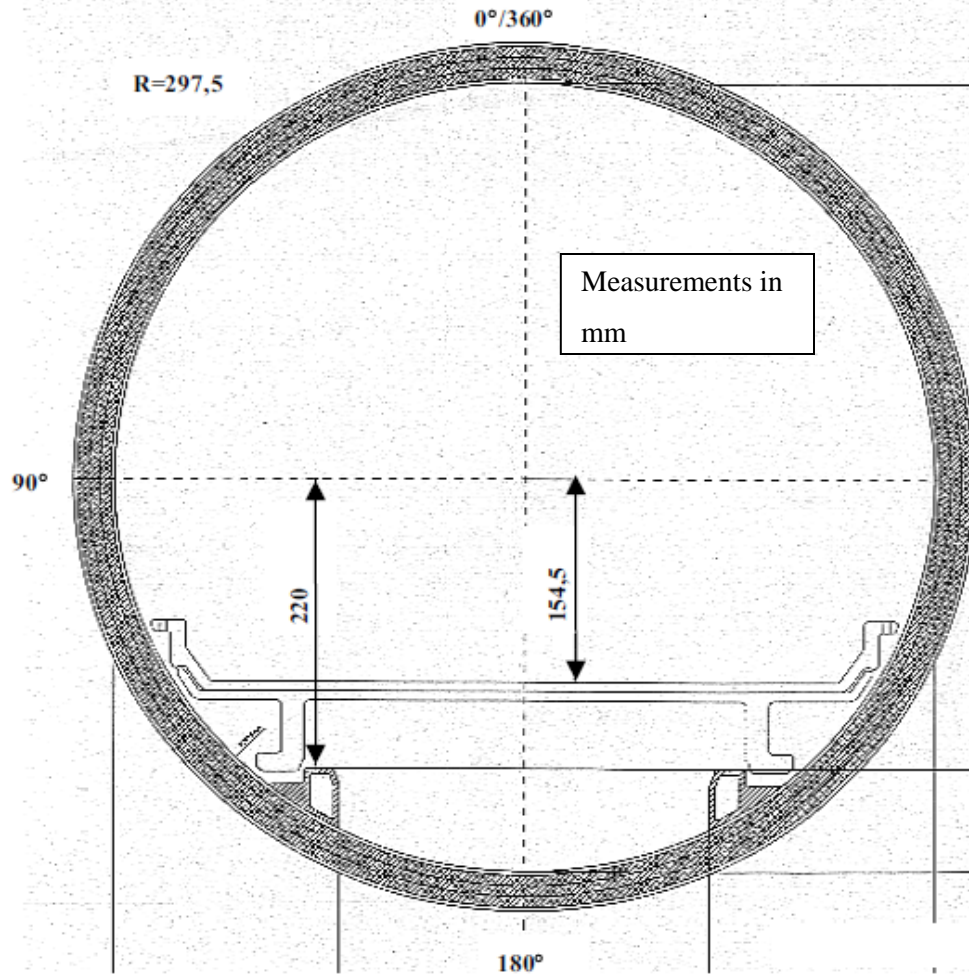


Figure 3-3: Siemens Bore Cross-section

The final constraint on our design is that the coil must have no ferromagnetic materials inside. This is because they will interfere with the magnetic fields used in the MR scanner. When ferromagnetic materials are used, there may be artifacts in the image. Due to the high strength of the magnetic field, ferromagnetic materials may even be pulled rapidly toward the scanner causing damage.

There are various methods of judging coil effectiveness. One method is to look at the sensitivity of the coil. The more sensitive the coil is, the larger the signal produced from the load. The problem with sensitivity is that noise may interfere with the signal. Even if a coil has a high sensitivity, the amount of noise might be large. A large amount of noise would degrade the image quality. Instead of using sensitivity as the factor to judge the effectiveness of the coil, the SNR is a more reasonable parameter to use.

3.3 Revised Client Statement

As seen from above, there are a number of constraints that the coil architecture must take into account. First, the SNR must be high in order to obtain clear images. This means that the coil must resonate at the Larmor frequency, which is 63.65 MHz. A high quality factor (Q) is also necessary to create a robust coil. A high Q means that the resonance frequency of 63.65 MHz divided by its -3dB bandwidth must be large. This is a measurement of how well the coil selects just the Larmor frequency.

An important constraint to consider is that the coil must fit inside the MR scanner, but must also be able to accommodate a person comfortably inside. It was decided that in order to accommodate the larger population of men, the top coil should be tilted at a slight angle of 10 degrees.

Another constraint was the budget. As part of an internally sponsored MQP, each student has \$125, which yields a total of \$375. This will be spent on the acrylic casing for the housing, as well as the copper tubing and various capacitors needed.

3.4 Project Approach

In order to reach our design goal of creating a prototype Helmholtz coil for prostate imaging, the MQP team has developed the following methodology for constraining, designing, and testing of our prostate imaging coil. The methodology can be split into the following sections:

- Initial design and constraint evaluation
- Simulation of coil design
- Designing the individual components of the coil
- Testing and evaluation of the coil

One result of the RF simulation is the circuit scattering (S) parameters. The S parameters are high frequency circuit parameters of how well the device performs, described using forward and reverse voltage gain, as well as input and output port voltage reflection coefficients. A reflection coefficient describes the amplitude of a reflected wave to an incident wave. These parameters can be exported to a MATLAB script to determine proper values for the tuning capacitors.

For testing and evaluation, a tuning and matching circuit is extremely important to the functioning of our Helmholtz coil. Tuning is the varying of circuit elements such that the coil resonates at a target frequency, this frequency being the Larmor frequency. For a 1.5T scanner, this frequency is 63.65 MHz. In order to obtain clear images of the body (those with a high SNR), tuning needs to be performed [27]. Matching optimizes the transfer between a form of energy between the source and the load. The goal of matching is

to maximize the power transfer, and to reduce the reflections from the load. It uses inductors and capacitors to match the source (input) impedance to the load (output) impedance [28].

Tuning and matching is also needed because voltages appearing on the coil will be smaller and there is less risk of high voltages or temperatures harming the patient. Therefore breaks must be included in the coils to allow for tuning and matching capacitors. These capacitors are used to tune and match the coil so that it resonates at the proper frequency and presents the correct 50 ohm impedance to the MRI scanner. An inductor is needed with the matching capacitor in order to form a proper matching network. This combination will adjust the bandwidth that the coil resonates at. Ideally, this bandwidth should be narrow, at about 20 kHz, in order to construct a coil that resonates only at 63.65 MHz.

This coil needs to be tuned, matched, and tested as if a human were in the coil. A phantom is a physical model that emulates electrical properties of the human body. These are essential for the testing of MRI coils because the human body acts as a lossy dielectric load.

These coils will then be connected to a network analyzer. We will then tune and match the coil to the Larmor frequency. The network analyzer should be able to tell us the input impedance of our coil. The input impedance is essential in determining the sensitivity of the coil. Specifically, the resistive component of the impedance gives us the efficiency of our coil. Because this value will change when the human load is introduced, the input impedance of the coil with both with and without a phantom load will be measured. Tuning the circuit (adjusting the caps) will adjust the frequency, while matching will narrow the bandwidth.

The capacitor values obtained from the RF simulations are ideal values. Because of the coil construction and the imperfectness in shape, the values needed to make the coil resonant will change. Therefore, we put a variable capacitor on each of the coils.

4 Design Alternatives

In order to reach our design goal of creating a RF coil for MR prostate imaging, the MQP team has developed the following methodology for constraining, designing, and testing of our prostate imaging coil. The methodology can be split into three tasks:

- Feasibility testing through DC Simulation
- Optimization
- Conceptual Designs
- Modeling
- Further Design Calculations

In the following sections we will go into a detailed discussion of each task.

4.1 Design and Simulation

As described previously, we needed to design a coil with high SNR. The coil needs to be large enough to fit most patients, but small enough to fit into the bore of an MR scanner. We selected a coil design first through DC simulations, and then used an RF simulation to determine additional parameters necessary to construct the coil.

4.1.1 Alternative Designs

The group members initially started a brainstorming session to come up with different design possibilities for this project. The first idea, and the simplest, was a fixed, rigid coil that patients would sit in. This design had the merit of being simple to build and create. However, the coil may not be optimized for all users. The second idea was a series of coils optimized to users of different sizes. We determined that this design would fall outside the scope of the project. Another idea was to create an adjustable coil. There would be a different set of tuning and matching capacitors that would be switched when the coil was adjusted. While the most flexible, this idea was also considered far too complex for the scope of this project. The team members thus selected the fixed coil design.

After selecting the fixed coil design, we determined different fixed layouts that could be used for this project. There are three different fixed coil designs that we investigated. The parameters that varied between the coil designs were the radius of the coils, the distance between the two loops and the tilt angle of the top loop. MATLAB was used to test the various parameters, and by observing the magnetic field strength at certain points, the coil parameters were decided.

These three coil designs were also chosen based on the anatomy of a human male. In the first coil design, the coil is positioned closest to the prostate. Having a coil in this location would greatly increase the

sensitivity. For the second coil design, the loop covers a larger area which includes some of the visceral fat. The distance between the loops has to be greater in this case. In the last case, the top coil is tilted allowing for larger people to be imaged.

Ideally, the two loops of the coil should be a distance R (radius) apart. As will be seen, the ideal case of the Helmholtz coil architecture was not implemented in any of the cases. Although the ideal coil allows for a very high magnetic field strength, the noise is also very large. This in turn decreases the SNR, which is not ideal for this application.

As stated previously, the first coil design only covers the area immediately above the prostate. The design consists of two coils of an equal radius of 0.1590 meters, with a distance between the loops of 0.3175 meters. The maximum SNR in this case is $1.9815e-006$, which is not the true SNR but a proportional value to it. An example of how this fits with the human body can be seen in Figure 4-1.

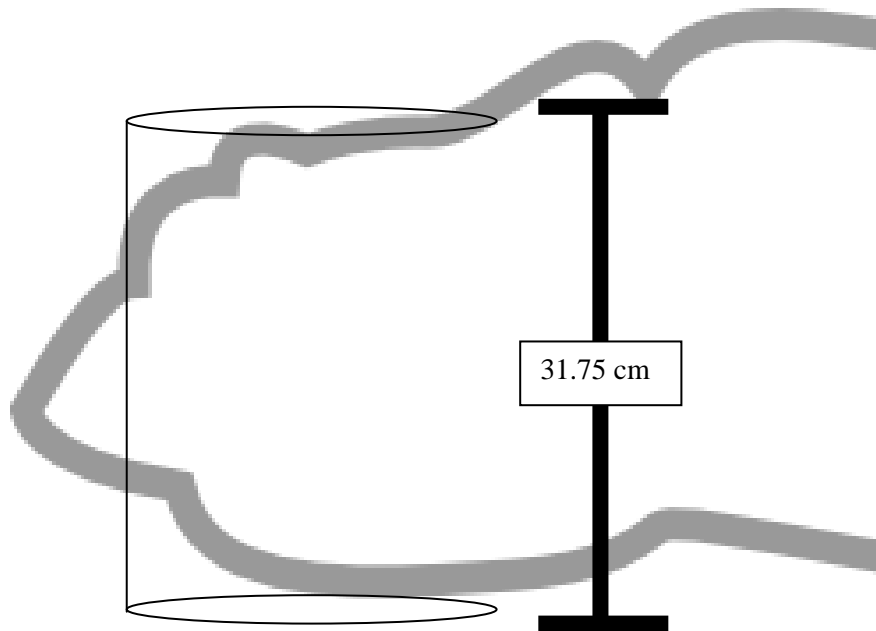


Figure 4-1: Coil Design 1 Placement

The second coil design consisted of a pair of parallel coils that were further apart to cover the visceral fat. The radius of the two coils is 0.1740 meters, and the distance between them is 0.346 meters. The maximum proportional SNR was calculated to be $1.7342e-006$. This can be seen in Figure 4-2.

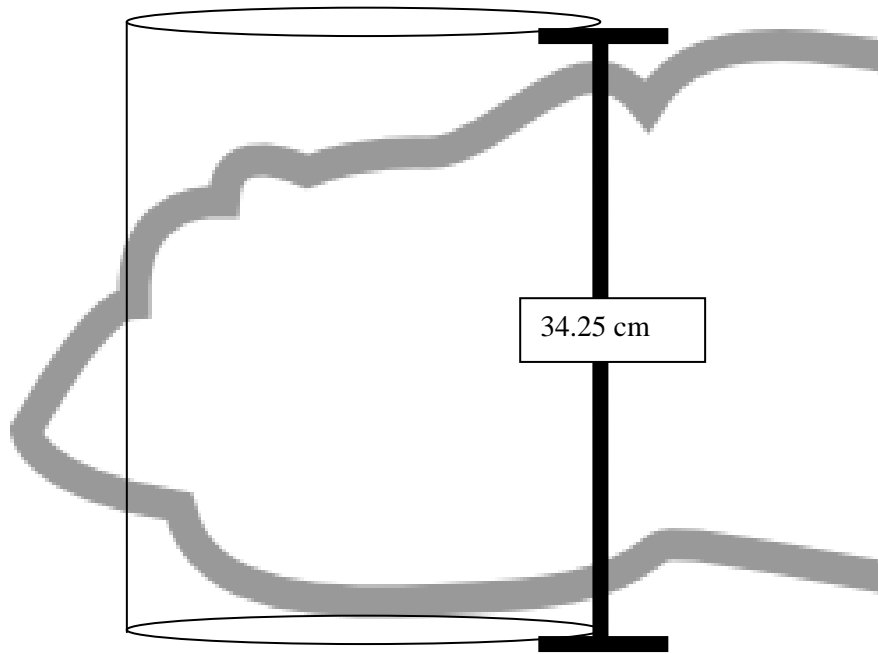


Figure 4-2: Coil Design 2 Placement

For the third coil design, the top coil was simulated at a tilt angle of 10 degrees. This was done to accommodate patients that may be larger at the stomach region, as are a significant portion of the population in the United States. The radius of the two coils is 0.1570 meters, and the distance between them 0.3425 meters. The maximum proportional SNR is $1.7757e-006$. This can be viewed in Figure 4-3.

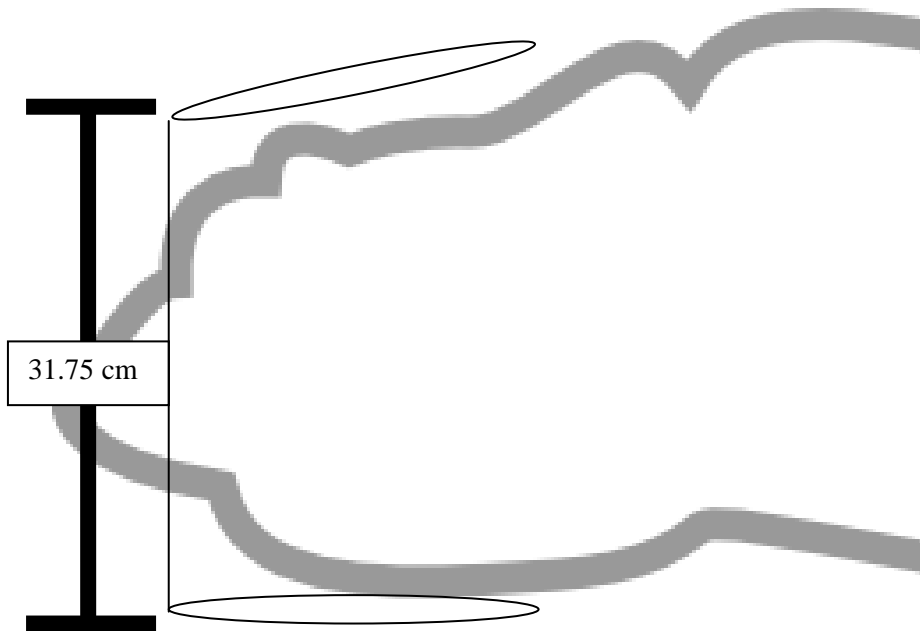


Figure 4-3: Coil Design 3 Placement

While these coils are sufficiently large to accommodate patients, the coil separation cannot be increased to the ideal Helmholtz coil design for two reasons. First, increasing the radius of the coil until it is equal to the height of the coil would create a system that was so large that it could not fit in a magnet. Second, as you increase the radius of the coil, you increase the length of the conductor in the coil, increasing overall resistance of the coil. In order to optimize the design we simulated the various coils in MATLAB.

4.1.2 Feasibility testing through DC Simulation

In order to verify the feasibility of our design possibilities, we needed to analytically compare the effectiveness of different coils through simulation. The first simulation was conducted under DC conditions. This simulation was performed through the use of MATLAB code. This code is explained in Appendix A. The results of the DC simulation should reflect the results of the RF simulation, and thus provide a measure of redundancy.

The relative SNR of each coil at each point due to the magnetic field of the coil, B_1 , and the total high-frequency resistance of the coil, R , can be found by the following equation

$$SNR \propto \frac{|B_1|}{\sqrt{Pwr}} \propto \frac{|B_1|}{\sqrt{I^2 R}} \propto \frac{|B_1|}{\sqrt{R}} \quad (1)$$

Here, the relationship of resistance and length was used, where l is the length of a conductor, ρ is the resistivity of the material, and A is the cross sectional area of our conductor. If we assume that all of our potential coils will be made with the same conductor, the term ρ/A will be constant. This means that:

$$SNR \propto \frac{|B_1|}{\sqrt{R}} \propto \frac{|B_1|}{\sqrt{\frac{l * \rho}{A}}} \propto \frac{|B_1|}{\sqrt{l} * \sqrt{\frac{\rho}{A}}} \propto \frac{|B_1|}{\sqrt{l}} \quad (2)$$

If we assume all other components of the SNR of the coils to be constant between coil designs, the value B_1/\sqrt{l} can be used to compare the design of each coil. Clearly B_1/\sqrt{l} is *not* the real SNR value of the coil, rather it is simply a useful way of comparing different coil designs under similar conditions. We will refer to this value at the proportionality SNR constant for each coil.

In the case of the Helmholtz coil, we assumed a zero-resistance connection between the two loops in the coil. The top coil is called *coil B* and the bottom coil *coil A*. The coils *A* and *B* have radii a and b , respectively. The length used in the relative SNR calculation is thus

$$l = 2\pi(a + b) \quad (3)$$

Knowing that the magnetic field will be oscillating in the X direction, we can use B_x instead of B_1 .

While equation (1) is simple to calculate, B_1 varies with position relative to the coil. A MATLAB script was next written to determine the theoretical uniformity of the field in the region of interest. These simulations are based on the theoretical magnetic field strength due to the Helmholtz coil.

First, we made the assumption that the Helmholtz coil can be modeled by two circular currents. The currents travel on circles with radii R . These circular loops have their center points on the Z axis, and are perpendicular to the Z axis, and are distance h apart. These two circles' center points are thus located at $+h/2$ and $-h/2$ on the Z axis. We will next find the magnetic field at each point through superposition. The formula for the magnetic field strength through the central axis of a single wire loop can be found by

Biot-Savart's Law. For the loop at position $z = \frac{-h}{2}$ we find:

$$B_{z-}(z) = \frac{\mu_0}{4\pi} \frac{2\pi R^2 I}{((z + h/2)^2 + R^2)^{3/2}} = \frac{\mu_0}{2} \frac{R^2 I}{((z + h/2)^2 + R^2)^{3/2}} \quad (4)$$

Where h is the space between the current loops, R is the radius of the current loop, I is the current through the loop, z is the position on z axis, and μ_0 is the magnetic permeability of free space.

The same law applied to the coil at position $+h/2$ yields:

$$B_{z+}(z) = \frac{\mu_0}{2} \frac{R^2 I}{((z - h/2)^2 + R^2)^{3/2}} \quad (5)$$

When added, the resulting B_z field is:

$$B_z = \frac{\mu_0 R^2 I}{2} \left(\frac{1}{((z - h/2)^2 + R^2)^{3/2}} + \frac{1}{((z + h/2)^2 + R^2)^{3/2}} \right) \quad (6)$$

In the ideal case, the radius of the Helmholtz coil is equal to the height of the Helmholtz coil. In this case, $h=R$. This results in the equation:

$$B_z = \frac{\mu_0 R^2 I}{2} \left(\frac{1}{(5/4 R^2 + Rz + z^2)^{3/2}} + \frac{1}{(5/4 R^2 - Rz + z^2)^{3/2}} \right) \quad (7)$$

When evaluated at $z = 0$, we get the maximum field strength of:

$$B_z = \frac{\mu_0 R^2 I}{2} \left(\frac{1}{\left(\frac{5}{4} R^2\right)^{3/2}} + \frac{1}{\left(\frac{5}{4} R^2\right)^{3/2}} \right) = \frac{\mu_0 R^2 I}{2} \left(\frac{2}{\left(\frac{5}{4} R^2\right)^{3/2}} \right) = \mu_0 I \left(\frac{4}{5}\right)^{3/2} \left(\frac{1}{R}\right) \quad (8)$$

The previously mentioned equations can be used to evaluate the magnetic field strength along an axis. The magnetic field strength is shown below in Figure 4-4. In this graph, the position on the axis is normalized to the radius of the coils, and the magnetic field strength is normalized to the maximum field strength.

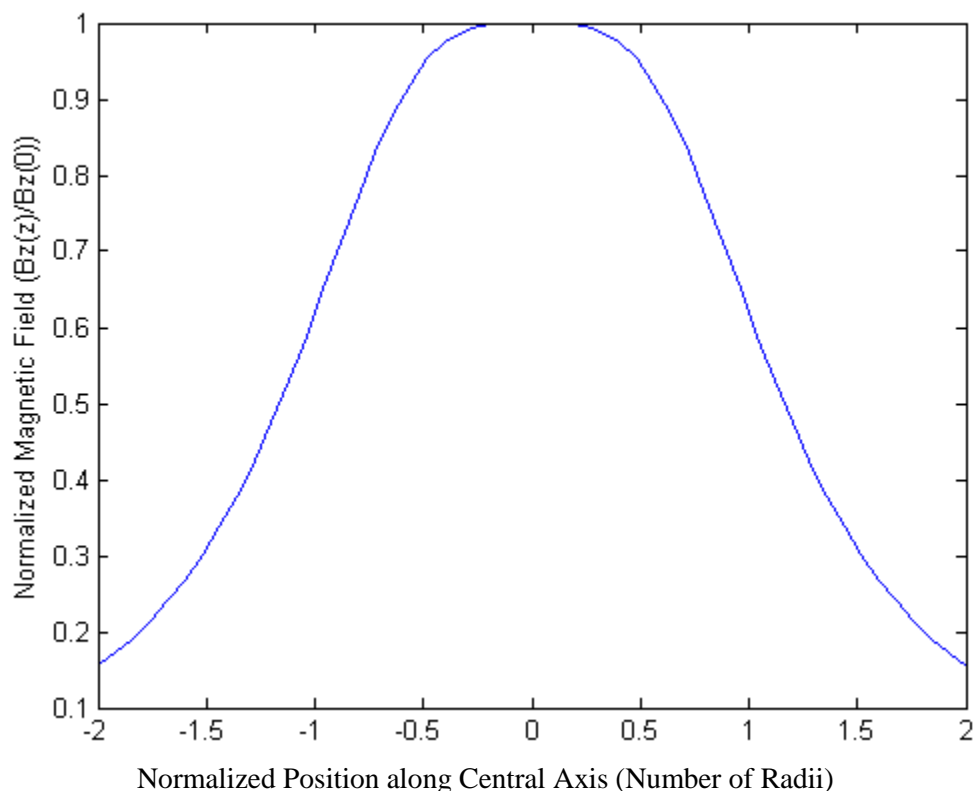


Figure 4-4: Helmholtz Coil 1D Magnetic Field Distribution

This is the numeric solution of the on-axis magnetic field strength of the dual loop [29]. The off-axis magnetic field strength is more complex. In order to compute this, we begin with the off axis magnetic field strength of a single loop by the Biot-Savart Law in a plane that bisects the current loop. The magnetic field strength is determined by a position z in direction of the central axis of the loop, and a position r in the direction of radius of the loop. The radius of the loop is R .

An analytical solution for the magnetic field can be developed by relying on elliptical functions $E(k)$, $K(k)$. These equations allow us to find the magnetic field strength components perpendicular to the radius of the coil (B_z) and parallel to the radius of the coil (B_r), as shown below [30, 31]:

$$B_z(r, z) = B_0 \frac{1}{\pi\sqrt{Q}} \left(E(k) \frac{1 - \alpha^2 - \beta^2}{Q - 4\alpha} + K(k) \right) \quad (9)$$

$$B_r(r, z) = B_0 \frac{\gamma}{\pi\sqrt{Q}} \left(E(k) \frac{1 + \alpha^2 + \beta^2}{Q - 4\alpha} - K(k) \right) \quad (10)$$

Where, $\alpha = \left| \frac{r}{R} \right|$, $\beta = \frac{z}{R}$, $\gamma = \frac{z}{r}$, $Q = |(1 + \alpha)^2 + \beta^2|$, $k = \sqrt{\frac{4\alpha}{Q}}$, $E(k)$ =the elliptical integral of the first kind, and $K(k)$ =the elliptical integral of the second kind.

If we allow $B(r, z) = B_z(r, z)\hat{z} + B_r(r, z)\hat{r}$, and the magnetic field caused by the top and bottom coil respectively is $B_{\text{top}}=B(r, z-h/2)$ and $B_{\text{bottom}}=B(r, z+h/2)$, we can find the magnetic field strength in a slice of our Helmholtz coil by simply adding the two. This answer can be projected around a cylinder to get the 3D representation of a Helmholtz coil's magnetic field strength. Figures 4-5 to 4-7 depict various view-points of our design. Also shown in these figures are regions where the magnitude of the B field remains within $\pm 5\%$ of its central location ($r=0, z=0$) field strength. Again, the magnetic field strength is normalized to the central magnetic field strength (B_0) and the position is normalized to the radius of the Helmholtz coil.

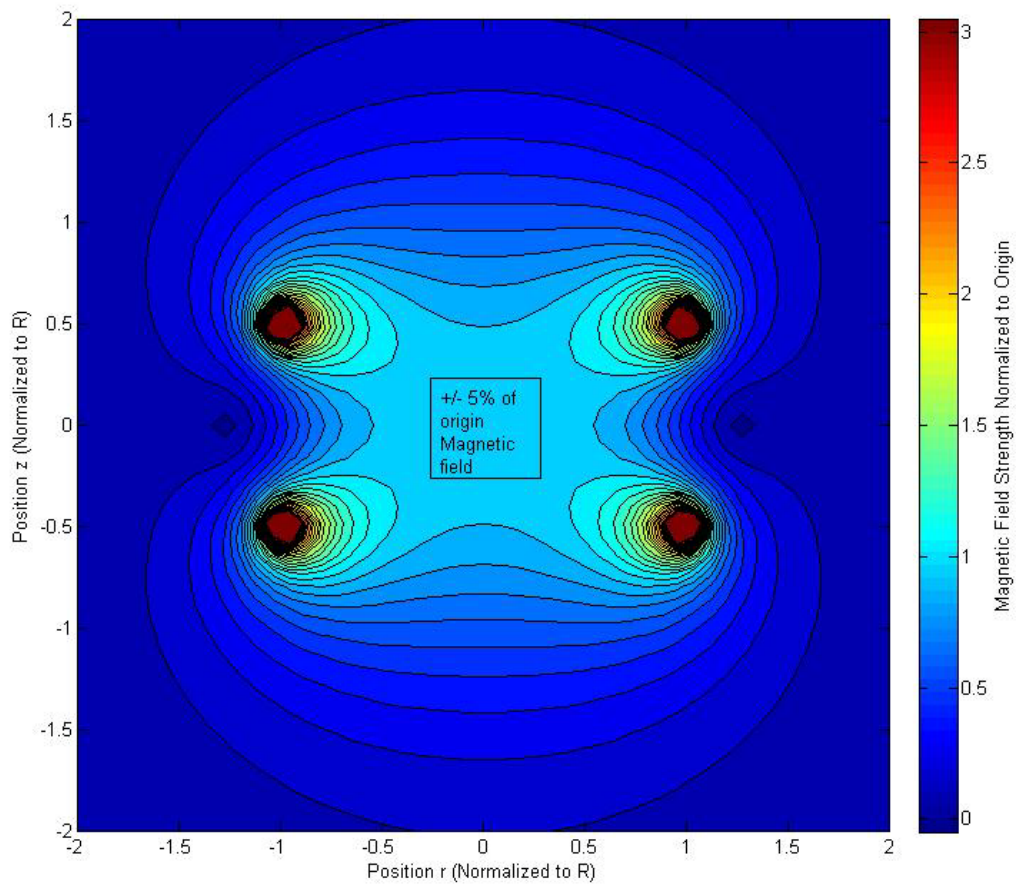


Figure 4-5: Helmholtz Coil 3D Magnetic Field Distribution (Cross section along central axis)

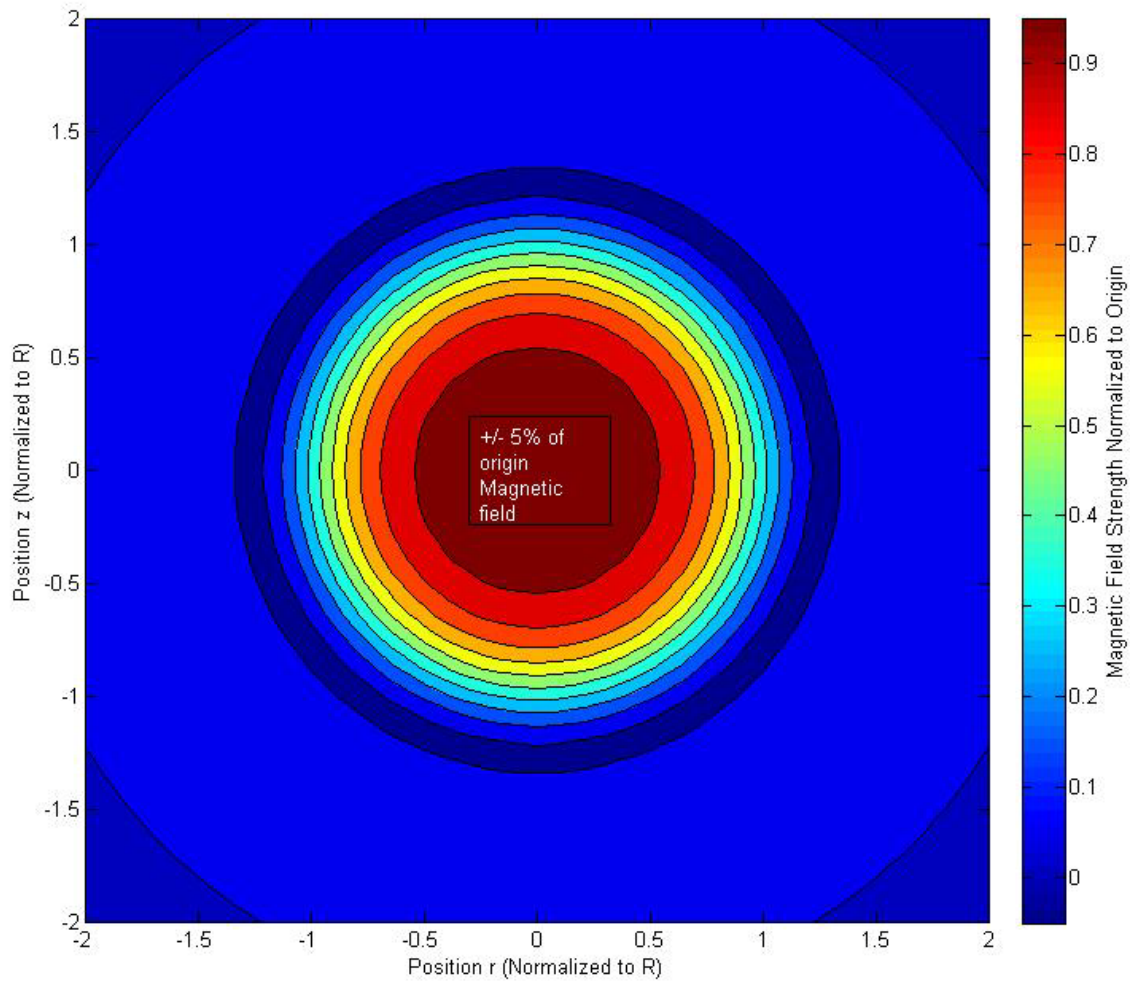


Figure 4-6: Helmholtz Coil 3D Magnetic Field Distribution (Cross section perpendicular to central axis)

Unfortunately, the simple case described above was determined to be insufficient for our project. We needed more flexibility in the upper loop configuration to better conform to the human body, which does not fit simply in an individual Helmholtz design. Our design may better be able to fit the human body if we can control the horizontal offset, and tilt angle (Θ) of the coil. An example of such a non-ideal Helmholtz coil simulation is shown in Figure 4.9. In this case, the field distribution is no longer radially symmetric. The field is thus only found and displayed for a central cross sectional of the coil.

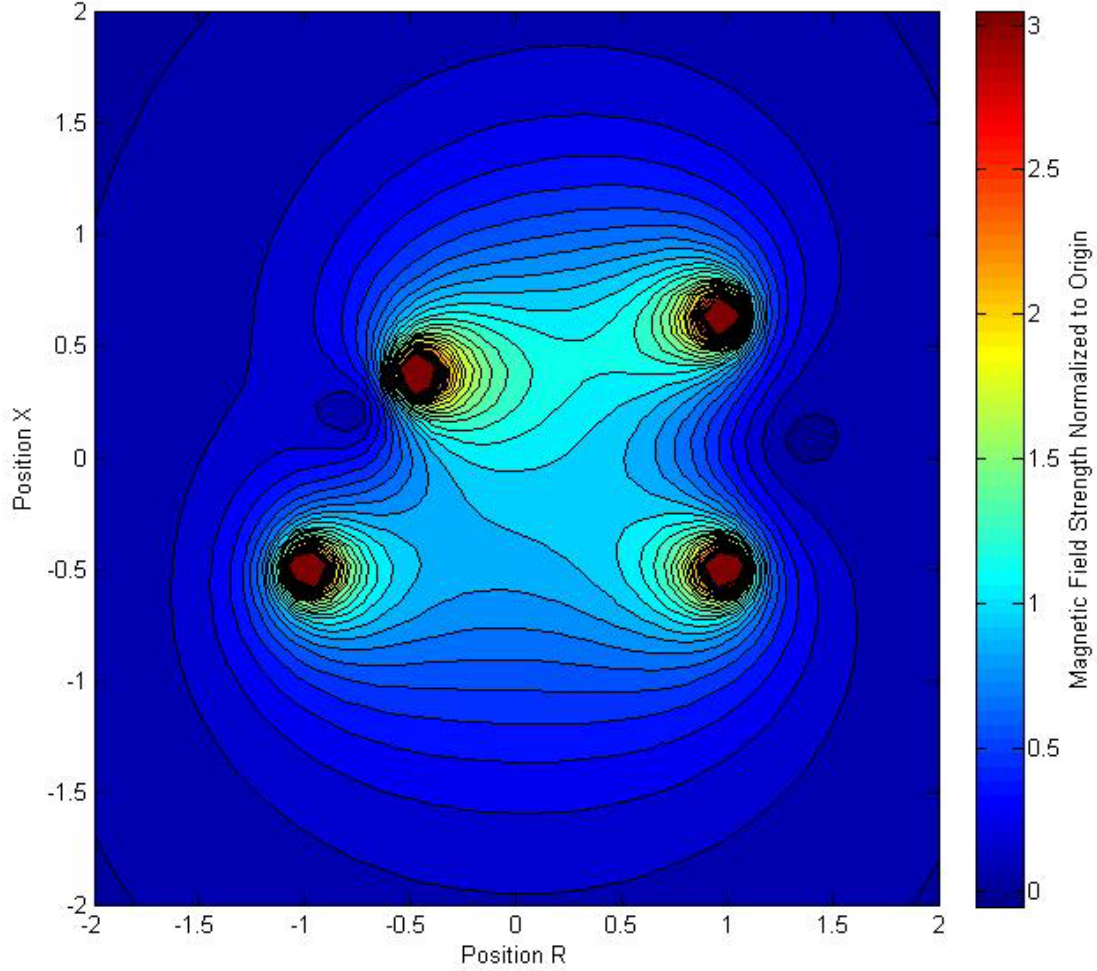


Figure 4-7: Non-Ideal Helmholtz Coil Example

After calculating the magnetic field produced by the coil at a specific point in space, we can find the SNR of the coil from equation (2). Because the MRI signal only oscillates in the Z direction, only the magnetic field of the coil in the z direction at a point, or $B_z(r,z)$, contributes to the SNR of the coil. The circumference of the top coil and bottom coil is used as the length. This is found from the radii of the top and bottom coils (a and b respectively) This gives the SNR at a point (r,z) as:

$$SNR(r, z) \propto \frac{|B_z(r, z)|}{\sqrt{2\pi ab}} \quad (11)$$

This can be used to find the SNR proportionality constant of the coil, which allows us to compare coil designs. We can also use this to determine the FOV of the MRI coil. The FOV of the coil can be determined by finding the -1 dB and -3 dB drop off of SNR when compared to the value of the SNR at the point of interest (the location of the prostate). This can be seen in Figure 4-8.

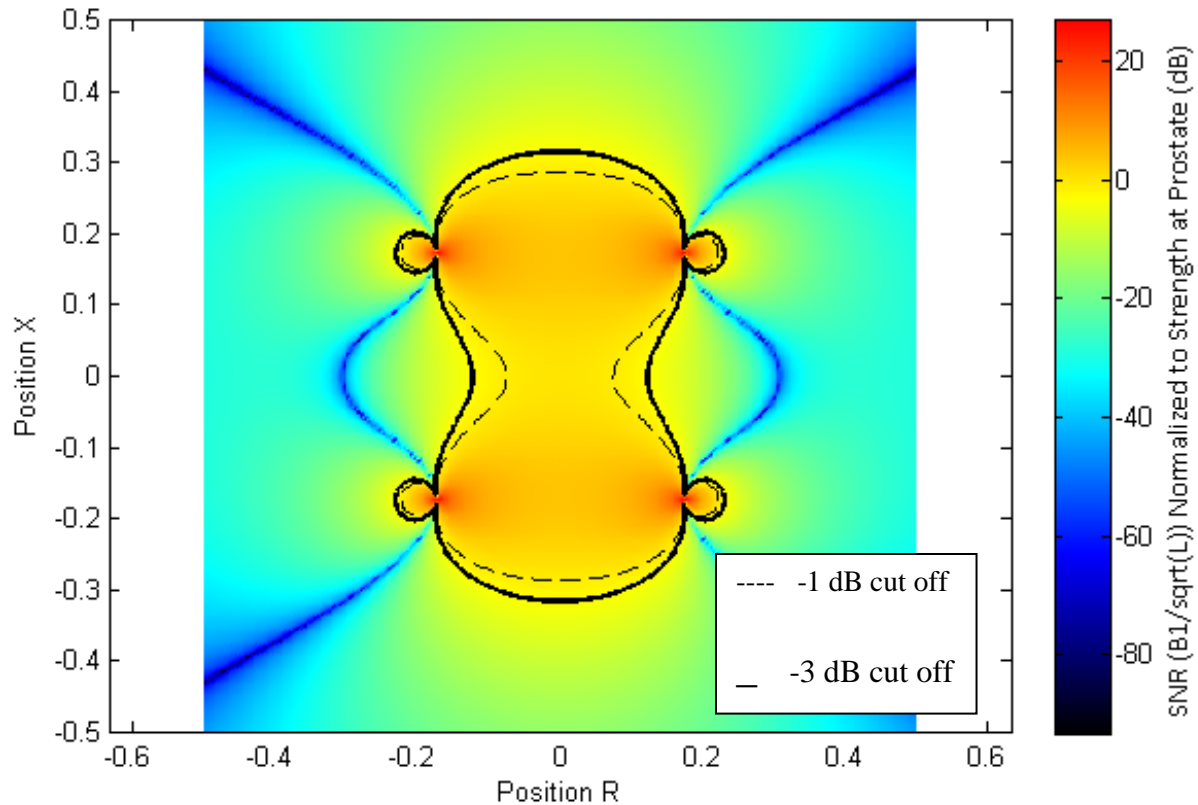


Figure 4-8: Example SNR Drop-off

These simulations will help us determine the optimal coil design for our project in terms of maximum SNR in the region of the prostate.

4.1.3 Optimization

The different designs discussed in Section 4.1.1 have vertical height constraints. However, we still need to find the radii for our coil for each design. This can be done by finding the SNR of the coil for different radii of the coil. An example relationship between the radius of the coil is shown below in Figure 4-9.

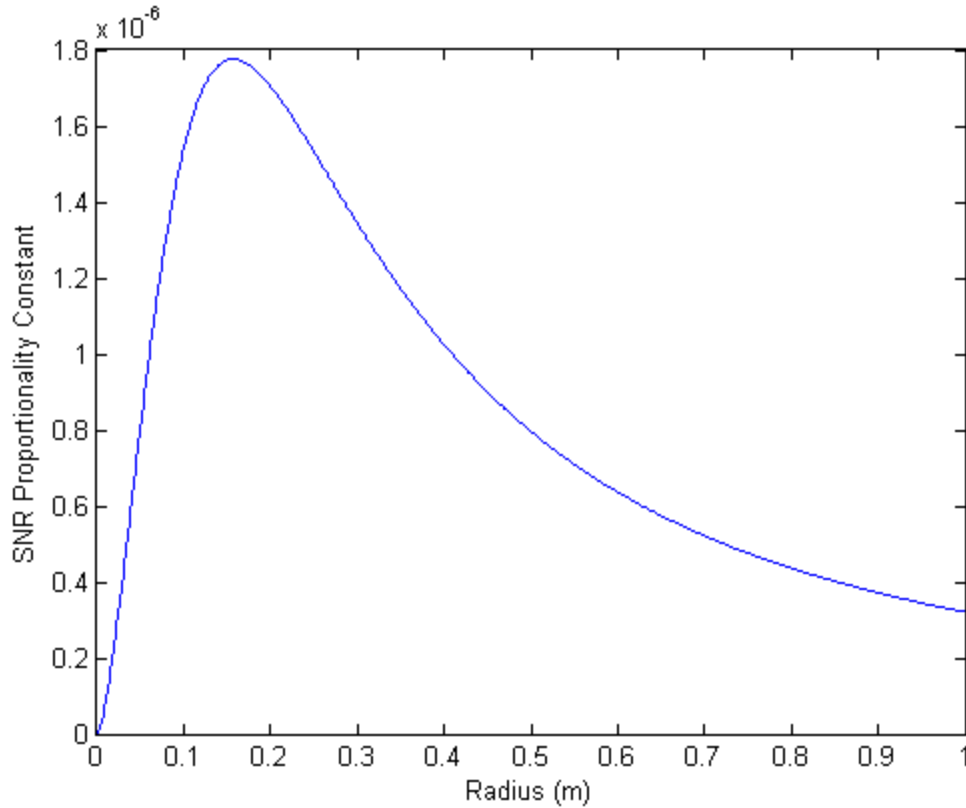


Figure 4-9: SNR Proportionality Constant (arbitrary units) at point of Prostate with Different Radii

When the coil is very small, the magnetic field (and thus, coil sensitivity) of the design does not penetrate very far into the coil. However, as the coil gets larger, it gets more and more resistive, causing a sharp drop-off in coil sensitivity. One thus needs to find the peak of the graph shown in Figure 4-9, and obtain an optimal radius at fixed heights. The point examined was the approximate point of the prostate for each coil. This point is approximately 11.9 cm above the bottom coil.

4.1.4 Conceptual Designs

After optimizing each design, we next ran the DC simulations with the MATLAB code described in the methodology section. This was done to confirm that the SNR cut off the coils was within the process and derivation of this simulation is described in the methodology section and in Appendix A.

This results initially produced SNR proportionality constants for each point in space. We know, however, that the third design has the highest central SNR. When looking at the 2D simulation results, we are more interested in the shape of the SNR regions. We thus normalized the data to the central point, and found the -1 dB and -3dB cut away from the central region. These results are shown in Figure 4-10.

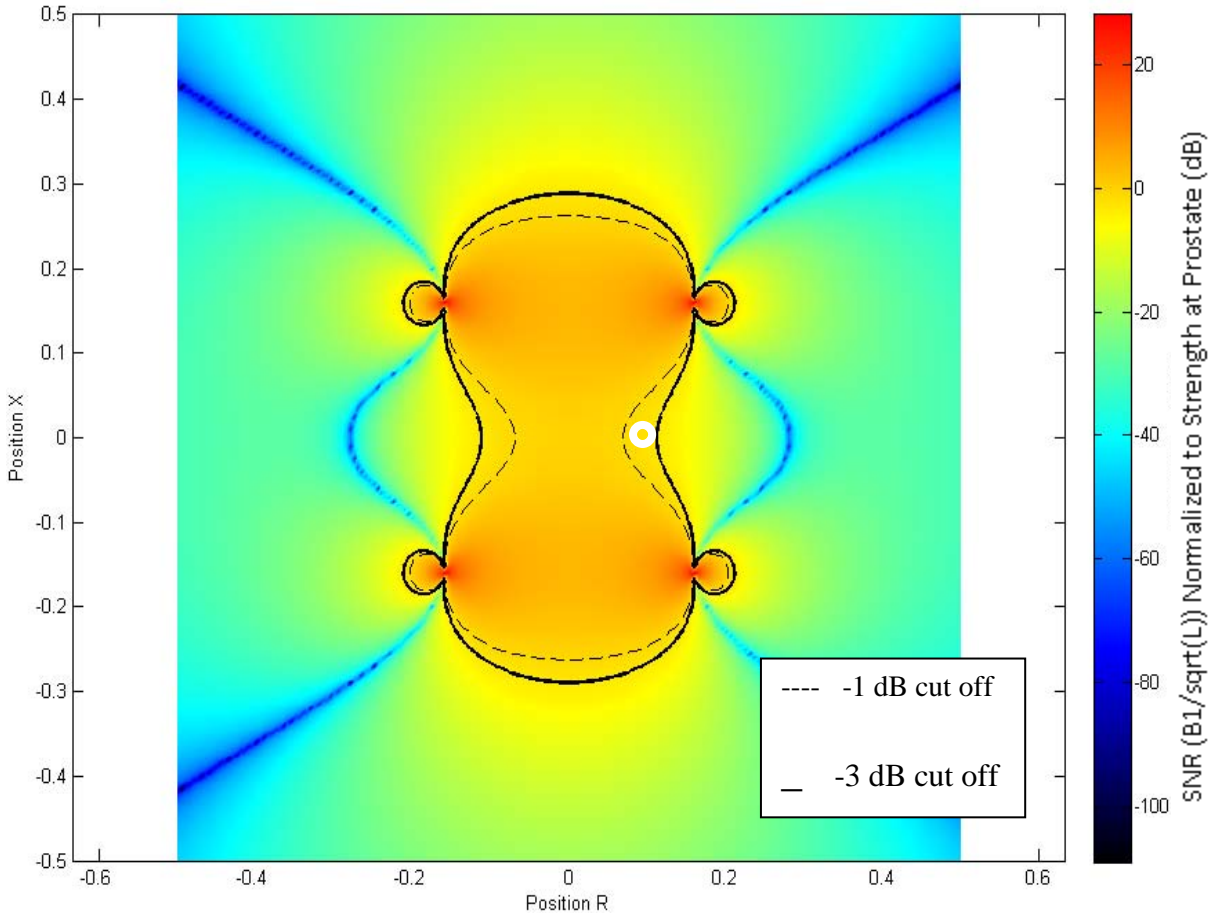


Figure 4-10: SNR Drop-off off coil design 1 (-3 dB Cutoffs Shown) (White circle is point of prostate)

The SNR at the origin of this coil was found to be $1.9831e-6$. However, this design will not allow patients to be centered under the coil. The actual SNR at the prostate may be within the -2, -3, or even -4 dB levels. We estimate that the SNR proportionality constant at the location of the prostate would be $1.5627e-6$.

For design number 2, the results are shown in Figure 4-11.

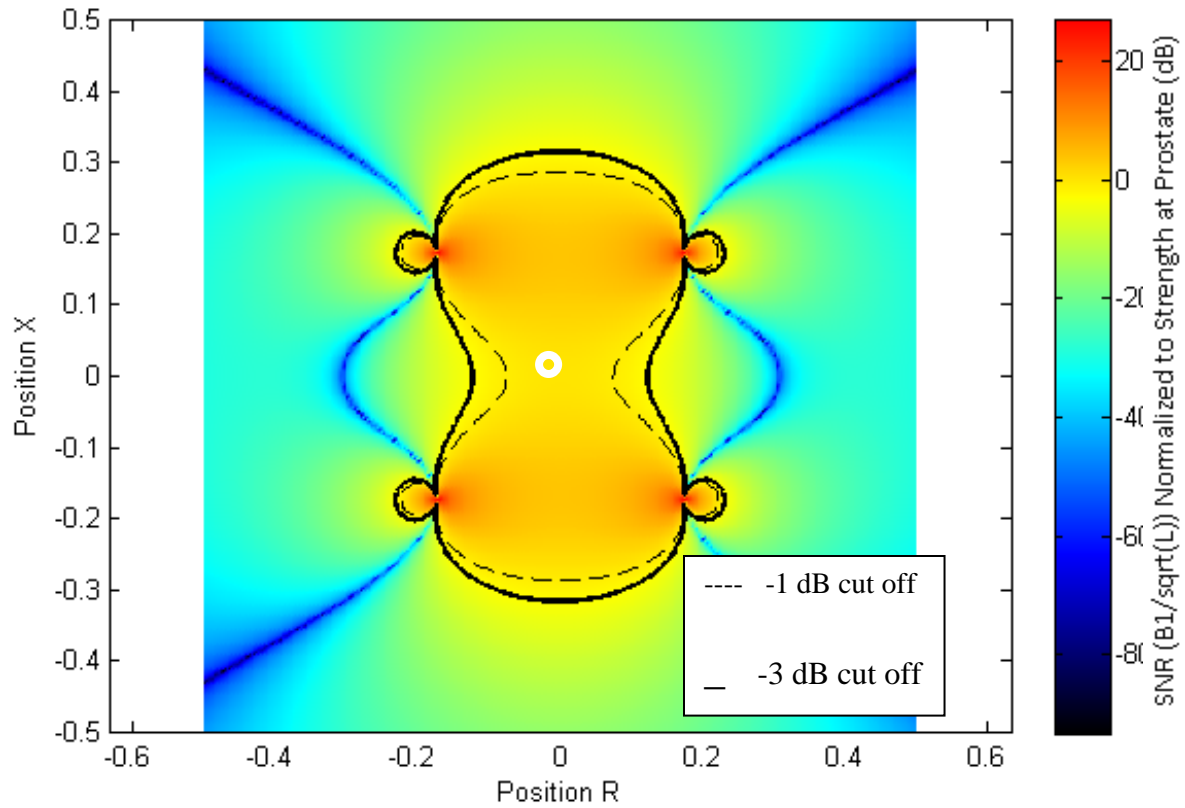


Figure 4-11: SNR Drop-off off coil design 2 (White circle represents point of Prostate)

The SNR proportionality constant at the point of the prostate was measured to be $1.7342e-6$.

For design number 3, the results are shown below in Figure 4-12.

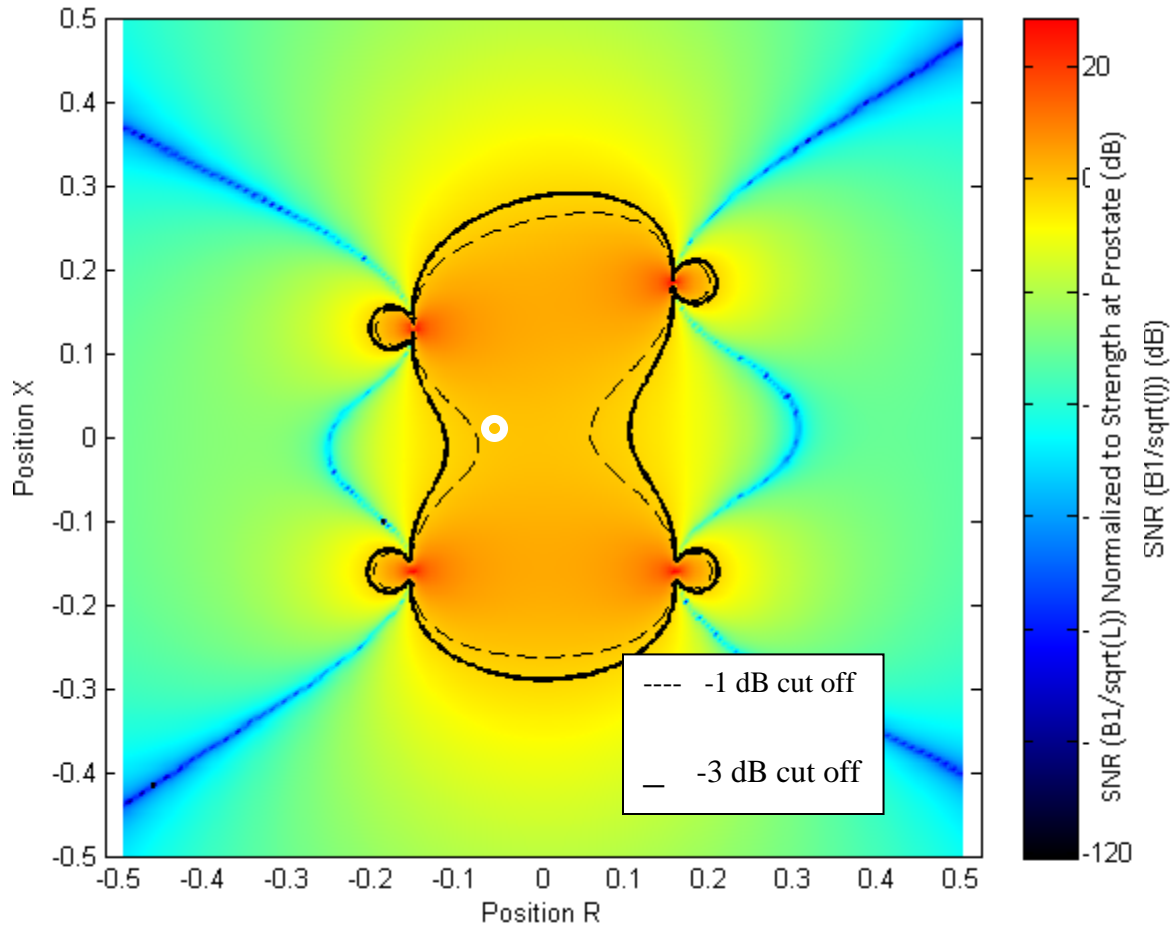


Figure 4-12: SNR Drop-off of coil design 3 (White circle is point of prostate)

The SNR proportionality constant the prostate was shown to be $1.7757e-006$.

In order to better compare the proportionality constant at the prostate, we normalized each SNR proportionality constant to the SNR proportionality constant of coil design three. Coils 1, 2 and 3 thus have an SNR proportionality constant of 0.8800, 0.9766, and 1.0000 respectively. Not only does this design have the highest central SNR, but the cut off regions for design 3 is similar to the cut off regions for the other two designs. Because of this, design number 3 was selected for our project.

4.1.5 RF Modeling

After we knew the dimensions of our coil, we conducted an RF simulation using Ansoft HFSS software. The main purpose of this simulation was to determine the scattering parameters of our coil. Because the coil has 8 ports, the matrix will have dimensions of 8x8. This matrix was then transferred into MATLAB which is used to determine the proper capacitance values for the coil breaks. The second purpose of this simulation is to confirm the results of our DC MATLAB simulations described in the prior sections.

RF simulation began with a CAD design of our coil that was created by a mechanical drawing program and exported in the so-called SAT file format. This file was then imported into Ansoft HFSS version 11 to complete the RF simulations. This file contained both the top and bottom loops of the coil, properly positioned and tilted, and with breaks for the capacitors. After being imported, the coil was defined to be copper.

Next, ports were created for the capacitors. Using the rectangle tool, a 2 dimensional strip interconnecting the tubes was created in the XZ plane between adjacent coil segments (see Figure 4-13). These rectangles are then defined as lumped ports with an impedance of 50 ohms. The lumped ports are not simulated as a conducting surface, but rather are used to define the space where a capacitor will be placed.

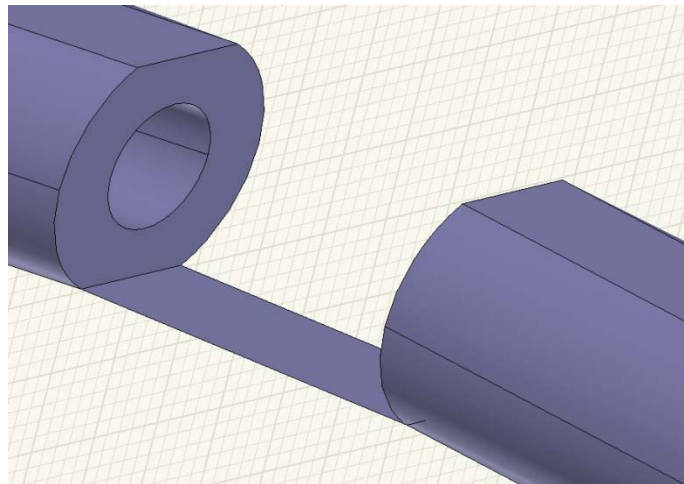


Figure 4-13: Port between Coil Segments

The next part of the simulation is the human body model. An existing model of the human body was imported into the HFSS simulation. The model offers an accuracy of 4mm. This model contains more detail than is required for this simulation, so organs were removed leaving only the prostate, intestines, and bladder. This causes the rest of the body to be simulated as muscle. The arms, lower legs, and upper body were then removed from the simulation. Although they do not greatly affect the simulation, a very

large amount of computing resources must be used to determine their effects on the coil system. Removing these parts of the body model simplifies the simulation and allows it to be analyzed easier. To remove the extremities, four boxes were created and subtracted from the human body model. The model was then shifted so that the prostate was in the center at position (0,0,0).

Finally, several properties of the simulation were set. A large radiation boundary was created surrounding the entire coil domain. This consists of a single box with sides of 5 meters in length and defined to be a vacuum. The frequency was set to 63.65 MHz and the simulation was set to run indefinitely until no more computer memory is available.

The entire simulation was then copied into a second file. This second simulation was set to 127.3MHz for a 3T MRI system. Both simulations were run on a server with 12GB of RAM. The resulting S-parameter matrix was exported into a MATLAB .m file.

4.1.6 Further Design Calculations

A MATLAB script called AnalyzerS was used to determine the values for the tuning and matching capacitors. This script takes the S-parameter input from HFSS and outputs a graph showing the S11 magnitude as a function of frequency. Our goal is to find capacitor values such that S11 will be close to zero at the target frequency. The AnalyzerS script is described in Appendix C.

5 Design Verification

5.1 Decisions and Construction

The construction of the coil can be divided into four main segments. The first choice to be made was for the copper medium. Either copper tape or copper tubing could be used to construct the coil. The skin effect plays an important role in this decision. Each of the coils (top and bottom) has four breaks where the tuning and matching capacitors were attached to. The coil was then shaped properly according to the radius of the design. The tubing was then cut and bent into the proper shape and radius. The copper tubing was attached to the surface mount boards. The ends of the tube were flattened and soldered to the board, which held the tuning and matching capacitors. The tuning and matching capacitors were then soldered to the boards. Finally, the coils were mounted in an acrylic casing, and were ready for testing.

5.1.1 Choice of copper medium

There were two available choices for the coil's conductor. Copper tape was the first option. The advantage of using tape would be the ease of construction, as it would be straightforward to cut the tape to the correct length and attach it to the tuning and matching capacitors.

The disadvantage of using copper tape is due to the skin effect. The skin effect is when the electromagnetic field (therefore the current) decays rapidly inside a conductor. Under DC conditions, the current flow is distributed uniformly over the conductor. On the other hand, in AC conditions, the current flow creates a magnetic field, which induces an electric field. The center of the conductor is where the effect is the strongest. Therefore the current flow is mostly towards the outer perimeter as frequency increases. Also, the effective resistance of the wire increases with frequency. When using copper tape, the current tends to flow on the edges of the tape, and decays closer to the center of the tape. This is not ideal for our application.

Copper tubing on the other hand effectively uses the skin effect with little loss of efficiency. When AC current is passed through a hollow conductor, the magnetic field is more concentrated at the outside diameter of the tube.

An important consideration is the skin depth, where as a function of the frequency f , it describes the spatial drop-off current density. The formula can be seen below, where f is the Larmor frequency at 1.5T, σ is the conductivity of the copper, and μ_o is the magnetic permeability.

$$\delta = \frac{1}{\sqrt{\pi \sigma \mu_o f}} \quad (12)$$

From the equation and the graph below, it can be seen that the skin depth is inversely proportional to frequency. When calculated:

$$\delta = \frac{1}{\sqrt{\pi * 64.5 * 4 * \pi * 10^{-7} * 63.65 * 10^6}} = 7.85 * 10^{-6} \text{ meters} \quad (13)$$

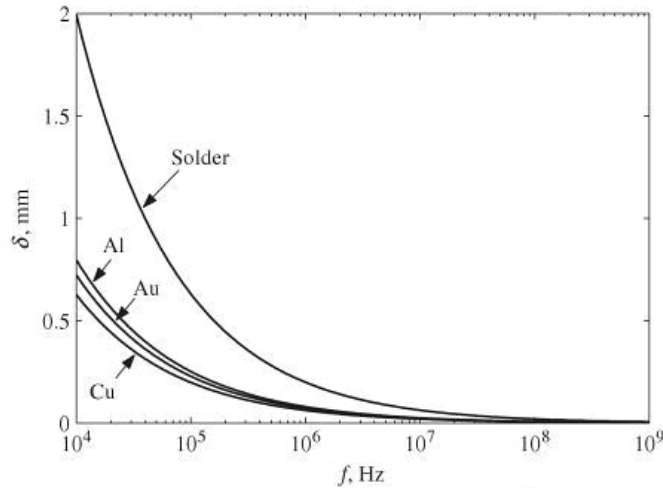


Figure 5-1: Skin depth vs. frequency

Related to skin depth, another important consideration is resistive loss. The surface resistance R_s is equal to:

$$R_s = \frac{1}{2\pi a \sigma \delta} \quad (14)$$

Where a is the radius of the coil, σ is the conductivity of copper, and δ is the skin depth.

As stated before, the higher the frequency, the lower the skin depth. As the skin depth decreases, the resistive loss of the conductor increases. When calculated:

$$R_s = \frac{1}{2 * \pi * 0.1570 * 64.5 * 10^6 * 7.85 * 10^{-6}} = 0.0020 \Omega \quad (15)$$

Figure 5-2 shows the magnetic field distribution for the inside and outside of a hollow conductor for a magnetic material carrying alternating current. The x-axis is distance from the inside of the conductor, and the y-axis is the magnetic field distribution.

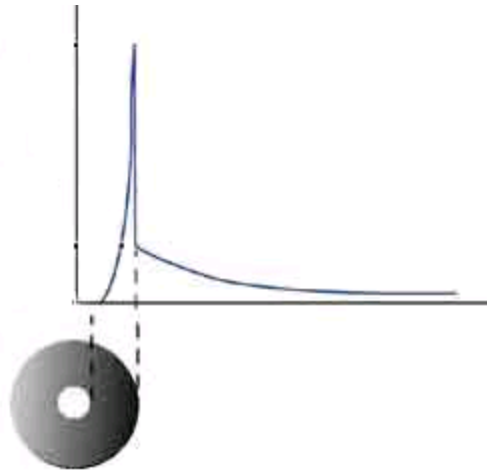


Figure 5-2: Magnetic Field Distribution inside and outside of a hollow conductor [3]

Based on this, it was decided that copper tubing would be the most suitable choice for the coil. McMaster Carr supplies products that are used to maintain manufacturing plants and large commercial facilities. After researching on their site, it was decided that copper tubing with 0.125" outer diameter and 0.061" inner diameter would be sufficient.

This particular type of copper is bendable (needed for our project) and was inexpensive.

5.1.2 Coil shaping

After receiving the copper tubing, it was then cut and shaped properly. The coil design chosen has a radius of 6.1811 inches, which gives a circumference of 38.837 inches. A 0.5" break was decided upon, as it would allow for sufficient room for the surface mount board with the tuning capacitor between two portions of the coil to be attached. Therefore the length of the each piece of copper tubing was determined to be 9.2".

The first portion of the coil construction was performed in the Higgins and Washburn machine shops with the help of machinist Neil Whitehouse. The copper tubing was first cut to 9.2 inches in length using a band saw. The ends of the tubing were then sanded using the electric sander. This can be seen below in Figure 5-3.



Figure 5-3: End of tubing after cut and sanded

These were then bent to the proper radius using the bendable tool in the Washburn machine shop. In Figure 5-4 below, a picture of the copper tubing can be seen. The imperfection in a smooth curve on the right hand side of the tubing is because of the initial bend when it was slid through the tool.

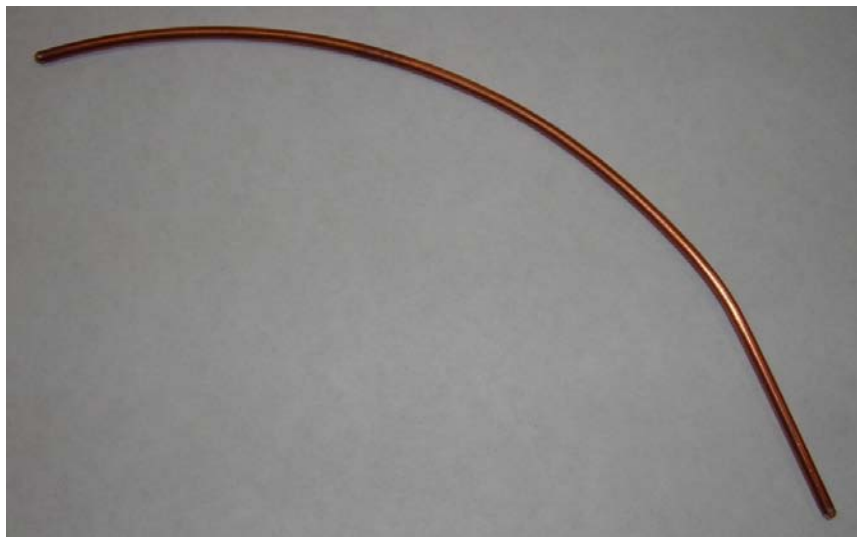


Figure 5-4: Bent copper tubing

In the ECE shop with the help of technician Tom Angelotti, a vice was used to flatten the ends of the tubing. This was done in order to solder the tubing to the surface mount board. Figure 5-5 below shows the copper tubing at the end of this stage.



Figure 5-5: Flattened end of the copper tubing

5.1.3 Attachment to surface mount boards

The final step was to attach the pieces of the tubing to surface mount boards. Capacitors were ordered to fit the particular type of surface mount boards that the ECE shop provided. The board within P/N 9161 could fit components of size 0805 (80 mils by 50 mils) and 1206 (120 mils by 60 mils). Half of each of these boards was used for each break in the coil. This was done so the coil could fit within the acrylic housing.

First the copper tubing was soldered to the surface mount boards. This can be seen in Figure 5-6.

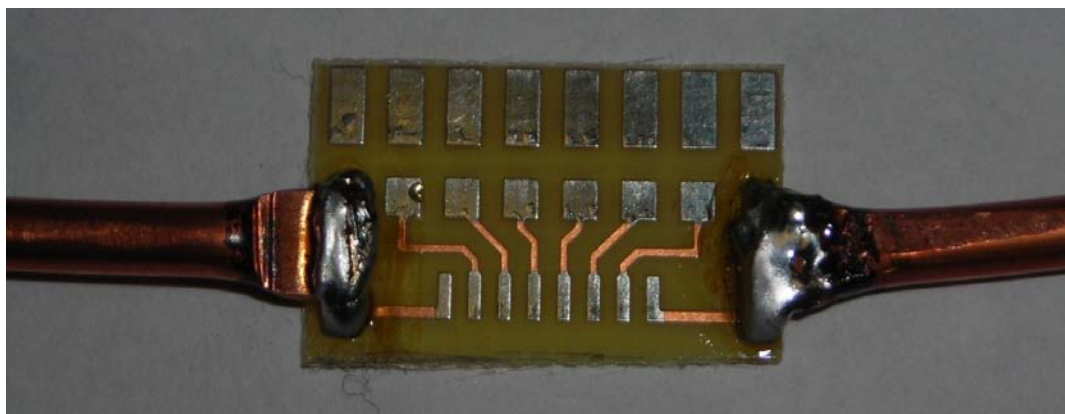


Figure 5-6: Soldering of copper tubing to the surface mount board

Next the capacitors were soldered to the board. Wire also had to be attached from the capacitor to the tubing. This can be seen below in Figure 5-7.

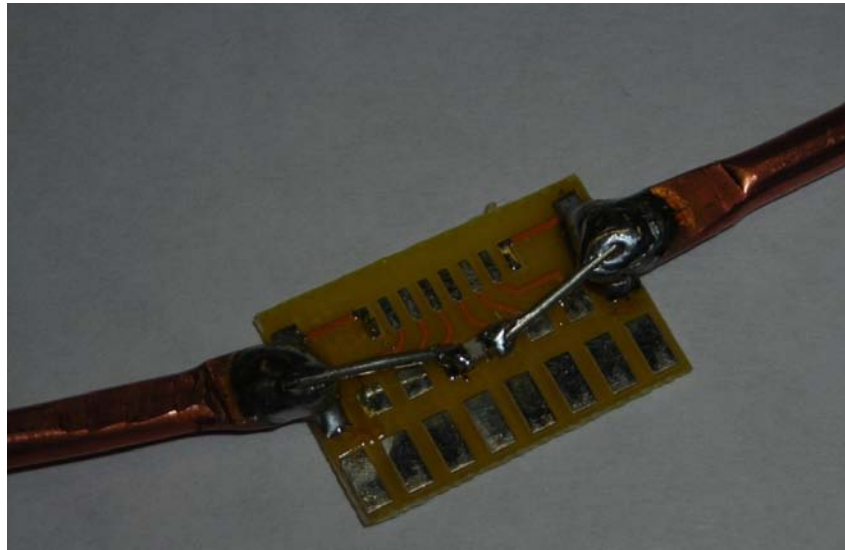


Figure 5-7: Capacitor soldered to the surface mount board

5.1.4 Casing

The first step in creating the casing was the selection of the material. The casing's material needed to be both non-magnetic, and easy to construct. We thus selected acrylic for the design. Acrylic is a non-magnetic insulator. In addition, we had access to an acrylic printer which greatly reduced the fabrication time.

The design of the casing is shown below. One safety requirement for MRI coils is that the MRI coil needs to be separated by at least 0.13 inches of solid material, and be at least 0.35 inches away from any crack or opening. We thus used 0.25" thick acrylic as the base material for our design.

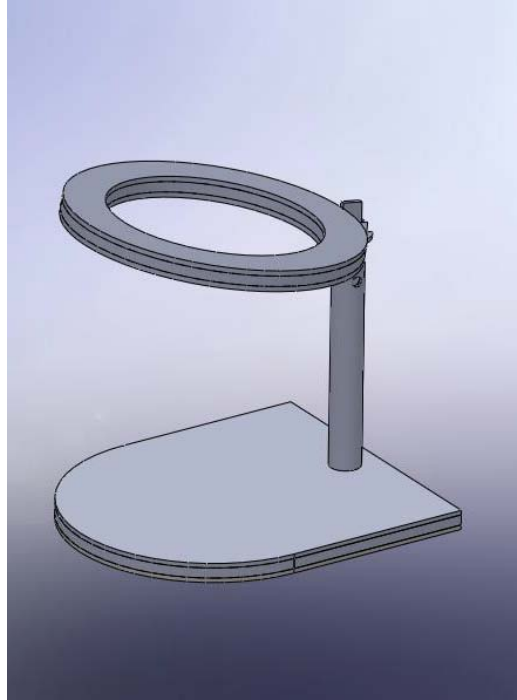


Figure 5-8: MRI Casing

5.2 Tuning and Matching the Coil

One essential part of testing the feasibility of our coil is the coils ability to be tuned and matched to a load. Any antenna system, such as an MRI coil, must be tuned and matched in order to work properly. A tuned coil means that the combined resistance, inductance, and capacitance of the coil causes the coil to resonate at a specific frequency. In our case, we want the coil to resonate at 63.65 MHz, the Larmor frequency of hydrogen in a 1.5T magnetic field. Matching the coil make the RF impedance of the coil 50 ohms, allowing for the lowest reflection of input power from the coil.

From RF simulations at 1.5T, it was determined that the tuning capacitor has an ideal value of 20 pF, and the matching capacitor has an ideal value of 35 pF. The capacitor values were also determined for the 3T scanner, and were 6 pF for the tuning capacitor, and 32 pF for the matching capacitor. While the values of 20 pF and 30 pF represent sufficiently large capacitances for stable operation, a 6 pF value at 3T is prone to parasitic influences.

The original layout for the capacitors can be seen below in Figure 5-9.

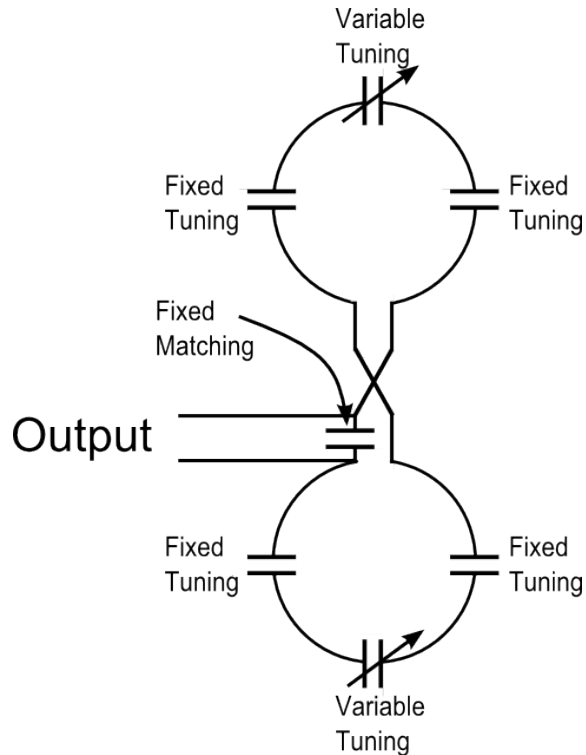


Figure 5-9: 2D Original Layout of capacitors

The capacitor values obtained from the RF simulations are ideal values. Because of the coil construction and the imperfectness in shape, the values needed to make the coil resonant will change. Therefore, we put a variable capacitor on each of the coils. These capacitors have a range of 8.5pF to 40 pF. Tuning the coil ensures that it resonates at the correct frequency; therefore slight adjustments must be made to the tuning capacitors. This is easily accomplished with the use of variable capacitors.

An inductor is needed with the matching capacitor in order to form a proper matching network. This combination will adjust the 3dB bandwidth that the coil resonates at. Ideally, this bandwidth should be narrow, at about 20 kHz, in order to construct a coil that resonates only at 63.65 MHz.

Before the coil can be tuned and matched, the system must be connected to the network analyzer. There are many ways of doing so, with the use of BNC, SMA or N connectors. Since the network analyzer uses an N connector, it was decided that an N connector would be attached to the linking coaxial cable between the network analyzer and the coil.

The network analyzer will be used to properly tune and match the coil. The S11 parameter represents the input port voltage reflection coefficient. In other words this is the ratio of the power wave exiting from port 1 (b1) to the incident power wave at port 1 (a1). A graph showing S11 (in dB) vs. frequency can be viewed when using the network analyzer, similar to the RF simulation results.

At the resonant frequency of 63.65 MHz, the reflection coefficient should be much less than zero, as $20 \cdot \log(0)$ is $-\infty$. This is because at this frequency, the power wave should not be reflected. At all other frequencies the S11 parameter will be zero, as the power wave will be reflected more. This is because at the target frequency, $20 \cdot \log(1) = 0$.

Tuning the coil, as discussed before, is performed to make sure the coil resonates at the correct frequency. Therefore by tuning the coil (on a graph of frequency vs. dB) will shift the wave along the frequency axis. Matching the coil adjusts the bandwidth, which will ideally be narrow.

5.2.1 Procedure for tuning and matching the coil

The procedure for tuning and matching the coil will next be outlined. First the variable tuning capacitors were adjusted so that the coil resonates at 63.65 MHz. Initially the variable capacitors were both be set to the ideal value of about 20 pF, and then adjusted one at a time from there. Once the target frequency was correct, the bandwidth was adjusted by use of the matching capacitor and inductor.

The coil was successfully matched to a human load at 63.65 MHz. However, slight modifications to the original design needed to be made. First, while we did keep a similar total capacitance, it was determined that two additional breaks would keep the coil from having excessive distance to travel before reaching a capacitor. This meant the addition of two additional capacitors. Because of the short time allotted, we were not able to re-simulate the coil with these new breaks. However, because the overall inductance and resistance of the coil did not change significantly, the required capacitance also did not change significantly. Capacitor values were thus selected in order to create a similar over all capacitance.

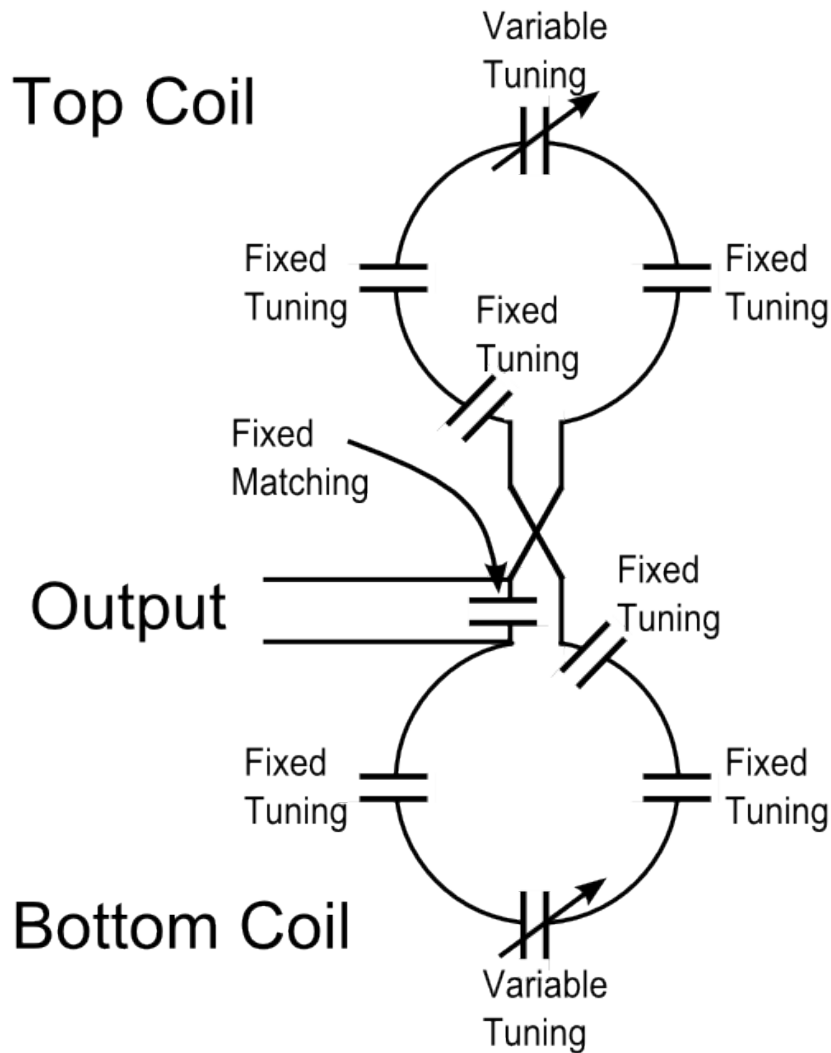


Figure 5-10: Layout with 2 additional breaks

After adding the two additional breaks, we determined that the tuning caps needed to be shifted significantly in order to tune the coil. The coil was giving abhorrent behavior, giving side resonances and could not be tuned to 63.65 MHz. This is most likely due to the fact that the tuning capacitance was not evenly distributed. With the fixed tuning capacitors at a value of 18 pF, the tuning capacitors were at a value of ~13 pF. This was most likely due to the fact that the real coil had a different overall impedance than found in simulation, causing the overall required capacitance to be different from the simulation. While the overall value of the capacitance changed slightly due to this difference, the individual caps were now in series with 6 capacitors. Small changes in these capacitors did not do much to change the overall capacitance.

In order to compensate, each tuning cap was selected as 21 pF. This allowed the coil to be tuned with fixed variable cap values of ~24 pF.

5.2.2 Verifying Tuning and Matching using Variable Volume Phantom

This coil needed to be tuned, matched, and tested as if a human were in the coil. This is typically done by simply using one of the designers as a “stand in” replacement, as the coil’s tuning and matching should not change significantly from person to person.

A phantom is a physical model that emulates electrical properties of the human body. These are essential for the testing of MRI coils because the human body acts as a lossy dielectric load. The implication of a lossy load is that as the quality factor decreases, it results in a shift in frequency.

Phantoms are typically made from containers of saline or protein. One of the requirements of this phantom is that it needs to allow for internal measurements. Based on this requirement, a phantom was constructed out of a paint bucket and PVC pipe. phantom was then filled with a saline solution to model the human body.

The electrical conductivity of the phantom can be adjusted using the molar conductivity of NaCl, which is $126.9 \text{ ohm}^{-1} \text{ cm}^2 \text{ mol}^{-1}$ [32]. The conductivity of the coil was thus selected to be similar to that of other phantoms, such as the one from Park (0.24 Siemens/M) [33].

After constructing the phantom, the phantom can be placed inside our coil to test the coil’s response to various loads. This was done by starting the phantom full with 19 Liters of solution. The solution was removed 1 liter at a time, and the S11 parameter was measured for each position using the network analyzer. The data from the network analyzer was dumped into a .CSV, where it could be opened in excel to find the necessary data to extract the quality factor and resonance frequency. The raw data for this section can be found in Appendix E.

Table 5-1: Coil Response for Different Loads

Volume (L)	Operating Frequency	Shift from 63.65 MHz	Lower Cutoff (MHz)	Upper Cutoff (MHz)	Bandwidth (MHz)	Q	Lowest point (dB)
19	63.3175	0.5224%	60.325	66.550	6.225	10.17	-14.10125
18	62.7250	1.4533%	60.175	65.575	5.400	11.62	-11.65601
17	62.7250	1.4533%	60.325	65.500	5.175	12.12	-10.61212
16	63.7750	0.1964%	59.875	68.050	8.175	7.801	-23.56484
15	63.7000	0.0786%	60.175	67.450	7.275	8.756	-16.30785
14	64.0750	0.6677%	60.700	67.675	6.975	9.186	-16.41481
13	63.7750	0.1964%	60.800	66.850	6.050	10.54	-12.54609
12	64.0000	0.5499%	60.850	67.225	6.375	10.04	-14.24805
11	63.8500	0.3142%	61.000	66.850	5.850	10.91	-12.23180
10	63.9250	0.4321%	61.075	66.850	5.775	11.07	-11.74341
9	63.9250	0.4321%	61.225	66.775	5.550	11.52	-11.14311
8	63.9250	0.4321%	61.375	66.625	5.250	12.18	-9.81950
7	64.0000	0.5499%	61.525	66.775	5.250	12.19	-9.66155
6	64.3000	1.0212%	61.525	67.075	5.550	11.59	-10.44105
5	64.3000	1.0212%	61.600	66.925	5.325	12.08	-10.04381
0	63.9000	0.3928%	62.700	65.300	2.600	24.58	-4.69000

There is some variability in this data. This is most likely due different positioning of the phantom within the coil. However, from this data we can find some general trends. First, the quality factor of the coil generally gets larger as the coil becomes less and less loaded. This can be seen especially from the range of 0-16 L, shown in Figure 5-11. This makes sense as the load adds a resistance to the coil.

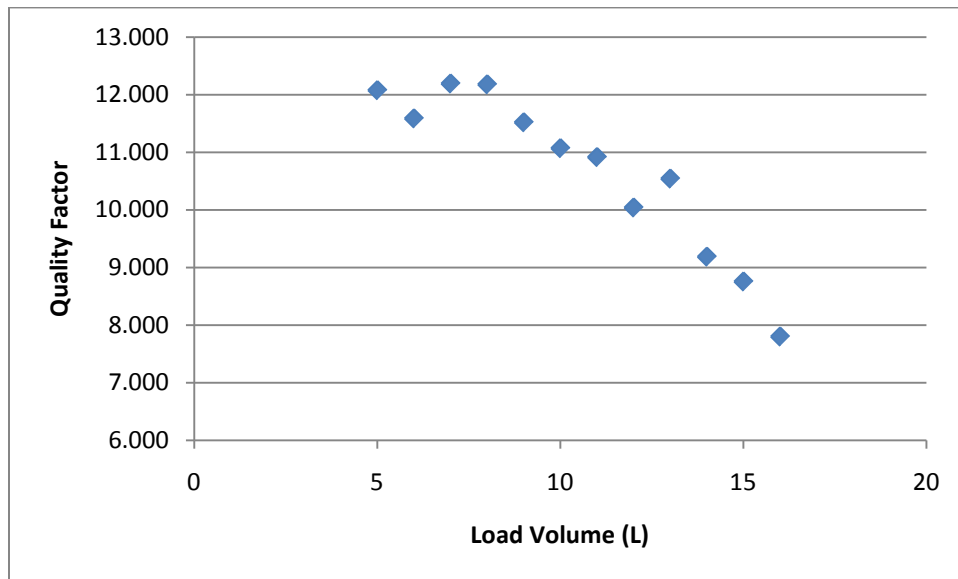


Figure 5-11: Q of coil based on Volume of Load

The resistance of the load is not the only thing that affects the quality factor, however. How well the coil is matched at the specific frequencies also affects the quality. Thus, the frequency shift due to the load can cause the coil to become unmatched, while approaching the matching point can increase the quality factor. The higher quality factor for the volumes 17-19 is most likely due to this. At point 16, the dip has

the lowest value of -23.56484 dB. This low value means that the load most acts as the stand in human load at that point.

Another thing to note is that the frequency shift due to the different loads is relatively small. Most shifts in frequency are within 1.5% of the target value of 63.64 MHz. This shift will be discussed more in the Discussion section.

5.2.3 Verifying Tuning and Matching using Biological Loads

While the phantom acts as a good model for the human body, it is not perfect. The human body's electrical properties vary significantly from person to person. Thus, another way to verify tuning and matching is to test human subjects in the coil. Different human loads can also be used to test whether or not the coil can be tuned and matched to a human load.

The following Institutional Review Board (IRB) approved test was performed on 11 student volunteers of varying weights, and genders. The IRB approval documents are shown in Appendix F. The students' names are kept confidential.

- 1.) WPI Students will be informed of the following information by one of the student researchers.
 - The purpose of this MQP is to design a Helmholtz MRI Receive Coil for imaging the prostate. In an actual imaging setting, the patient will emit a signal that would be picked up by this coil.
 - For the scope of the project, we will not be imaging any patients.
 - We will be testing whether or not the coil behaves correctly outside of a magnet.
 - This coil has different RF behavior depending on the type of load placed inside of it. The size, weight, and electrical conductivity of the load can change the frequency which the coil resonates, as well as the quality of the resonance.
 - This experiment is designed to test our coil only
 - The student will be asked to empty his/her pockets and remove any belts
 - The student will be asked to sit in the coil as a patient would
 - While in the coil, the student will not be exposed to any dangerous electromagnetic radiation
 - The student will be exposed to less than 1 mW of radio waves centered around 63.65 MHz. This frequency and power level will have no effect on you.
 - The behavior of the coil will be recorded and saved independent of his/her name or any other personal information
 - The entire test will take less than 5 minutes.
- 2.) The students will be asked to sign a consent form.
- 3.) One of the student researchers will demonstrate how to sit in the coil.
- 4.) The students will be asked individually to sit in the coil.

- 5.) A RF frequency sweep from 50 to 70 MHz will be used on the network analyzer. The data for the S11 parameter for the patient will be dumped into a .CSV file, which will be saved as Patient followed by a number.
- 6.) A Smith chart display will be saved from the network analyzer for the same frequency range.
- 7.) The patient will then be allowed to leave.

The raw data for this test is shown in Appendix G.

Eleven students volunteered for the testing of the loaded coil. Proper IRB approval was granted for this test. Each student was made to lie in the coil, and various measurements were recorded from the network analyzer. On the S11 parameter graph, marker 1 specified the target frequency of 63.65 MHz. Marker 2 displayed the lowest point on the graph, while Markers 3 and 4 annotated the -3dB points.

An example of the S11 graph for a student can be seen:

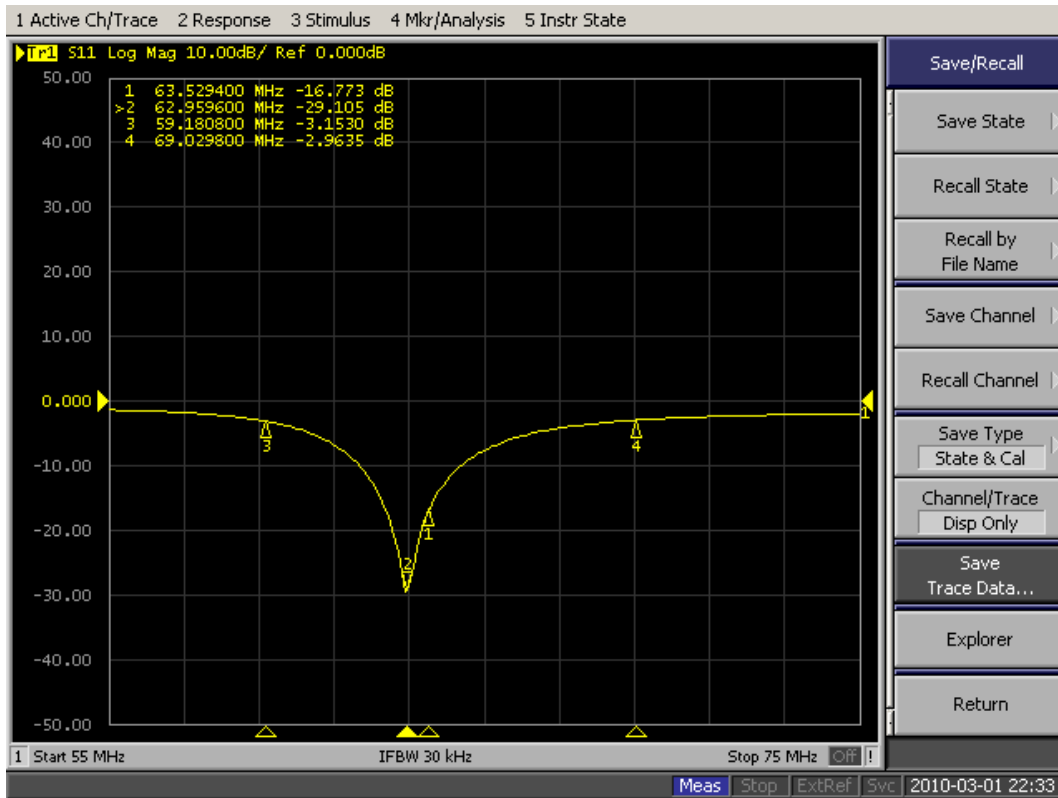


Figure 5-12: Example S11 parameter graph from a student

Trace data was captured from the network analyzer and saved onto a flash drive. A screen image of the S11 parameter graph was also saved for each student. In order to properly analyze the data, a Smith chart was also viewed for each student. Marker 1, which denotes the target frequency, is very close to middle of the graph. Marker 2 denotes the lowest point, and ideally it should be exactly in the middle of the Smith

chart. A perfectly matched coil would have Marker 2 at the center indicating a perfect match; our coil may have become a bit detuned. An example can be seen:

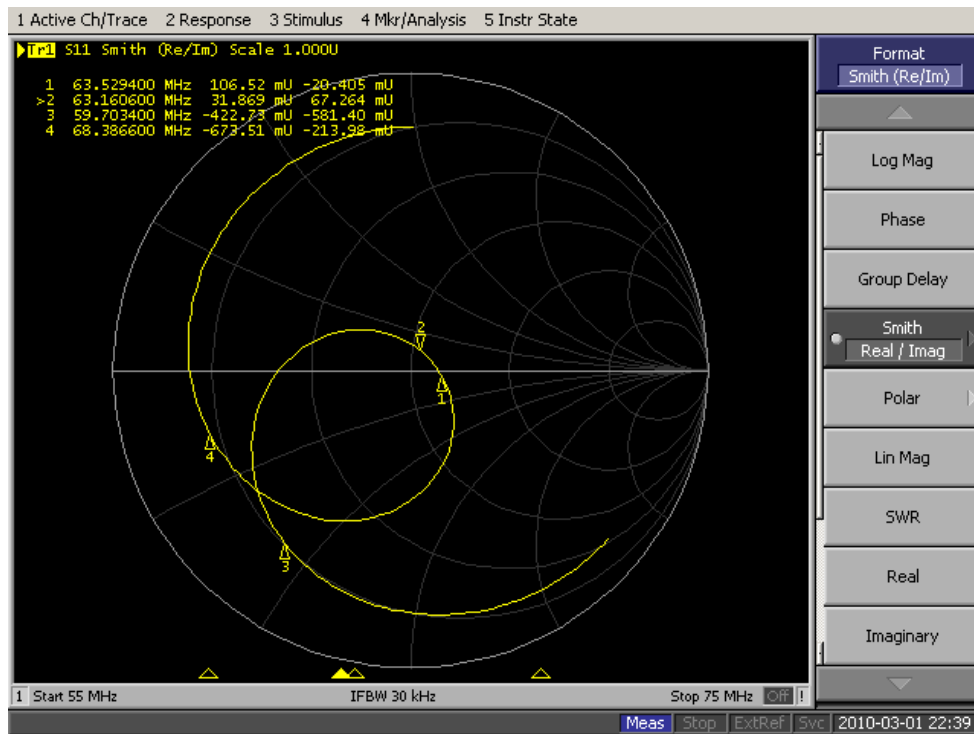


Figure 5-13: Example Smith chart from a student

Data was gathered from the eleven students. The individual student data can be found in Appendix G. The data for the entire population was then compiled. The operating frequency for the population was 63.0 ± 0.2 MHz. This range does not include the value of 63.65 MHz. This shows that our coil has a shift from the 63.65 MHz value of 0.63294 MHz. However, this error is only 0.994%.

The standard deviation of this value can be used to show how our coil's tuning changes when exposed to different loads. The change of 0.2 MHz is relatively small, being only 0.308% of the total value. This shows that our coil will stay relatively tuned for many different loads.

The quality measured for the students was also measured. This value was found to be 7.1 ± 0.7 . The variability in this value was a little larger than that for the tuned frequency: 10.04%. This shows a greater variability in the coils performance due to the different human loads.

The final part of the population measurements were the lowest point measurements. This value was found to be -9.8 ± 0.2 dB for the S11 parameter. This variability of this measurement is 1.76%. This change shows that our coil behaves similarly at the Larmor frequency for different biological loads.

5.3 SNR Uniformity Testing

After verifying the tuning and matching of the coil, we can turn our attention to the magnetic field uniformity and magnetic field strength. The magnetic field strength is a contributing factor to the coils' sensitivity. This field must be uniform across the region of interest to prevent the appearance of dark or light spots in the image.

We tested the magnetic field uniformity using a small magnetic dipole loop. This dipole loop is much smaller than the actual coil, only around 1 inch. The magnetic dipole loop sensor will be placed within the Helmholtz coil, creating the network shown in Figure 5-14. As our coil consists of only resistance, capacitance, and inductance, the coil is a linear passive system. We can thus set S_{12} and S_{21} equal to each other. Setting S_{12} equal to S_{21} ensures that the forward and reverse voltage gains are equal to each other.

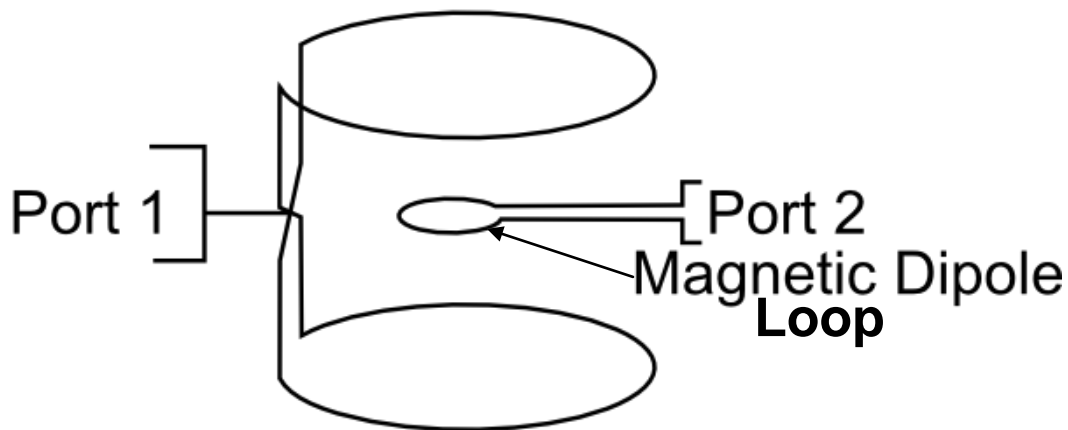


Figure 5-14: Magnetic Field Test Arrangement to Investigate Helmholtz Receive Coil Sensitivity

In this setup, the power injected into port 1 will create a current in the magnetic dipole. The power out of port 2 will be proportional to the strength of the B_1 field. Thus, the S_{21} parameter of this network is proportional to the B_1 field. For the purposes of this test, we will verify the magnetic field strength distribution for the 2 axis tested in the DC simulation: the vertical direction, and the front to back direction.

The absolute value of the B_1 field cannot be determined from this setup. However, the relative value of B_1 can be found. We can thus find the magnetic field *distribution* by the S_{21} parameter through the coil. The magnetic dipole was placed every 1 cm within the coil, and the S_{21} parameter was recorded. The raw data for this test is shown in Appendix H.

We first did this test unloaded in the vertical direction. This data was normalized to the lowest value in the set. This is shown in Figure 5-15, as well as the corresponding theoretical data.

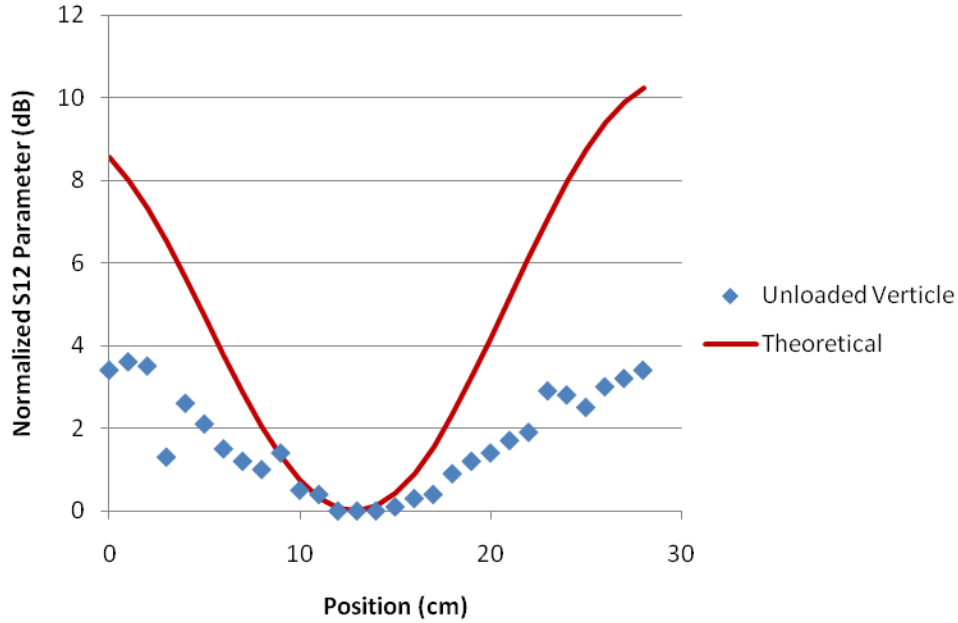


Figure 5-15: Magnetic Field Distribution in Vertical Direction

While of similar shape, the actual MRI coil’s magnetic field strength does not grow as fast as the magnetic field of the theoretical coil. In this case, this allows a greater area to be within +/- 3 dB of the center coil. The difference in this value is most likely due scaling issues associated with this method of measuring field strength.

In order to find how good of a fit the theoretical data is to the actual measured data, we can find the coefficient of determination between the two data sets. Using the individual measured data points y_i , the mean measured value \bar{y} , and the individual theoretical values, f_i , this can be found from the equations

$$SS_{tot} = \sum_i (y_i - \bar{y})^2 \tag{14}$$

$$SS_{err} = \sum_i (y_i - f_i)^2 \tag{15}$$

$$R^2 = 1 - \frac{SS_{err}}{SS_{tot}} \tag{16}$$

This reveals an R^2 value of -7.7, showing that this is a fairly poor fit.

Next, we compared the magnetic field in the front to back direction. In this test, we were able to use a specialized phantom to test the magnetic field distribution for both the loaded and unloaded case. These results are shown below.

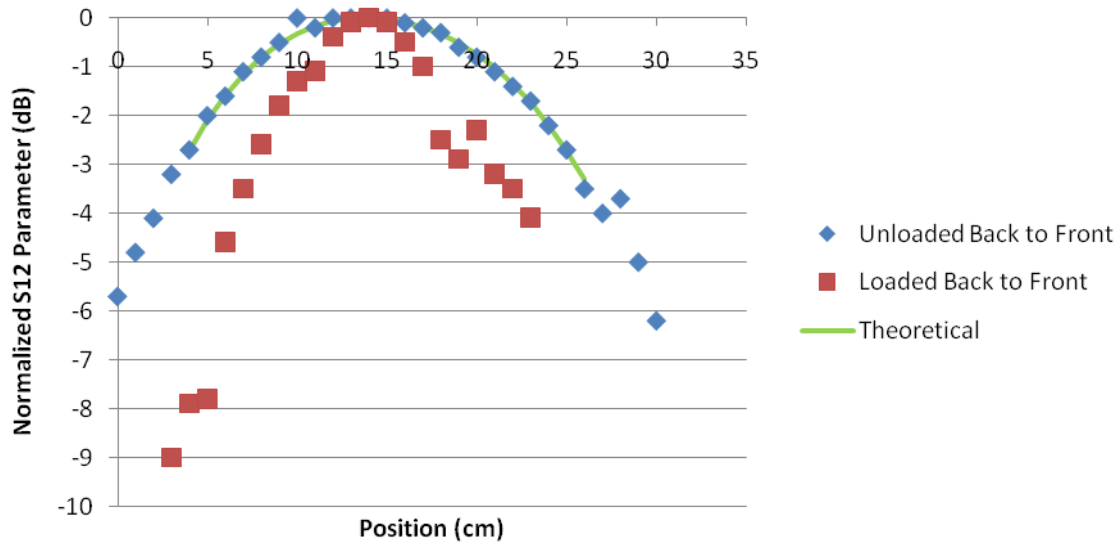


Figure 5-16: Front to Back Magnetic Field Strength Distribution

While each magnetic field distribution follows generally the same shape. We can use the R^2 calculation from equation 14 to find how closely our data matches the model. In the loaded case, the data departs from the model, with a R^2 value of -0.28822. While this value is still small, it does correspond much better than the vertical case. The unloaded case corresponded very well with the theoretical data, with 0.893.

6 Discussion

6.1 Coil Bench Testing Behavior

The testing performed on the coil had mixed results. First, we tested the coil's ability to be tuned and matched. While it was successfully tuned and matched to one individual, variations in the population will change whether or not it is tuned and matched during bench testing. Our first testing in Section 5.2.2 used a phantom to test the coil under different loading conditions. Overall, the coil responded very well to the phantom. In the unloaded case, the coil had a relatively high quality factor of 24.58. This quality factor is good considering the size of the coil. The quality factor also drops when loaded. While this is not the desired behavior, it does demonstrate that our coil is sensitive to the different loading levels. In addition, the different loads caused a shift in frequency from the desired 63.65 MHz by a maximum of 1.5%. This shows that the coil behavior is robust enough to handle different loads.

The coil's behavior was confirmed when we performed the S11 parameter testing on different student subjects. First, the coil was successfully tuned to 63.65 MHz. With a systematic error of 0.994%, the coil is very close to the actual value of the Larmor frequency. The Larmor frequency is well within the bandwidth for all students. In addition, the tuned frequency only had a variance over the population of 0.308%. This shows that our coil maintains its tuned frequency under many different loads.

The coil's quality factor is relatively low (7.1 ± 0.7). This is a concern for creating a well functioning coil, and is most likely due to the large size of the coil. However, certain changes can be made to reduce the resistance of the coil and thus increase the Q that were outside the scope of this project. First, the coil's Q could be increased by using larger diameter tubing. The larger diameter tubing would have more surface area, and thus reduce the resistance of the coil at high frequencies. Another way to increase the coil's Q would be to decrease the size of the coil. While the coil would be less able to accommodate patients, the coil would be able to get both higher SNR and quality factor.

The magnetic field distribution is either the same or has a wider range than the theoretical DC simulation as shown previously in a plot. In the vertical direction, the ± 3 dB range was much wider than simulation, causing the R^2 value, a measure of correlation, to be very poor (-7.7, a very poor fit). While the departure from the simulation may be due to RF behavior of the dipole loop and not of coil behavior, this is good data.

The R^2 value for the front to back unloaded case was 0.89, showing that the coil did behave as expected in this particular direction. However, loading the coil significantly changed this shape, causing the fit to

have an R^2 value of 0.2882. The different behavior may be due to the difficulty of finding accurate placement within the phantom.

6.2 Safety features

Safety features are a crucial part to the MQP project of creating an external Helmholtz coil for prostate MR imaging. There are four main safety features to be discussed. First is the PIN diode, which controls the switching between transmit and receive mode. Next is the DC choke, which is used in parallel with each of the tuning and matching capacitors in order to avoid damage. Another important safety feature is the fuse. The last safety feature is the importance of the thickness of the casing.

A PIN diode is a device that is ideal for fast switching. Therefore, it is used as an RF switch to change between receive and transmit mode within an MRI machine. This is an important safety feature; if the switching between the transmit and receive coil is not performed properly, the patient could be harmed. PIN diodes are also used to reduce the insertion loss of the system, which will in turn lessen SNR degradation.

Another important safety aspect is the DC choke. Across the tuning and matching capacitors, a diode should be placed in parallel. Placing a diode in this manner will protect the capacitor from sudden large changes in voltage, and in turn will not harm the patient.

Fuses are a crucial part of safety for the MRI system. It protects the system in the case of too much current, which can easily damage the coil. It could potentially harm the patient, as even a few mA of alternating current can be painful and interfere with breathing and with the heart.

The last safety feature to be considered is the thickness of the acrylic casing. There are strict spacing requirements to keep patients electrically isolated from all metal surfaces in an MRI coil. All metal surfaces must be at least 0.35" from any crack in the casing. In addition, all surfaces must have at least 0.18" of plastic between them and the patient. These requirements are met by the acrylic casing.

6.3 Economics and social issues

The results of our project can influence the economy of everyday living. Creating an external coil for prostate MR imaging will greatly increase the level of comfort experienced by older men. By using this coil, it is hoped that prostate cancer will be detected at earlier stages, as men will be more willing to have an external coil rather than an internal one.

On top of being used specifically for prostate imaging, this coil modality may be helpful in imaging other diseases in the pelvic area, and could be modified for different diseases. For example, the coil could focus on imaging the rectum for rectal cancer, or imaging other organs in the region.

If our product were introduced in other countries, it would affect the culture. It would allow men of varying proportions to be imaged comfortably. Men would most likely be more willing to be imaged because of the level of comfort and accommodations. Use of this product would hopefully improve the detection of prostate cancer.

Our product will address a good and satisfying life for older men that are prone to prostate cancer. By using an external coil, men will be more willing to get imaged. The level of comfort and ease of use with an external coil is also increased.

As engineers we also have a responsibility to create a safe and effective product. If our product fails and misdiagnoses a disease, patients could either miss vital treatment, or undergo painful treatment unnecessarily. In addition, patients you use our product must be ensured of the safety of our product. We cannot cause physical harm to patients who use the product, and thus before reaching the market our product must be made as safe as possible.

Our project greatly influences the health and personal safety of people. Specifically, it affects the health of older men that are prone to prostate cancer. By using an external Helmholtz coil design to image the prostate, men are more likely to be imaged compared to if an endorectal coil were to be used. This external coil provides a greater ease of use and comfort, and can also accommodate larger patients.

Safety is an important aspect to this project, as the coil must properly only receive the signal and not transmit. Within the MRI machine, it must switch rapidly from receiving and transmitting, and if this is not done properly, the patient can be harmed.

6.4 Manufacturability

The subject matter of our MQP could be easily reproduced. First, it is possible to recreate the DC and the RF simulations. For the DC MATLAB simulations, a clear guide and code has been provided for the magnetic field distribution plots. For the RF simulations, a guide has been provided in importing CAD models, use of a human torso as a load, and using a script to solve for the tuning and matching capacitor values.

As for the construction of the coil itself, a number of pictures and specifications accompany the building process. This includes the shaping of the coil, and the attachment of the tuning and matching capacitors.

The design of the coil casing is made from acrylic, and was designed with specific dimensions in CAD. Therefore, it can also be reproduced.

7 Final Design and Validation

This section will describe how the project was conducted through the specific aims. The reader will also be provided with information if the work is to be repeated. The experimental methods will be discussed, as well as the procedure for the data analysis.

7.1 Specific Aims

The specific aims of our project were met. As described previously, we needed to design a coil with high SNR. The coil needed to be large enough to fit most patients, but small enough to fit into the bore of an MR scanner. We selected a coil design first through DC simulations, and then performed an RF simulation to determine additional parameters as necessary to construct the coil, such as tuning and matching capacitor values.

Our coil was tested in various ways. First, to verify the tuning and matching, it was tested with the phantom filled to different solution levels and biological loads. From these tests we obtained the quality factor for each case. For the loaded case, the average quality factor is 7.1, while with the unloaded case the quality factor was 24.58. Though the quality factor is low in the loaded case, it is expected for a large coil. A magnetic dipole was then used to obtain measurements of the magnetic field distribution. A higher SNR and quality factor could be obtained by ideally decreasing the diameter of the coil.

The coil was designed to accommodate most patients, and to also fit properly into the bore of an MR scanner. As a larger population of men today are more overweight, it was of importance for our project to accommodate men of varying sizes. The radius of the coil is 0.1570 meters, with a height of 0.3425 meters.

7.2 Repetition of Work

The subject matter of our MQP can be easily reproduced. First, it is possible to recreate the DC and the RF simulations. For the DC MATLAB simulations, a clear guide and code has been provided for the magnetic field distribution plots. For the RF simulations, a guide has been provided in importing CAD models, use of a human torso as a load, and using a script to solve for the tuning and matching capacitor values.

As for the construction of the coil itself, a number of pictures and specifications accompany the building process. This includes the shaping of the coil, and the attachment of the tuning and matching capacitors. The design of the coil casing is made from acrylic, and was designed with specific dimensions in CAD. Therefore, it can also be reproduced.

7.3 Experimental Methods

Below is a general outline describing our methods, which can be divided into four main portions, simulation, design, construction, and testing and debugging.

Simulation

- MATLAB DC simulations
- ANSOFT HFSS RF simulation
- Simulate alternate coils

Coil

- Design coil's housing
- Build housing

Construction

- Build coils
- Attach coils
- Coax cable
- Solder capacitors on

Testing and Debugging

- Test coil
- S11, Smith for tuning and matching – with phantom
- S11, Smith for tuning and matching – with biological loads
- Magnetic Dipole Test

The first part of simulation was to perform DC and RF simulations. To perform DC simulations of the coil architecture, MATLAB was used. ANSOFT HFSS was used to do RF simulations. From here the values of the tuning and matching capacitors were obtained. Alternate coil designs were also simulated, which ranged in the radius of the coil, distance between the two loops, and the presence of a tilt to the top loop.

After a comparison between the simulations, a coil design was decided upon. Next the housing of the coil was designed in CAD and constructed. At the same time, work on the actual coils began. Copper tubing was cut and bent, and attached to the surface mount boards. Coaxial cable was used to connect between the coils, as well as to the network analyzer through an N connector. Surface mount capacitors and variable capacitors were soldered and connected the tubing within the breaks in the coil.

Lastly, the coil was tested and debugged extensively. First the variable tuning capacitors were adjusted to yield the best response. After many iterations of adjusting the capacitors, the coil was tested with the phantom and biological loads to verify the tuning and matching. The phantom was filled with different levels of solution and data and screenshots of the S11 parameter and the Smith chart were obtained. After,

the same data was gathered from eleven volunteers that acted as biological loads for the coil. Lastly, a magnetic dipole test was performed to verify the magnetic field distribution.

7.4 Data Analysis

As stated previously, extensive data was gathered from the phantom testing, biological load testing, and the magnetic field distribution simulations. For the phantom testing, data such as the operating frequency, -3dB points, and quality factor were obtained. We then created a plot of quality factor vs. volume of solution in the phantom.

For the biological load testing, a similar data analysis was performed. Once again, parameters such as the operating frequency, -3dB points, and quality factor were obtained. Statistical analyses were performed, and the mean and standard deviation of parameters such as the operating frequency and quality factor was obtained.

For the magnetic field distribution, data was gathered in the unloaded and loaded cases. For the unloaded case, data points were gathered in the horizontal direction from side to side, and front to back, and also in the vertical direction, each varying with distance. For the loaded case, over distance data was gathered in the two horizontal directions. Data was analyzed using Microsoft Excel, graphed, and compared to theoretical data.

8 Conclusions and Recommendations

The goal of this MQP was to create a viable MRI RF coil suitable for prostate imaging. Our data supports the fact that this design is a viable design and warrants further research. The data collected thus far allows us to form specific conclusions about our coil.

First, the coil can be tuned accurately to the Larmor frequency, having a resonance frequency over a population of varying loads within 0.994% of the Larmor frequency.

Second, the coil maintains its tuning for a variety of different loads. With testing on multiple subjects, the population had a standard deviation of the operating frequency of only 0.308%, demonstrating a low variability of the coil's operating frequency.

Third, the quality factor Q of this coil is low. While this is mostly due to the large size of the coil, it may also be due to the coil's matching at the frequency. In addition, it may be due to high resistance caused by some of the manufacturing practices. This should be investigated further.

Fourth, the FOV of this coil includes the range of the prostate. Because the magnetic field strength matches, or exceeds the simulated DC uniformity, we can conclude that the SNR of the coil is reasonable.

Based on these conclusions, the group recommends that further research be done into transforming this product into a marketable system. First, methods of increasing the quality factor of the device should be investigated. The next step towards creating a marketable product is testing in a clinical MRI system. This would require several additions to the coil. Safety systems, such as a PIN diode controlled RF chokes, DC current blocks, and fuses need to be implemented in order to keep patients safe. In addition, we would need to install a preamplifier to boost the received signal to levels expected by an MRI scanner. We would finally need to obtain the proprietary connector to interface our coil to a clinical MRI scanner.

After adjusting the coil to work in an MRI scanner, we suggest a clinical study be performed to determine the effectiveness of the coil at imaging prostate cancer and other diseases in the pelvic area. This will ensure that this receive only RF coil can be used as an effective medical tool.

References

- [1] National Cancer Insititute, "Prostate-Specific Antigen (PSA) Test," vol. 2009, 18 March 2009. 2009.
- [2] P. Wood BS, J. Kurhanewicz Ph.D., D. Vigneron Ph.D., M. Swanson Ph.D. and S. Li MD. The role of combined MRI & MRSI in treating prostate cancer. Presented at National Conference on PC.
- [3] N. M. deSouza, D. J. Gilderdale, R. Puni, G. A. Coutts and I. R. Young, "A solid reusable endorectal receiver coil for magnetic resonance imaging of the prostate: design, use, and comparison with an inflatable endorectal coil," *J. Magn. Reson. Imaging*, vol. 6, pp. 801-804, Sep-Oct. 1996.
- [4] Y. Kim, I. C. J. Hsu, J. Pouliot, S. M. Noworolski, D. B. Vigneron and J. Kurhanewicz. (2005, Expandable and rigid endorectal coils for prostate MRI: Impact on prostate distortion and rigid image registration. *Med. Phys.* 32pp. 3569.
- [5] J. J. Fütterer, M. R. Engelbrecht, G. J. Jager, R. P. Hartman, B. F. King, C. A. Hulsbergen-Van de Kaa, J. A. Witjes and J. O. Barentsz. (2007, Prostate cancer: Comparison of local staging accuracy of pelvic phased-array coil alone versus integrated endorectal–pelvic phased-array coils. *Eur. Radiol.* 17(4), pp. 1055-1065.
- [6] H. Hricak, S. White, D. Vigneron, J. Kurhanewicz, A. Kosco, D. Levin, J. Weiss, P. Narayan and P. R. Carroll. (1994, Carcinoma of the prostate gland: MR imaging with pelvic phased-array coils versus integrated endorectal–pelvic phased-array coils. *Radiology* 193(3), pp. 703-709.
- [7] M. D. Schnall, Y. Imai, J. Tomaszewski, H. M. Pollack, R. E. Lenkinski and H. Y. Kressel. (1991, Prostate cancer: Local staging with endorectal surface coil MR imaging. *Radiology* 178(3), pp. 797-802. Available: <http://radiology.rsna.org/content/178/3/797.full.pdf+html>
- [8] M. D. Schnall, R. E. Lenkinski, H. Y. Kressel, H. M. Pollack, T. C. Claiborne, G. J. Misic, T. R. Welch and E. J. Rhinehart, "Intracavity probe and interface device for MRI imaging and spectroscopy," United States 5348010, 1994, 1994.
- [9] H. Matsuoka, A. Nakamura, T. Masaki, M. Sugiyama, T. Takahara, J. Hachiya and Y. Atomi. (2003, Comparison between endorectal coil and pelvic phased-array coil magnetic resonance imaging in patients with anorectal tumor. *The American Journal of Surgery* 185(4), pp. 328-332.

- [10] P. J. Drew, R. Farouk, L. W. Turnbull, S. C. Ward, J. E. Hartley and J. R. T. Monson. (1999, Preoperative magnetic resonance staging of rectal cancer with an endorectal coil and dynamic gadolinium enhancement. *Br. J. Surg.* 86(2),
- [11] Radiology Info., "Prostate Ultrasound," vol. 2009, 20 June 2009. 2009.
- [12] Department of Family Medicine at Virginia Commonwealth University, "Should You Get a PSA Test," vol. 2009,
- [13] National Institute of Health, "What Are the Technological Advantages and Limitations (Disadvantages) of MRI?" *Health Services and Technology Assessment Text*, vol. 2009,
- [14] Diffen, "CT Scan vs. MRI," vol. 2009,
- [15] M. Fuchsjager, O. Akin, A. Shukla-Dave, D. Pucar and H. Hricak, "The role of MRI and MRSI in diagnosis, treatment selection, and post-treatment follow-up for prostate cancer," *Clin. Adv. Hematol. Oncol.*, vol. 7, pp. 193-202, Mar. 2009.
- [16] C. Bartolozzi, I. Menchi, R. Lencioni, S. Serni, A. Lapini, G. Barbanti, A. Bozza, A. Amorosi, A. Manganelli and M. Carini. (1996, Local staging of prostate carcinoma with endorectal coil MRI: Correlation with whole-mount radical prostatectomy specimens. *Eur. Radiol.* 6(3), pp. 339-345.
- [17] A. C. Yung, A. Y. Oner, J. M. Serfaty, M. Feloney, X. Yang and E. Atalar. (2001, Phased array coils for high resolution prostate MR imaging.
- [18] S. W. Heijmink, J. J. Futterer, T. Hambrock, S. Takahashi, T. W. J. Scheenen, H. J. Huisman, C. A. Hulsbergen-Van de Kaa, B. C. Knipscheer, L. A. L. M. Kiemeny and J. A. Witjes. (2007, Prostate cancer: Body-array versus endorectal coil MR imaging at 3 T--comparison of image quality, localization, and staging performance. *Radiology* 244(1), pp. 184.
- [19] T. R. McCauley, S. McCarthy and R. Lange, "Pelvic phased array coil: image quality assessment for spin-echo MR imaging," *Magn. Reson. Imaging*, vol. 10, pp. 513-522, 1992.
- [20] J. Sosna, I. Pedrosa, W. C. Dewolf, H. Mahallati, R. E. Lenkinski and N. M. Rofsky. (2004, MR imaging of the prostate at 3 tesla comparison of an external phased-array coil to imaging with an endorectal coil at 1.5 tesla. *Acad. Radiol.* 11(8), pp. 857-862.

- [21] I. Straus. (2002, Magnetic field calibration: Unwinding the helmholtz coil. [[Online]]. Available: <http://journals.iranscience.net:800/www.conformity.com/www.conformity.com/0205iz.pdf>
- [22] Magnetic Resonance - Technology Information Portal. (2009, 28 September 2009). Helmholtz pair coil. [[Online]]. 2009(28 September), Available: <http://www.mrtip.com/serv1.php?type=db1&db=Helmholtz%20Pair%20Coil>
- [23] T. Reiman, J. Heiken, W. Totty and J. Lee. (1988, Clinical MR imaging with a helmholtz-type surface coil. *Radiology* 169(2), pp. 564-566.
- [24] ETS-Lindgren, "Helmholtz Coil User Manual - Model 6400 Series," 2009.
- [25] S. Serfaty, L. Darrasse and S. Kan. (1995, Double-bracelet resonator helmholtz probe for NMR experiments. *Rev. Sci. Instrum.* 66pp. 5522.
- [26] V. M. Spitzer, D. G. Whitlock and National Library of Medicine. (1998, *Atlas of the Visible Human Male : Reverse Engineering of the Human Body*.
- [27] Magnetic Resonance - Technology Information Portal, "Tuning," vol. 2009, 28 September 2009. 2009.
- [28] Magnetic Resonance - Technology Information Portal. (2009, 28 September 2009). Matching. [[Online]]. 2009(28 September), Available: <http://www.mrtip.com/serv1.php?type=db1&db=matching>
- [29] Embry-Riddle Aeronautical University, "Helmholtz Coil," vol. 2009,
- [30] E. Dennison, "Off-Axis Field Due to a Current Loop," vol. 2009, 28 October 2000. 2000.
- [31] Vizimag. Calculator for on-axis or off-axis magnetic fields of air-cored solinoids using current loops. [[Online]]. 2009(2 November 2009), Available: <http://www.vizimag.com/calculator.htm>
- [32] B. E. Conway. (1952, *Electrochemical Data*.
- [33] S. Park, J. Nyenhuis, C. Smith, E. Lim, K. Foster, K. Baker, G. Hrdlicka, A. Rezai, P. Ruggieri and A. Sharan. (2003, Gelled versus nongelled phantom material for measurement of MRI-induced temperature increases with bioimplants. *IEEE Trans. Magn.* 39(5), pp. 3367-3371.

Glossary of Terms and Acronyms

BHP: Benign Prostatic Hyperplasia

Biot-Savart law: The law that defines the magnetic field created by a loop with a DC current flowing through it. Used to conduct our DC simulations.

DC simulation: Frequency independent simulations. In our case used to model magnetic field strength using simpler calculations for resistance than RF simulations.

Dipole loop: A small antenna in a loop shape, used to measure magnetic field perpendicular to the loop.

DRE: Digital Rectal Exam

Endorectal Coil: An MRI coil architecture designed for prostate imaging in which a collapsible planar coil is inserted into the patient's rectum and inflated with saline.

Ferromagnetic materials: Materials with a significant magnetic permeability, usually containing iron. These materials will be attracted to magnets.

FOV: Field of View

Helmholtz Coil: An MRI coil architecture in which two loops are placed parallel to each other and connected such that the current through each loop flows in the same direction.

IRB: Institutional Review Board

Larmor frequency: The rotational frequency of atoms subjected to a strong magnetic field. The Larmor frequency of hydrogen atoms in a 1.5T magnetic field is 63.65MHz.

Load: A mass that alters the magnetic field at a point in space. A load in close proximity to an antenna will change its RF behavior.

Magnetic field or B1 field. The field surrounding an electric current. In our case we will be using electric currents to measure the magnetic fields given off by the body as it is subjected to other magnetic fields.

Matching: The process of altering an antenna so that it performs in the desired manner when subjected to a load. In our case accomplished through a capacitor.

MR(I): Magnetic Resonance (Imaging)

Network analyzer: A device used to determine the properties of an antenna system over a range of frequencies. Used in our application to determine the S11 and S12 parameters.

Oncologist: A medical doctor specializing in the field of cancer treatment and detection.

Phantom: A load designed to simulate the electrical properties of the human body. Used to simulate a human during testing.

Phased array coil MRI systems: An MRI coil architecture in which multiple coils are placed on the patient's abdomen for the purpose of imaging a large area.

Planar coil: A flat piece of conducting material. Used for imaging in close proximity to the coil, for example in the endorectal coil.

PSA: Prostate-Specific Antigen

Receive coil: A coil used as part of an MRI system to detect the magnetic field generated by rotating atoms in the body.

RF simulation: Simulations for the purpose of creating high frequency circuits. Used in our application to model our coil system and determine the high frequency S-Parameters.

RF: Radio frequency

S11 parameter: A frequency dependant property of an antenna system that relates the amount of RF power inserted into a port with the power being reflected back. S11 magnitudes close to zero indicate an ideal transfer of power into a port.

S12 parameter: A frequency dependant property of an antenna system that relates the amount of power transferred from one port to another. Used in our application to determine the energy transferred from our coil to a dipole loop and used to determine the magnetic field in space.

SNR: Signal to Noise Ratio

TIM: Total Imaging Matrix

TRUS: Trans-Rectal Ultrasound

Tuning: The process of altering an antenna so that it will resonate at the proper frequency. In our case accomplished through the addition of capacitors, but in other applications often accomplished by altering the size or shape of the antenna.

Appendix A MATLAB DC Simulation of Helmholtz Coil

Simple 1-Dimensional On Axis Simulation	i
Simple 2-D Central Plane Simulation.....	iii
Simple 3-D Helmholtz Simulation	vii
Advanced 2D-Coil Simulation.....	xi
SNR Approximations.....	xv
Optimizing SNR.....	xviii

One essential part of our project was the DC simulation of our coil in MATLAB. The goal of this simulation was to be able to compare different coil designs to determine the coil that would have the highest SNR at the prostate. This was iterated through many times in increasing complexities to accurately model our project.

Simple 1-Dimensional On Axis Simulation

The simulation started by simulating the magnetic field strength in one dimension. We began using the simplest cast: where the two coils are parallel and share the same axis. The theoretical on-axis magnetic field strength is:

$$B_z = \frac{\mu_0 R^2 I}{2} \left(\frac{1}{\left(\left(z - \frac{h}{2} \right)^2 + R^2 \right)^{3/2}} + \frac{1}{\left(\left(z + \frac{h}{2} \right)^2 + R^2 \right)^{3/2}} \right)$$

With a theoretical maximum field strength of:

$$B_{zmax} = \mu_0 * I \left(\frac{4}{5} \right)^{\frac{3}{2}} \left(\frac{1}{R} \right)$$

This was used to create the code block shown below:

```

function [ Bz,Bzmax ] = helmholtz_onaxis( z,i,a,h )
%HELMHOLTZ_ONAXIS simulates the on axis field strength of a helmholtz coil
% [ Bz ] = helmholtz_onaxis( z,i,a,h )
% Bz-Magnetic field strength
% z=position on perpendicualar axis
% a=radius of helmholtz coil
% h=hight between coils

u0=4.*pi.*10.^-7;
Bz=u0.*a.^2.*i.^2./2.*(1./((z-h./2).^2+a.^2).^(3./2)+1./...
    ((z+h./2).^2+a.^2).^(3./2));
Bzmax=u0*i*(4/5)^(3/2)*(1/a);
end

```

We can use this function to create a normalized magnetic field strength by using a current of 1 A and a radius of 1 m. The position z is thus easily normalized into unitless measurement by dividing the position by 1 m. The magnetic field strength is normalized to the maximum field strength by dividing by the maximum field strength at 1 Ampere and 1 meter. This is shown below:

```

>> [Bz,B0]=helmholtz_onaxis(-2:0.08:2,1,1,1);
>> Bz=Bz./B0;
>> plot(-2:0.08:2,Bz);

```

This reveals the graph shown below:

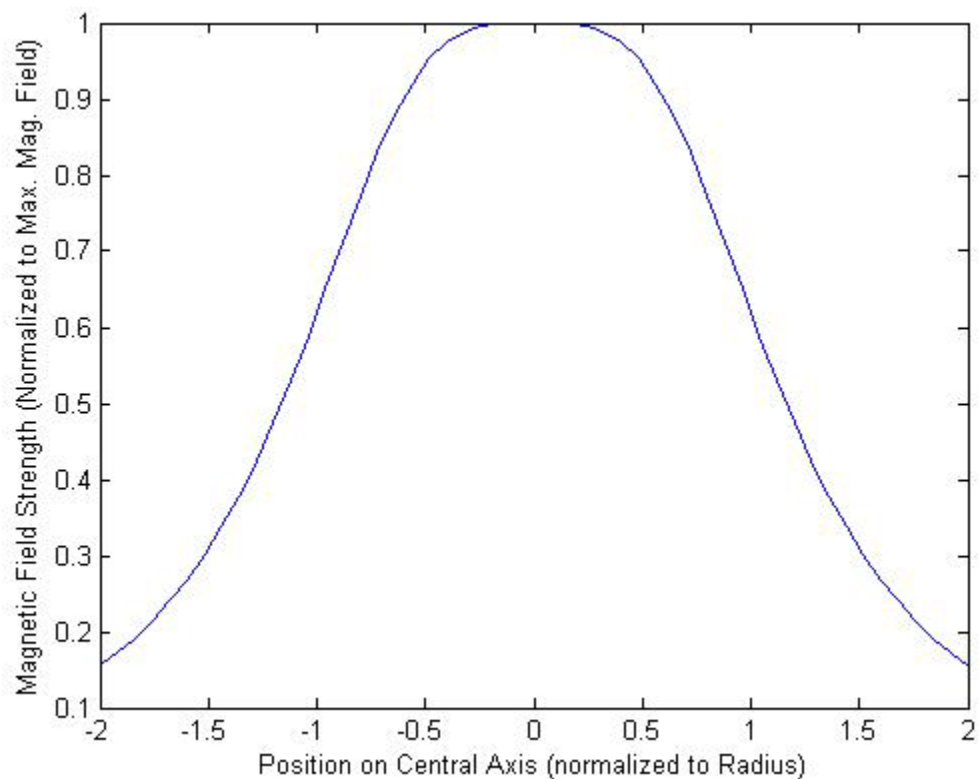


Figure A.1: Helmholtz Coil 1D Magnetic Field Distribution

Simple 2-D Central Plane Simulation

For our design, we needed to expand this code to allow for a 2-D case.

The off-axis magnetic field strength is more complex. In order to compute this, we begin with the off axis magnetic field strength of a single loop by the Biot-Savart Law in a plane that bisects the current loop. The magnetic field strength is determined by a position z in direction of the central axis of the loop, and a position r in the direction of radius of the loop. The radius of the loop is R .

This solution to the Biot-Savart Law cannot be determined exactly, but uses the elliptical integral approximation to determine the magnetic field strength. These equation find the magnetic field strength components perpendicular to the radius of the coil (B_z) and parallel to the radius of the coil (B_r). shown below[30, 31]:

$$B_z(r, z) = B_0 * \frac{1}{\pi * \sqrt{Q}} * \left(E(k) \frac{1 - \alpha^2 - \beta^2}{Q - 4\alpha} + K(k) \right) \quad (1)$$

$$B_r(r, z) = B_0 * \frac{\gamma}{\pi * \sqrt{Q}} * \left(E(k) \frac{1 + \alpha^2 + \beta^2}{Q - 4\alpha} - K(k) \right) \quad (2)$$

$$\alpha = \left| \frac{r}{R} \right| \quad \text{Where,} \quad \beta = \frac{z}{R} \quad \gamma = \frac{z}{r}$$

$$Q = |(1 + \alpha)^2 + \beta^2| \quad k = \sqrt{\frac{4\alpha}{Q}}$$

$E(k)$
= elliptical integral of the first kind

$K(k)$
= elliptical integral of the second kind

If we allow $B(r,z)=\{B_z(r,z),B_r(r,z)\}$, and the magnetic field caused by the top and bottom coil respectively is $B_{top}=B(r,z-h/2)$ and $B_{bottom}=B(r,z+h/2)$, we can find the magnetic field strength in a slice of our Helmholtz coil by simply adding the two.

```

function [ Bx,Br] = singleloop( r,x,i,a )
%SINGLELOOP models a single loop coil in 2D space
% [ Bx,Br] = singleloop( r,x,i,a )
% Bx=magnetic field in the direction along the axis of the coil
% (perpandicular to the radius)
% Br=magnetic field in the direction of the radius of the coil
% r=position parellel to the radius
% x=position perpandicular to the radius
% i=current in coil
% a=radius of coil
%
% The data for this code was taken from
% [1] Vizimag. Calculator for on-axis or off-axis magnetic fields of
% air-cored solinoids using current loops. [[Online]]. 2009(2 November
% 2009), Available: http://www.vizimag.com/calculator.htm
% [2] E. Dennison, "Off-Axis Field Due to a Current Loop," vol. 2009, 28
% October 2000. 2000.
%
% This code utilizes the elliptic12 function, downloaded from
% http://www.mathworks.com/matlabcentral/fileexchange/8805
%
% This code was written by Nathan Climer in October of 2009 as part of an
% MQP project for Worcester Polytechnic Institute
r=(abs(r)>1e-15).*r;

u0=4*pi*10.^(-7);
B0=i*u0./(2*a);
alpha=abs(r./a);
beta=x./a;
gamma=x./r;
Q=abs((1+alpha).^2+beta.^2);
k=sqrt(4.*alpha./Q);
[K,E]=elliptic12(pi./2,k.^2);
%the angle pi/2 is in accordance with the Quarter Period for elliptic
%functions, briefly mention in wikipedia
%Note: i don't really understand this, but the angle of pi/2 causes the
%output to coincide with the theoretic on-axis exact solution

Bx=B0./(pi.*sqrt(Q)).*(E.*((1-alpha.^2-beta.^2)./(Q-4.*alpha))+K);
if r~=0
Br=B0.*gamma./(pi.*sqrt(Q)).*(E.*((1+alpha.^2+beta.^2)/(Q-4.*alpha))-K);
else
Br=0;
end
end

```

```

function [ Bx,Br ] = helmholtz_2Dpoint( x,r,i,a,h )
%HELMHOLTZ_2DPOINT Finds the 2D magentic field in a helmholtz coil
% [ Bx,Br ] = helmholtz_2Dpoint( x,r,i,a,h )
% Bx=magnetic field in the direction along the axis of the coil
% (perpandicular to the radius)
% Br=magnetic field in the direction of the radius of the coil
% r=position parellel to the radius
% x=position perpandicular to the radius
% i=current in coil
% a=radius of coil
% h=height between two coils
%
% This code was written by Nathan Climer in October of 2009 as part of an
% MQP project for Worcester Polytechnic Institute

[Bx1,Br1]=singleloop(r,x-h/2,i,a);%find mag field due to upper loop
[Bx2,Br2]=singleloop(r,x+h/2,i,a);%find mag field due to lower loop
Bx=Bx1+Bx2;%add the x values
Br=Br1+Br2;%add the y values
end

```

The Helmholtz function can be used to create the image shown below:

```

>> [Bx,Br]=helmholtz(1,1,1,-2,2,0.08);
>> Bx=Bx./B0;
>> Br=Br./B0;
>> B=sqrt(Bx.^2+Br.^2);
>> contourf(-2:0.08:2,-2:0.08:2,Bx,-2.05:.1:2.05)
>> axis square
>> t= colorbar;
>> set(get(t,'ylabel'),'string','Magnetic Field Strength Normalized to
Origin');
>> xlabel('Position x');
>> ylabel('Position z');

```

The levels in the contour plots are selected to include a level of 0.95 to 1.05. This would be a difference of +/- 5% of the central value.

The figures below show both absolute field strength and the field strength in the +z direction. The +z direction is the most important as that this will be the direction in which the MRI signal will be oscillating.

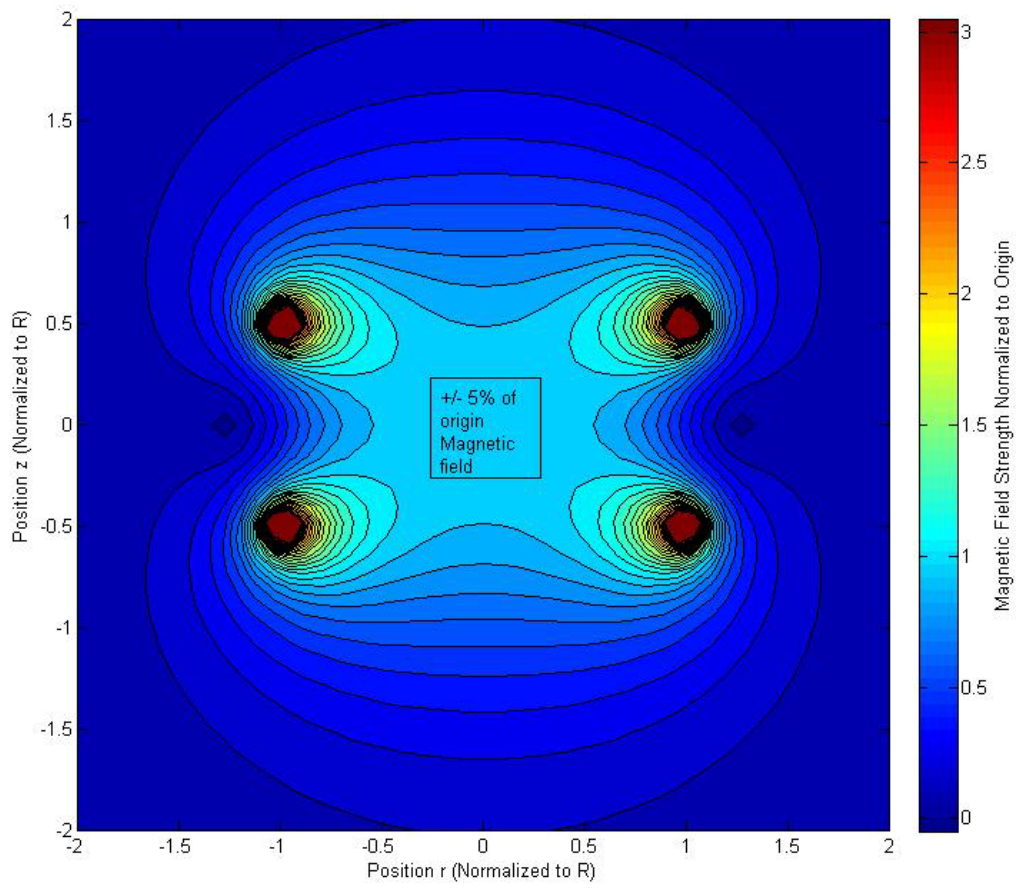


Figure A.2: Helmholtz Coil 3D Magnetic Field Distribution (Cross section along central axis)

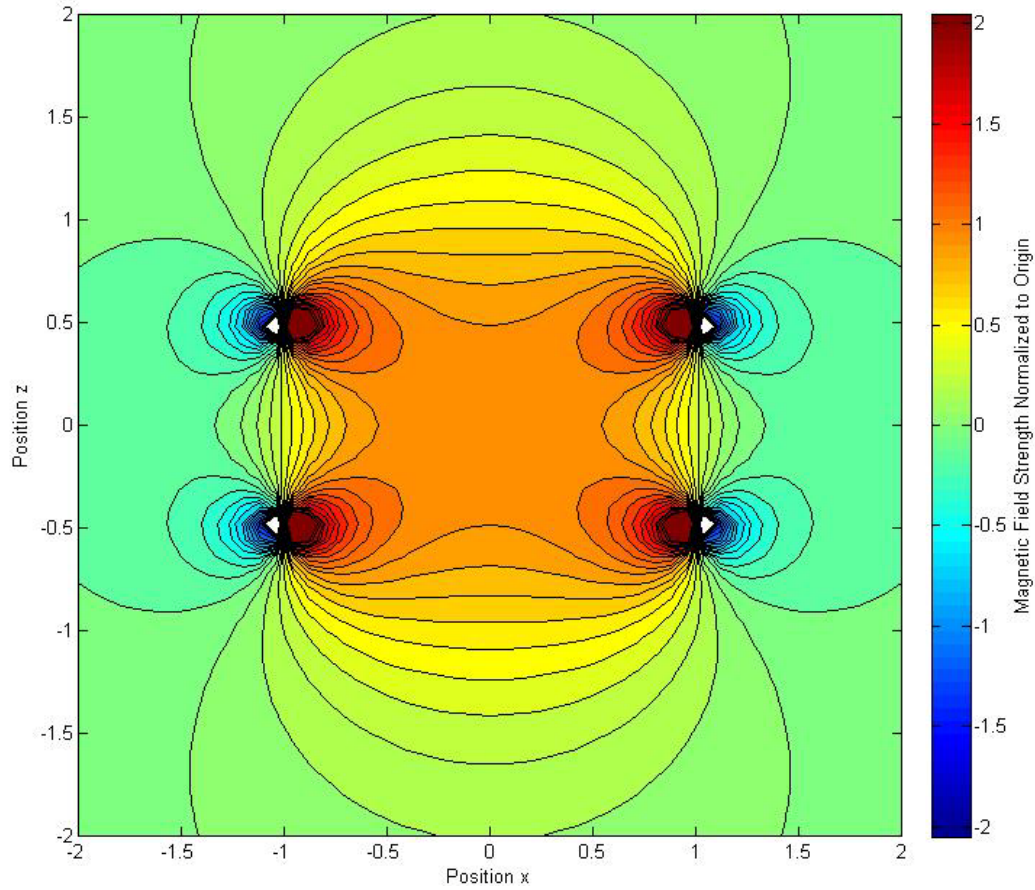


Figure A.3: Helmholtz Coil 3D Z Magnetic Field Distribution (Cross section along central axis)

Simple 3-D Helmholtz Simulation

This 2D solution can be projected around a cylinder to get the 3D representation of a Helmholtz coil's magnetic field strength. This code is shown below:

```

function [ Bx,By,Bz ] = helmholtz_3Dpoint( x,y,z,i,a,h )
%HELMHOLTZ_3DPOINT Finds the 3D magnetic field of a helmholtz coil
% [ Bx,By,Bz ] = helmholtz_3Dpoint( x,y,z,i,a,h )
% Bx=magnetic field in the x direction (along radius of coil)
% By=magnetic field in the y direction (along radius of coil,
%   perpendicular to x direction)
% Bz=magnetic field in the z direction (along axis of coil)
% x=position in x direction
% y=position in y direction
% z=position in z direction
% i=current in coil
% a=radius of coil
% h=height between two coils
%
% This code was written by Nathan Climer in October of 2009 as part of an
% MQP project for Worcester Polytechnic Institute

r=sqrt(x.^2+y.^2);%find the radius in cylindrical coordinates
theta=atan2(y,x);%find the theta in cylindrical coordinates
[Bz,br]=helmholtz_2Dpoint(z,r,i,a,h);%find the 2D data in cylindrical
coordinates
Bx=br.*cos(theta);%convert from cylindrical into cartesian
By=br.*sin(theta);
end

```

```

function [ rng, bx, by, bz, Bmag ] = helmholtz3D( i, a, h, max, step )
%HELMHOLTZ3D populates 3D cubic matrixes with 3D field data for a DC
helmholtz
%coil simulation
%
% [ rng, bx, by, bz, Bmag ] = helmholtz3D( i, a, h, max, step )
% rng=position range per index
% bx=magnetic field in the x direction (along radius of coil)
% by=magnetic field in the y direction (along radius of coil,
%     perpendicular to x direction)
% bz=magnetic field in the z direction (along axis of coil)
% Bmag=magnitude of magnetic field strength
% i=current in coil
% a=radius of coil
% h=hight between two coils
% max=max position to simulate
% step=step between positions
%
% This code was written by Nathan Climer in October of 2009 as part of an
% MQP project for Worcester Polytechnic Institute

rng=0:step:max;
Bx=zeros(length(rng),length(rng),length(rng));%Bx positive octant
By=zeros(length(rng),length(rng),length(rng));%By positive octant
Bz=zeros(length(rng),length(rng),length(rng));%Bz positive octant
A=1:length(rng);
%walk through matrix and populate each position
for(xx=A)
    for(yy=A)
        for(zz=A)

[Bx(xx,yy,zz),By(xx,yy,zz),Bz(xx,yy,zz)]=helmholtz_3Dpoint(rng(xx),rng(yy),
rng(zz),i,a,h);
            end
        end
    end
end
mid=length(rng);

bx=zeros(length(rng)*2-1,length(rng)*2-1,length(rng)*2-1);%full matrix
by=zeros(length(rng)*2-1,length(rng)*2-1,length(rng)*2-1);%full matrix
bz=zeros(length(rng)*2-1,length(rng)*2-1,length(rng)*2-1);%full matrix

bx(mid:end,mid:end,mid:end)=Bx;%fill in positive octant
bx(mid:-1:1,mid:end,mid:end)=-Bx;%mirrors and inverts values over xy plane
bx(:,mid:-1:1,mid:end)=bx(:,mid:end,mid:end);%mirrors and copies over yz
plane
bx(:, :, mid:-1:1)=bx(:, :, mid:end);%mirrors and copies over xz plane

by(mid:end,mid:end,mid:end)=By;%fill in positive octant
by(mid:end,mid:-1:1,mid:end)=-By;%mirros and inverts over yz plane
by(mid:-1:1, :, mid:end)=by(mid:end, :, mid:end);%mirrors and copies of xy plane
by(:, :, mid:-1:1)=by(:, :, mid:end);%mirrors and copies over xz plane

bz(mid:end,mid:end,mid:end)=Bz;%fills in positive octant
bz(mid:-1:1,mid:end,mid:end)=Bz;%mirros and copies over xy plane

```

```

bz(:,mid:-1:1,mid:end)=bz(:,mid:end,mid:end);%mirrors and copies over yz
plane
bz(:,:,mid:-1:1)=bz(:,:,mid:end);%mirrors and copies over xz plane

Bmag=sqrt(bx.^2+by.^2+bz.^2);%finds magnitude
end

```

This code can be used as shown below to display different slices in 2-D of the Z direction magnetic field:

```

>> [rng,Bx,By,Bz,Bmag]=helmholtz3D(1,1,1,2,0.08);
>> B0=(4/5)^(3/2)*(4*pi*10^-7)*1/1;
>> Bz=Bz./B0;
>> contourf(-2:0.08:2,-2:0.08:2,Bz(:,:,26));
>> axis square
>> t= colorbar;
>> set(get(t,'ylabel'),'string','Magnetic Field Strength Normalized to
Origin');
>> xlabel('Position x');
>> ylabel('Position z');

```

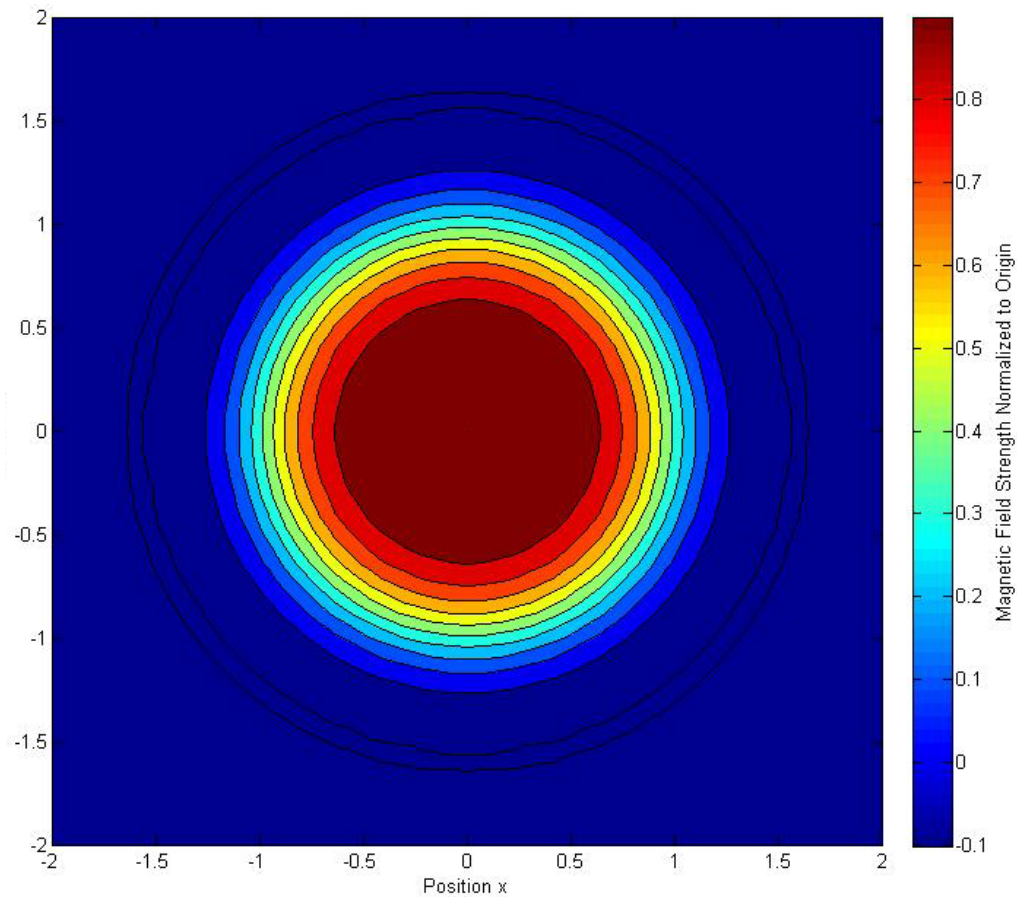


Figure A.4: Cross Section of 3D simple simulation

Advanced 2D-Coil Simulation

The simple case described above was determined to be insufficient for our project. We needed more flexibility in the coil to better target the human body, which does not fit simply in an individual Helmholtz design. Our design may better be able to fit the human body if we can control the horizontal offset ($B_{xoffset}$) and angle (Θ) of the coil. Because of the increased complexity, we will call this round of simulation the Advanced simulations.

The first step in creating an advanced 2D-coil simulation was to be able to control the angle and offset of the top coil. This was done through the use of coordinate system shifting, shown in the code below:

```

function [ Bx,Br] = singleloop_comp( offsetx,offsetr,rr,xx,i,a,angle )
%SINGLELOOP models a single loop coil in 2D space
% [ Bx,Br] = singleloop( r,x,i,a )
% Bx=magnetic field in the direction along the axis of the coil
% (perpendicular to the radius)
% Br=magnetic field in the direction of the radius of the coil
% rr=position parallel to the radius
% xx=position perpendicular to the radius
% i=current in coil
% a=radius of coil
% offsetx=offset of center point of top coil in the x direction
% offsetr=offset of centerpoint of the top of the coil in the r direction
% angle=tilted coil
%
%
% The data for this code was taken from
% [1] Vizimag. Calculator for on-axis or off-axis magnetic fields of
%     air-cored solenoids using current loops. [[Online]]. 2009(2 November
%     2009), Available: http://www.vizimag.com/calculator.htm
% [2] E. Dennison, "Off-Axis Field Due to a Current Loop," vol. 2009, 28
%     October 2000. 2000.
%
% This code utilizes the elliptic12 function, downloaded from
% http://www.mathworks.com/matlabcentral/fileexchange/8805
%
% This code was written by Nathan Climer in October of 2009 as part of an
% MQP project for Worcester Polytechnic Institute

%apply offset
r=rr-offsetr;
x=xx-offsetx;
%apply tilt
c=sqrt(r.^2+x.^2);
theta=atan2(x,r);
phi=theta-angle;
rprime=c.*cos(phi);
xprime=c.*sin(phi);
%find value
[bxp,brp]=singleloop(rprime, xprime, i, a);
%remove tilt
bp=sqrt(bxp.^2+brp.^2);
bang=atan2(bxp,brp);
Bx=bp.*sin(bang+angle);
Br=bp.*cos(bang+angle);
end

```

Using this function, we can make a more advanced solver for a single point in the range of the Helmholtz coil.

```

function [ Bx,Br ] = helmholtz_2Dpoint_comp( r,x,i,a,b,offsetbx,h,theta )
%HELMHOLTZ_2DPOINT_COMP Finds the 2D magentic field in a helmholtz coil
% [ Bx,Br ] = helmholtz_2Dpoint( x,r,i,a,h )
% Bx=magnetic field in the direction along the axis of the coil
% (perpandicular to the radius)
% Br=magnetic field in the direction of the radius of the coil
% r=position parellel to the radius
% x=position perpandicular to the radius
% i=current in coil
% a=radius of coil
% h=height between two coils
% offsetbx=offset of center point of top coil
% angle=tilted coil
%
% This code was written by Nathan Climer in October of 2009 as part of an
% MQP project for Worcester Polytechnic Institute

[Bx1,Br1]=singleloop_comp(h/2,offsetbx,r,x,i,b,theta);%find mag field due to
upper loop
[Bx2,Br2]=singleloop(r,x+h/2,i,a);%find mag field due to lower loop
Bx=Bx1+Bx2;%add the x values
Br=Br1+Br2;%add the y values
end

```

This function in turn can be used to populate a 2D matrix of values, as in the code below:

```

function [ Bx,Br ] = helmholtz_comp( i,a,b,offsetbx,h,theta,max,step )
%HELMHOLTZ_COMP Finds the 2D magentic field in a helmholtz coil
% [ Bx,Br ] = helmholtz_2Dpoint( x,r,i,a,h )
% Bx=magnetic field in the direction along the axis of the coil
% (perpandicular to the radius)
% Br=magnetic field in the direction of the radius of the coil
% i=current in coil
% a=radius of coil
% h=height between two coils
% offsetbx=offset of center point of top coil
% angle=tilted coil
% max=maximum position to simulate
% step=step in between each simulated position
%
% This code was written by Nathan Climer in November of 2009 as part of an
% MQP project for Worcester Polytechnic Institute
range=-max:step:max;
Bx=zeros(length(range));
Br=zeros(length(range));
A=1:length(range);
for(n=A)
    for(q=A)
        [Bx(n,q),Br(n,q)]=helmholtz_2Dpoint_comp(range(q),range(n),i,...
            a,b,offsetbx,h,theta);
    end
end
end

```

Finally, this function can be used to generate an image of the magnetic field strength of the coil, an example of which is shown below:

```
>> [Bx,Br]=helmholtz_comp(1,1,.75,.25,1,10*pi/180,2,0.08);  
>> B=sqrt(Bx.^2+Br.^2);  
>> B0=(4/5)^(3/2)*(4*pi*10^-7)*1/1;  
>> B=B./B0;  
>> contourf(B,-0.05:.1:3.05)  
>> contourf(-2:0.08:2,-2:0.08:2,B,-0.05:.1:3.05)
```

This generates the figure shown below:

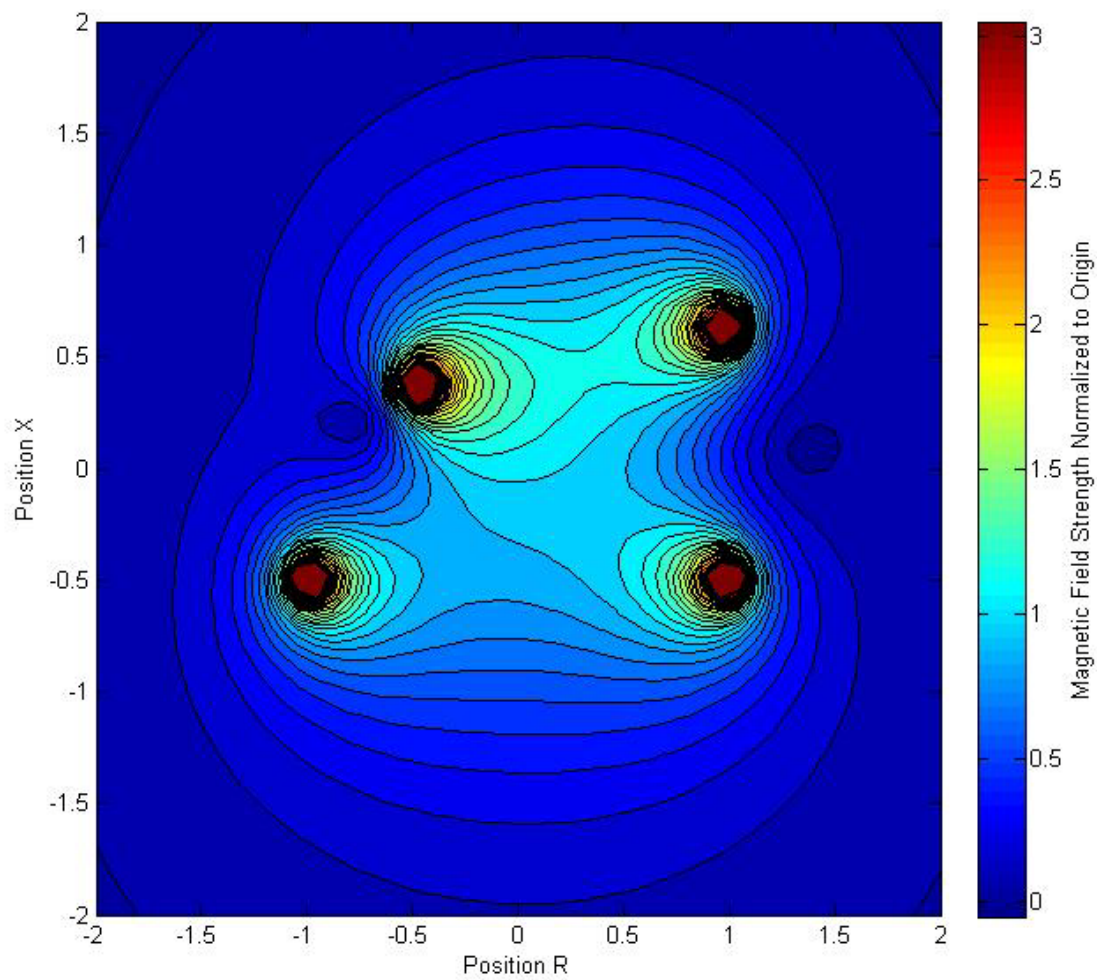


Figure A.5: Non-Ideal Helmholtz Coil Magnetic Field Strength

SNR Approximations

The relative SNR of each coil at each point due to the magnetic field of the coil, B_1 , and the resistance of the coil, R , can be found by the following equation:

$$SNR \propto B_1/\sqrt{R}$$

Resistance can be found by:

$$R = \frac{l\rho}{A}$$

Where l is the length of a conductor, ρ is the resistivity of the material, and A is the cross sectional area of our conductor. If we assume that all of our potential coils will be made with the same conductor, the term ρ/A will be constant. This means that:

$$SNR \propto \frac{B_1}{\sqrt{R}} = \frac{B_1}{\sqrt{\frac{l\rho}{A}}} = \frac{B_1}{\sqrt{l} \sqrt{\frac{\rho}{A}}}$$

$$SNR \propto \frac{B_1}{\sqrt{l}}$$

If we assume all other components of the SNR of the coils to be constant between coil designs, the value B_1/\sqrt{l} can be used to compare the design of each coil. B_1/\sqrt{l} is *not* the SNR of the coil, but is simply a useful way of comparing different coil design under similar conditions.

In the case of the Helmholtz coil, we will assume a zero-resistance connection between the two loops in the coil. The top coil will be called *coil B* and the bottom coil *coil A*. The coils *A* and *B* has radii a and b respectively. The length used in the relative SNR calculation is thus:

$$l = 2\pi i(a + b)$$

Knowing that our signal will be primarily oscillating in the X direction, we can use B_x as B_1 . Using this relationship, the SNR of a coil can be found using the function shown below:

```

function [ SNR ] = Helmholtz_SNR( i,a,b,offsetbx,h,theta,max,step )
%HELMHOLTZ_SNR populates a matrix with the relative SNR values for a coil
% [ SNR ] = Helmholtz_SNR( i,a,b,offsetbx,h,theta,max,step)
% i=current in coil
% a=radius of coil
% h=height between two coils
% offsetbx=offset of center point of top coil
% theta=tilted coil
% max=maximum position to simulate
% step=step in between each simulated position
%
% This code was written by Nathan Climer in November of 2009 as part of an
% MQP project for Worcester Polytechnic Institute
[Bx,Br]=helmholtz_comp( i,a,b,offsetbx,h,theta,max,step );
SNR=Bx./sqrt((2*pi*(a+b)));

end

```

This can be used to plot the relative SNR of different coils. An example of this is shown below:

```

>> snr=helmholtz_SNR(1,.1570,.1570,0,.3175,10*pi/180,.5,.005);
>> contourf(-.5:0.005:.5,-.5:0.005:.5,snr,-2e-5:0.1e-5:2e-5)

```

This generates the figure below:

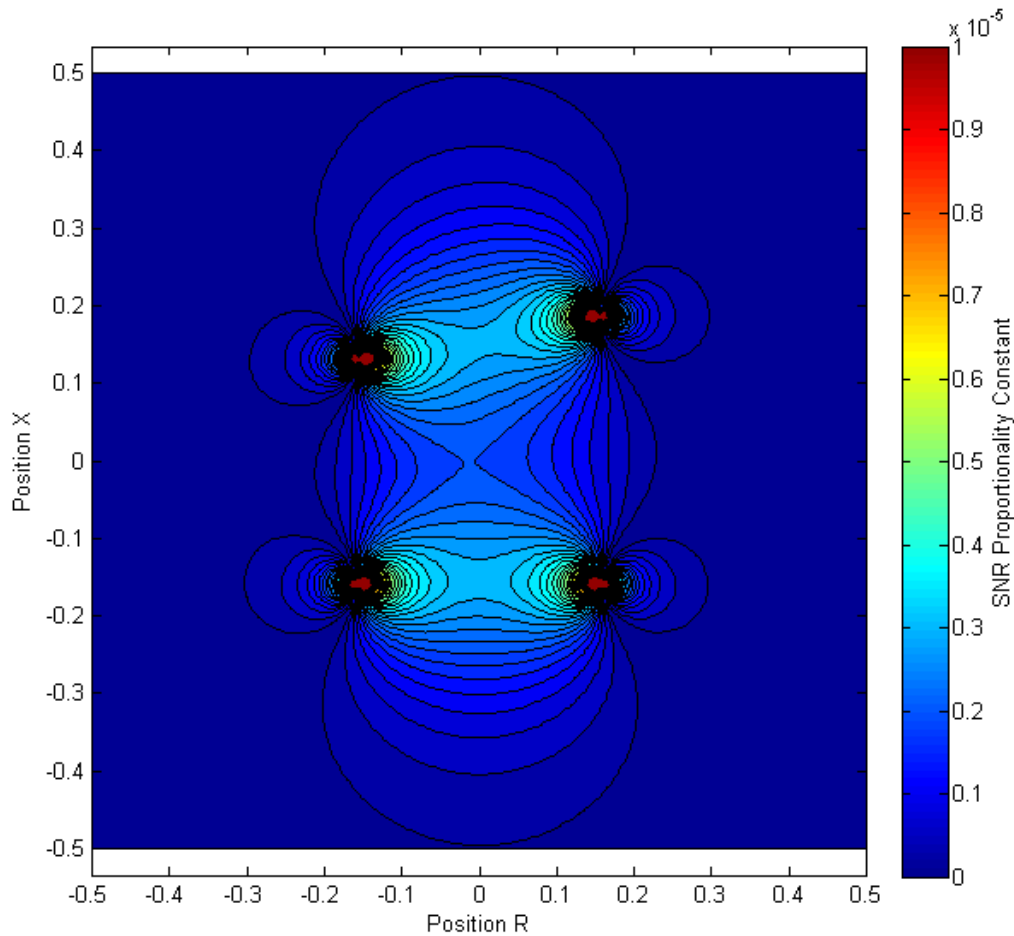


Figure A.6: SNR Example

The code below shows how the -3 dB cutoff for the coil, compared to the center magnetic field strength, can be displayed:

```
>> snr=helmholtz_SNR(1,.1570,.1570,0,.3175,10*pi/180,.5,.005);  
>> snrdcb=20*log(snr./(snr(100,100)))./log(10);  
>> rng=-.5:.005:.5;  
>> pcolor(rng,rng,snrdcb)  
>> shading interp  
>> axis equal  
>> hold on  
>> contour(rng,rng,snrdcb,-110:109:-1,'EdgeColor','black','LineStyle','--')  
>> contour(rng,rng,snrdcb,-110:107:-3,'EdgeColor','black','LineWidth',2)  
>> t=colorbar;  
>> set(get(t,'ylabel'),'string','SNR (B1/sqrt(I)) (dB compared to origin)');  
>> xlabel('Position R');  
>> ylabel('Position X');
```

This generates the figure below:

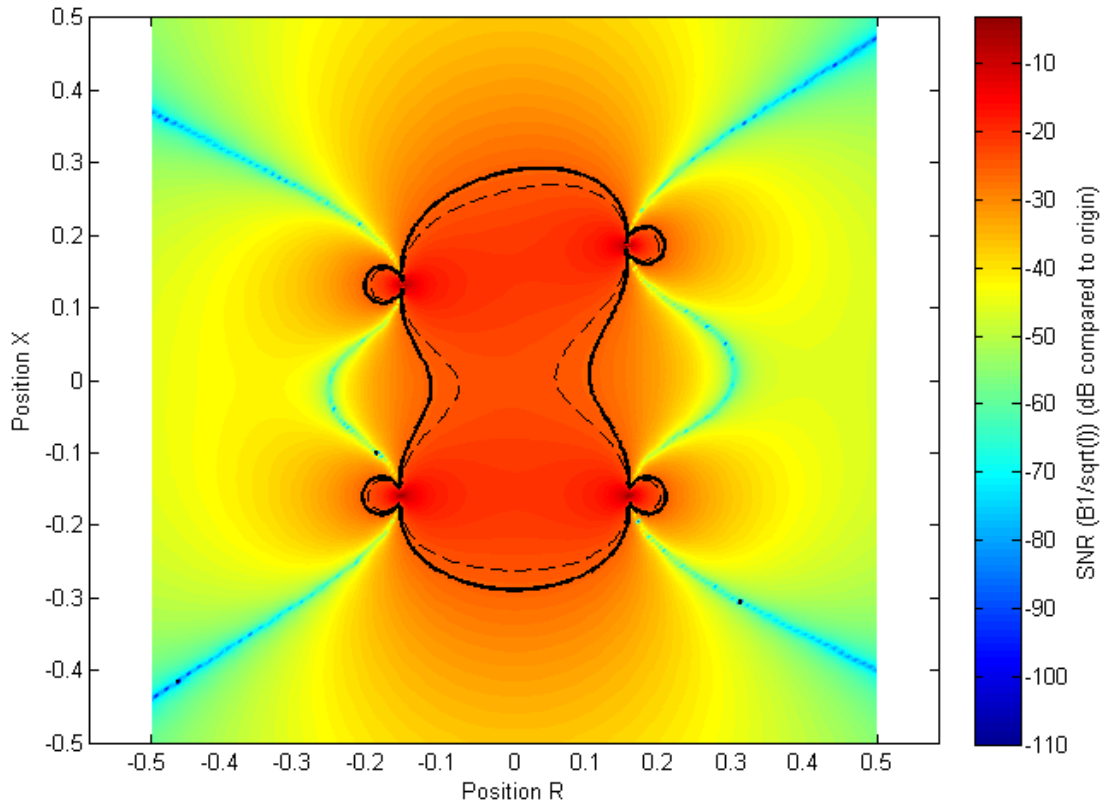


Figure A.6: SNR Drop-off Example

Optimizing SNR

As shown above, the SNR is heavily dependent on both a and b . However, the relationship between the SNR and a and b is non-linear, and difficult to predict. It can thus be hard to find the correct radii to optimize SNR. In addition, the radii are limited only by the SNR and the size of the magnetic bore. Based on this, the other parameters (such as height and angle) are dependent mainly on the dimensions of the human body. Using these data points as inputs, the following code finds the best possible radii for a and b to make the highest SNR.

```

function [ r,snr ] = findbesthelmholtzr( ang,h,testz )
%FINDBESTHELMHOLTZR finds the radius of a and b such that the SNR is
maximized
% [r, snr] = findbesthelmholtzr( ang,h,testz )
% r=radius
% snr = snr at test point
% ang = angle of top coil
% h = height between coils
% testz = test position
%
% This code was written by Nathan Climer in November of 2009 as part of an
% MQP project for Worcester Polytechnic Institute

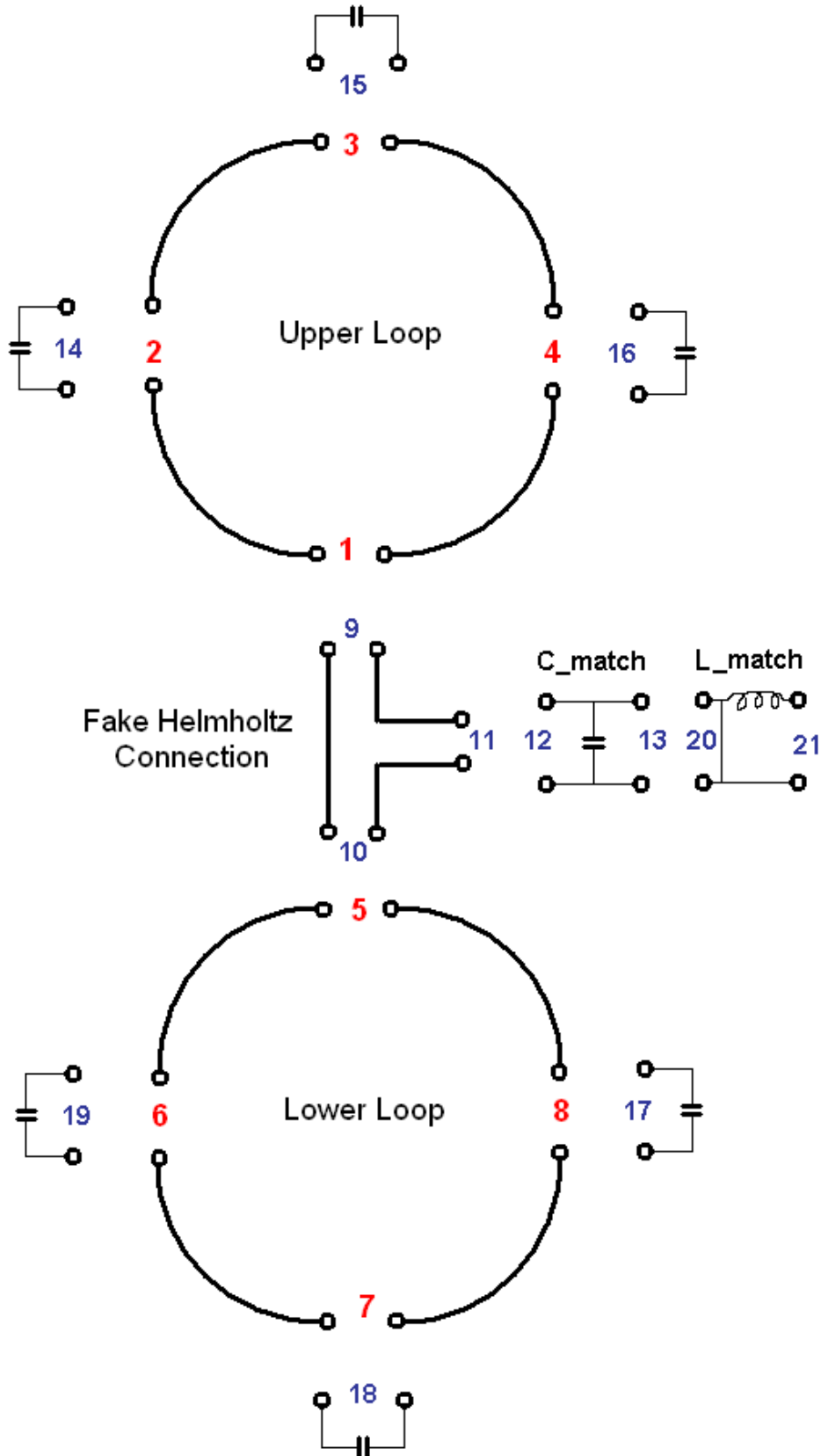
range=0.001:0.001:1;
S=zeros(1000);
for (n=1:1000)
    %select center point such that lowest point is at h
    hh=h+range(n)*sin(ang*pi/180);
    %find magnetic field
    [Bx,Br]=helmholtz_2Dpoint_comp(0,testz-hh/2,1,range(n),range(n),0,hh,...
        ang*pi/180);
    %find SNR
    S(n)=Bx./sqrt(4*pi*range(n));
end
%find radius that gives the max SNR
r=range(find(S==(max(S))));
%find the max SNR
snr=max(S);

end

```

It was determined through experimentation that changing the focus by growing or shrinking coil B with respect to A has a more drastic effect in reducing FOV than raising the SNR at the point of interest.

Appendix B Port numbers used in HFSS and AnalyzerS



Appendix C AnalyzerS MATLAB script

AnalyzerS contains several parameters that must be defined. Several of these are basic, such as the target impedance and the desired frequency. The tuning and matching circuits must also be defined. This is accomplished by assigning port numbers (Appendix B) to each circuit component and defining the impedance of that port in the lumped elements definition file (Appendix C). Ports 1 through 8 do not need to be defined in this file because this information is determined from the S-parameters. AnalyzerS contains three vectors that describe which ports are connected to each other. The Port_first vector contains the port number of the first input to each connection. The Port_second vector contains the port number of the second input to each connection. The Port_free vector identifies the port that will be used for the external connection to the MR system. This is the port that will become port 1 in our completed coil, and is the port that should have an impedance of 50Ω . For our simulation these vectors are defined as:

```
% interconnections
Port_first =[ 1  2  3  4  5  6  7  8 11 13];
Port_second=[ 9 14 15 16 10 19 18 17 12 20];
Port_free=[21];
```

This defines that ports 1 and 9 are connected, port 2 and 14 are connected, etc.

```

clc; clear all; close all;
%*****
f=127.3e6/2;
Z0=50;
BW=.2*f;
f1=f-0.5*BW;
f2=f+0.5*BW;
omega=2*pi*f;

N_Network=8;

% interconnections
Port_first =[ 1 2 3 4 5 6 7 8 11 13];
Port_second=[ 9 14 15 16 10 19 18 17 12 20];

Port_free=[21];

N_Inter=length(Port_first);
Ports_free=length(Port_free);
N=max([max(Port_first), max(Port_second), max(Port_free)]);

Channell=1;
Channel2=0;

%%%%%%%%%%%% introduce lumped elements
R_cap = 0.05;

% 1.5T design 3 with series L
C_tune = 20e-12;
C_match = 35e-12;

% 3T design 4 with series L
%C_tune = 6e-12;
%C_match = 32e-12; % 30-35 works ok

Sweep=101;

%Load S Parameters from HFSS
design_3;
%design_4;

S1 = S;
save coil_info;

%S matrix
S=zeros(N,N);

U=diag(ones(N_Network,1));
Y=1/50*(U-S1)*inv(U+S1);
for m=1:N_Network

```

```

    for n=1:N_Network
        R(m,n)=real(1/Y(m,n));
        L(m,n)=imag(1/Y(m,n))/omega;
    end
end

for sweep=1:Sweep
    disp(strcat(num2str(sweep), ' / ', num2str(Sweep)));
    if(Sweep~=1)
        freq(sweep)=f1+(f2-f1)*(sweep-1)/(Sweep-1);
        freq_scaled(sweep)=(freq(sweep)-f)/(0.5*BW);
    end
    if(Sweep==1)
        freq(sweep)=f;
    end
    omega=2*pi*freq(sweep);
    % reconstruct S1 matrix
    for m=1:N_Network
        for n=1:N_Network
            Y(m,n)=1/(R(m,n)+j*omega*L(m,n));
        end
    end
    S1star=inv(U+Y*Z0)*(U-Y*Z0);

    S=zeros(N,N);
    S(1:N_Network,1:N_Network)=S1star;

counter=N_Network;

analyzerS_lumped_elements;

if(((Sweep+1)/2==round((Sweep+1)/2))&&(sweep==(Sweep+1)/2))
    S_center_notmod=S;
end

for k=1:N_Inter

    k1=Port_first(k);
    k2=Port_second(k);
    S(k1,k2) = S(k1,k2)-1;
    S(k2,k1) = S(k2,k1)-1;

    % DO SECOND ROW
    % figure out which number is bigger
    if(abs(S(k2,k1))>abs(S(k2,k2)))
        Bigger=k1;
        Smaller=k2;
    end
end

```

```

else
    Bigger=k2;
    Smaller=k1;
end

% remove Bigger column
S(k2,:)=S(k2,:)*(-1.0/S(k2,Bigger));
row=S(k2,:);
S=S+S(:,Bigger)*row;
S(k2,:)=row;

% DO FIRST ROW
% remove Smaller column
S(k1,:)=S(k1,:)*(-1.0/S(k1,Smaller));
row=S(k1,:);

S=S+S(:,Smaller)*row;
S(k1,:)=row;

end

if(((Sweep+1)/2==round((Sweep+1)/2))&&(sweep==(Sweep+1)/2))
    S_center=S;
end

% find new S-matrix
S_new=zeros(Ports_free,Ports_free);
S_new(:,:)=S(Port_free(:),Port_free(:));

if(((Sweep+1)/2==round((Sweep+1)/2))&&(sweep==(Sweep+1)/2))
    S_new_center=S_new;
    S_new_center_dB=20*log10(abs(S_new));
end

% define channels to look at
Sfirst(sweep)      =S_new(Channel1,Channel1);
if(Channel2~=0)
    Ssecond(sweep)      =S_new(Channel2,Channel2);
    Ssecondfirst(sweep)=S_new(Channel2,Channel1);
end

SfirstdB(sweep)    =20*log10(abs(Sfirst(sweep)));
if(Channel2~=0)
    SseconddB(sweep)    =20*log10(abs(Ssecond(sweep)));
    SsecondfirstdB(sweep)=20*log10(abs(Ssecondfirst(sweep)));
end

end %sweep

%Plot

```

```

figure(1)
subplot(2,1,1)
smith(2)
hold on
realSfirst=real(Sfirst);
imagSfirst=imag(Sfirst);
scatter(realSfirst,imagSfirst,20,'r');
scatter(realSfirst((Sweep+1)/2),imagSfirst((Sweep+1)/2),'r','filled');
hold off

title(strcat('S',num2str(Channel1),num2str(Channel1)));
subplot(2,1,2);
plot(freq/1e6,SfirstdB); grid on; xlabel('f, MHz');
ylabel(strcat('S',num2str(Channel1),num2str(Channel1),' dB'));
hold on
plot_lines(f/1e6,[],'r:');
title(strcat('S',num2str(Channel1),num2str(Channel1),'=',num2str(SfirstdB((Sweep+1)/2))));
hold off

if(Channel2~=0)
figure(2)
subplot(2,1,1)
smith(2)
hold on
realSsecond=real(Ssecond);
imagSsecond=imag(Ssecond);
scatter(realSsecond,imagSsecond,20,'r');
scatter(realSsecond((Sweep+1)/2),imagSsecond((Sweep+1)/2),'r','filled');
hold off

title(strcat('S',num2str(Channel2),num2str(Channel2)));
subplot(2,1,2);
plot(freq/1e6,SseconddB); grid on; xlabel('f, MHz');
ylabel(strcat('S',num2str(Channel2),num2str(Channel2),' dB'));
hold on
plot_lines(f/1e6,[],'r:');
title(strcat('S',num2str(Channel2),num2str(Channel2),'=',num2str(SseconddB((Sweep+1)/2))));
hold off

figure(3)
subplot(2,1,1)
smith(2)
hold on
realSsecondfirst=real(Ssecondfirst);
imagSsecondfirst=imag(Ssecondfirst);
scatter(realSsecondfirst,imagSsecondfirst,20,'r');
scatter(realSsecondfirst((Sweep+1)/2),imagSsecondfirst((Sweep+1)/2),'r','filled');
hold off

title(strcat('S',num2str(Channel2),num2str(Channel1)));

```

```

subplot(2,1,2); plot(freq/1e6,SsecondfirstdB); grid on; xlabel('f, MHz');
ylabel(strcat('S',num2str(Channel2),num2str(Channel1),' , dB'));
hold on
plot_lines(f/1e6,[],'r:');
title(strcat('S',num2str(Channel2),num2str(Channel1),'=',num2str(Ssecondfirst
dB((Sweep+1)/2))));
hold off
end

% find minimum of first resonance
SfirstdB_min=0;
freqfirst_min=0;
for sweep=1:Sweep
    if(SfirstdB(sweep)<SfirstdB_min)
        sweepfirst_min=sweep;
        SfirstdB_min=SfirstdB(sweep);
        freqfirst_min=freq(sweep);
    end
end
disp('suggestion: multiply tuning cap by:');
freqfirst_min^2/f^2

if(Channel2~=0)
% find minimum of second resonance
SseconddB_min=0;
freqsecond_min=0;
for sweep=1:Sweep
    if(SseconddB(sweep)<SseconddB_min)
        sweepsecond_min=sweep;
        SseconddB_min=SseconddB(sweep);
        freqsecond_min=freq(sweep);
    end
end
disp('suggestion: multiply tuning cap by:');
freqsecond_min^2/f^2
end

% calculate new solution vectors
B=zeros(N,1);
Power_Scaling = zeros(N_Network,2*Ports_free);
Holder = zeros(N_Network,Ports_free);

for m=1:Ports_free
    B=zeros(N,1);
    B(Port_free(m))=sqrt(2);
    for n=1:Ports_free
        S_center(Port_free(n),:)=0;
        S_center(Port_free(n),Port_free(n))=1;
    end
    v=inv(S_center)*B;

    b=S_center_notmod*v;

```

```

V_port=sqrt(Z0)*(v+b);
I_port=1/sqrt(Z0)*(v-b);
for ss=1:N
    P_port(ss)=0.5*real(V_port(ss)*conj(I_port(ss)));
end

FileName=strcat('V_port',num2str(m),'.dat');
FID=fopen(FileName,'w');
for mm=1:N
    fprintf(FID, ' %5.0f',mm);
    fprintf(FID, ' %g',real(V_port(mm)));
    fprintf(FID, ' %g',imag(V_port(mm)));
    fprintf(FID, ' %g\n',abs(V_port(mm)));
end
fprintf(FID, 'Port voltages, real, imaginary parts and absolute value');
fclose(FID);
FileName=strcat('I_port',num2str(m),'.dat');
FID=fopen(FileName,'w');
for mm=1:N
    fprintf(FID, ' %5.0f',mm);
    fprintf(FID, ' %g',real(I_port(mm)));
    fprintf(FID, ' %g',imag(I_port(mm)));
    fprintf(FID, ' %g\n',abs(I_port(mm)));
end
fprintf(FID, 'Port currents, real, imaginary parts and absolute value');
fclose(FID);
FileName=strcat('P_port',num2str(m),'.dat');
FID=fopen(FileName,'w');
for mm=1:N
    fprintf(FID, ' %5.0f',mm);
    fprintf(FID, ' %g\n',P_port(mm));
end
fprintf(FID, 'Port powers, real and imaginary parts');
fclose(FID);

for n=1:N
    vv(n)=v(n)^2/2;
end
Power_Scaling(:,2*m-1) = abs(vv(1:N_Network));
Power_Scaling(:,2*m) = angle(v(1:N_Network))*180/pi;
Holder(:,m) = v(1:N_Network);

end

Power_Scaling

writepowerscaling(Power_Scaling, Channel1, 'design_3')

```

Appendix D MATLAB Lumped Elements Definition

```

% Helmholtz Connection
counter=counter+1;
S(counter,counter)=(1/3);
S(counter,counter+1)=(-1)*(2/3);
S(counter,counter+2)=(-1)*(-2/3);
S(counter+1,counter)=(2/3);
S(counter+1,counter+1)=(1/3);
S(counter+1,counter+2)=(2/3);
S(counter+2,counter)=(-2/3);
S(counter+2,counter+1)=(2/3);
S(counter+2,counter+2)=(1/3);
counter=counter+2;
%Define Cap and Output as Port 12/13
counter=counter+1;
Z=R_cap+1/(j*omega*C_match);
S(counter,counter)=-Z0/(2*Z+Z0);
S(counter,counter+1)=2*Z/(2*Z+Z0);
S(counter+1,counter)=2*Z/(2*Z+Z0);
S(counter+1,counter+1)=-Z0/(2*Z+Z0);
counter=counter+1;
%Define Capacitor as Port 14
counter=counter+1;
Z=R_cap+1/(j*omega*C_tune);
S(counter,counter)=(Z-Z0)/(Z+Z0);
%Define Capacitor as Port 15
counter=counter+1;
Z=R_cap+1/(j*omega*C_tune);
S(counter,counter)=(Z-Z0)/(Z+Z0);
%Define Capacitor as Port 16
counter=counter+1;
Z=R_cap+1/(j*omega*C_tune);
S(counter,counter)=(Z-Z0)/(Z+Z0);
%Define Capacitor as Port 17
counter=counter+1;
Z=R_cap+1/(j*omega*C_tune);
S(counter,counter)=(Z-Z0)/(Z+Z0);
%Define Capacitor as Port 18
counter=counter+1;
Z=R_cap+1/(j*omega*C_tune);
S(counter,counter)=(Z-Z0)/(Z+Z0);
%Define Capacitor as Port 19
counter=counter+1;
Z=R_cap+1/(j*omega*C_tune);
S(counter,counter)=(Z-Z0)/(Z+Z0);
%Define L as port 20/21
counter=counter+1;
Z=R_cap+j*omega/(omega*omega*C_match);
S(counter,counter)=Z/(Z+2*Z0);
S(counter,counter+1)=2*Z0/(Z+2*Z0);
S(counter+1,counter)=2*Z0/(Z+2*Z0);
S(counter+1,counter+1)=Z/(Z+2*Z0);
counter=counter+1;

```

Appendix E Raw Data for Phantom Load Testing

This section contains the raw data used in testing the S11 parameter for the MRI phantom load. The results are summarized below in Table E-1.

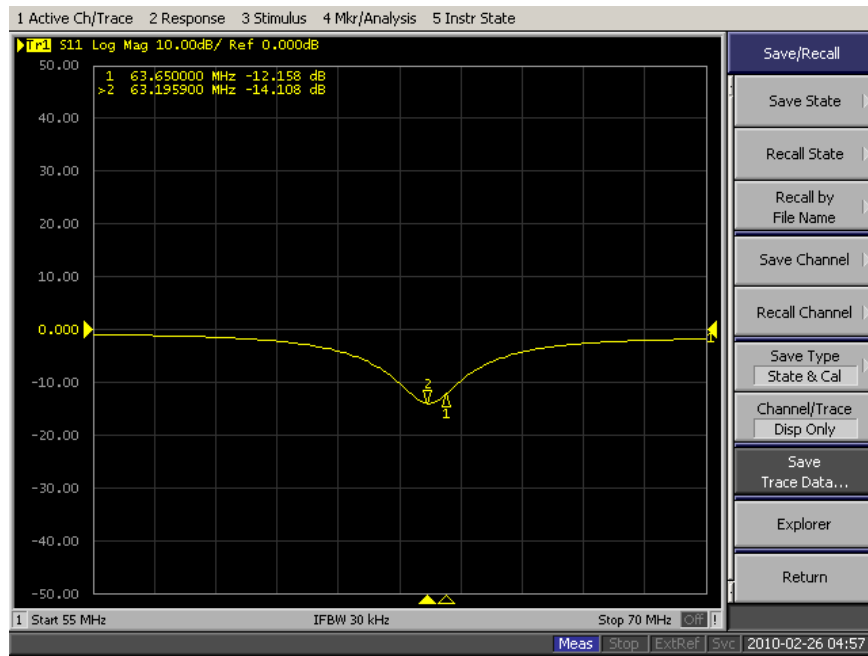
Table E-1: Summary of Variable Volume Phantom Load Testing

Volume (L)	Operating Frequency	Shift from 63.65 MHz	Lower Cutoff (MHz)	Upper Cutoff (MHz)	Bandwidth (MHz)	Q	Lowest point (dB)
19	63.3175	0.5224%	60.325	66.550	6.225	10.17	-14.10125
18	62.7250	1.4533%	60.175	65.575	5.400	11.62	-11.65601
17	62.7250	1.4533%	60.325	65.500	5.175	12.12	-10.61212
16	63.7750	0.1964%	59.875	68.050	8.175	7.801	-23.56484
15	63.7000	0.0786%	60.175	67.450	7.275	8.756	-16.30785
14	64.0750	0.6677%	60.700	67.675	6.975	9.186	-16.41481
13	63.7750	0.1964%	60.800	66.850	6.050	10.54	-12.54609
12	64.0000	0.5499%	60.850	67.225	6.375	10.04	-14.24805
11	63.8500	0.3142%	61.000	66.850	5.850	10.91	-12.23180
10	63.9250	0.4321%	61.075	66.850	5.775	11.07	-11.74341
9	63.9250	0.4321%	61.225	66.775	5.550	11.52	-11.14311
8	63.9250	0.4321%	61.375	66.625	5.250	12.18	-9.81950
7	64.0000	0.5499%	61.525	66.775	5.250	12.19	-9.66155
6	64.3000	1.0212%	61.525	67.075	5.550	11.59	-10.44105
5	64.3000	1.0212%	61.600	66.925	5.325	12.08	-10.04381
0	63.9000	0.3928%	62.700	65.300	2.600	24.58	-4.69000

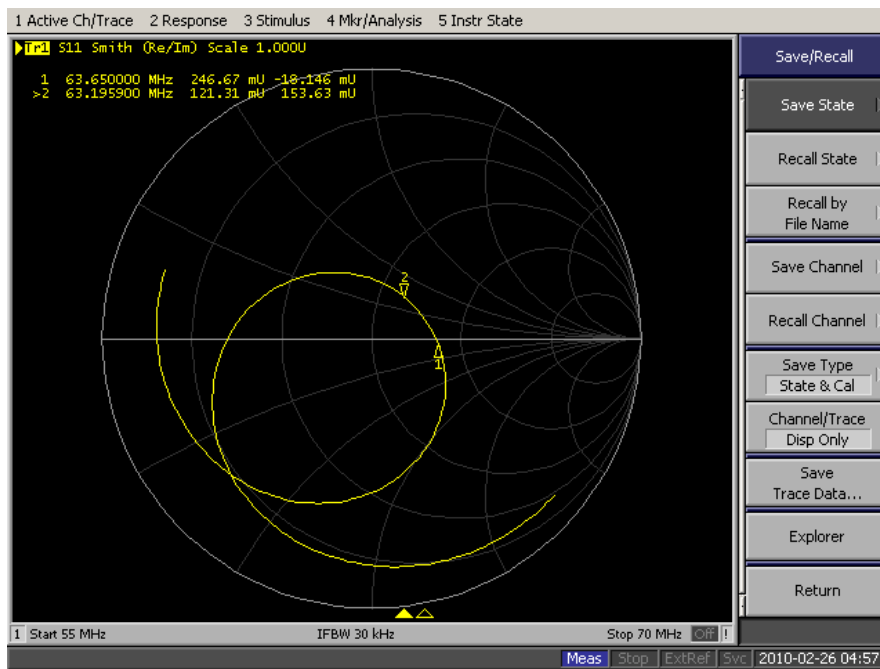
For each volume, the -3 dB cutoff was used to find the bandwidth of the coil. The lowest point in the dip was used to find the resonance frequency of each coil. The quality factor Q for each coil was found from

$$Q = \frac{\text{Resonance Frequency}}{\text{Bandwidth}}$$

Loaded 19 Liters

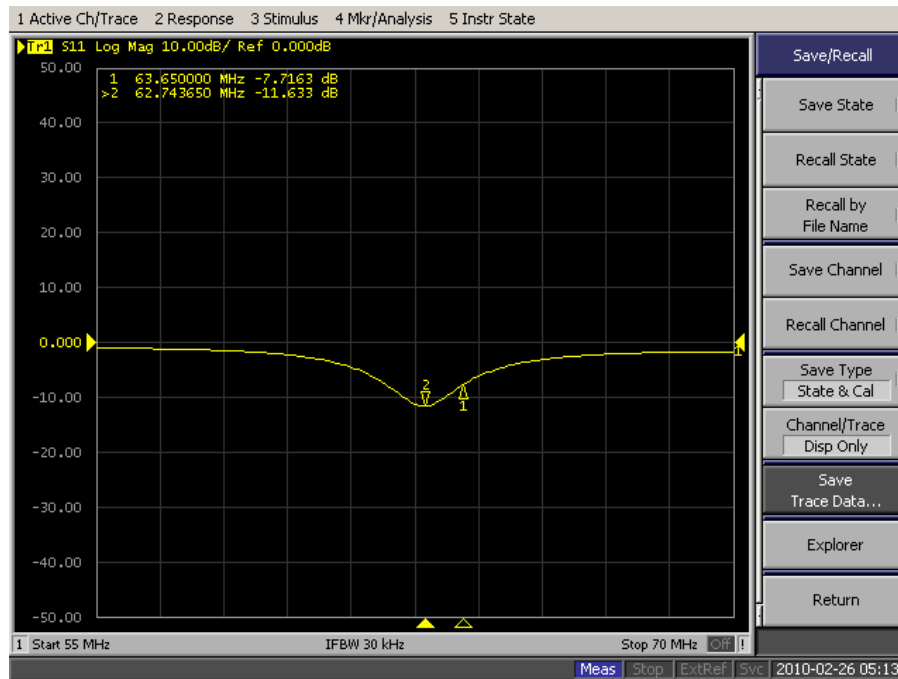


Loaded 19 Liters S11 Plot

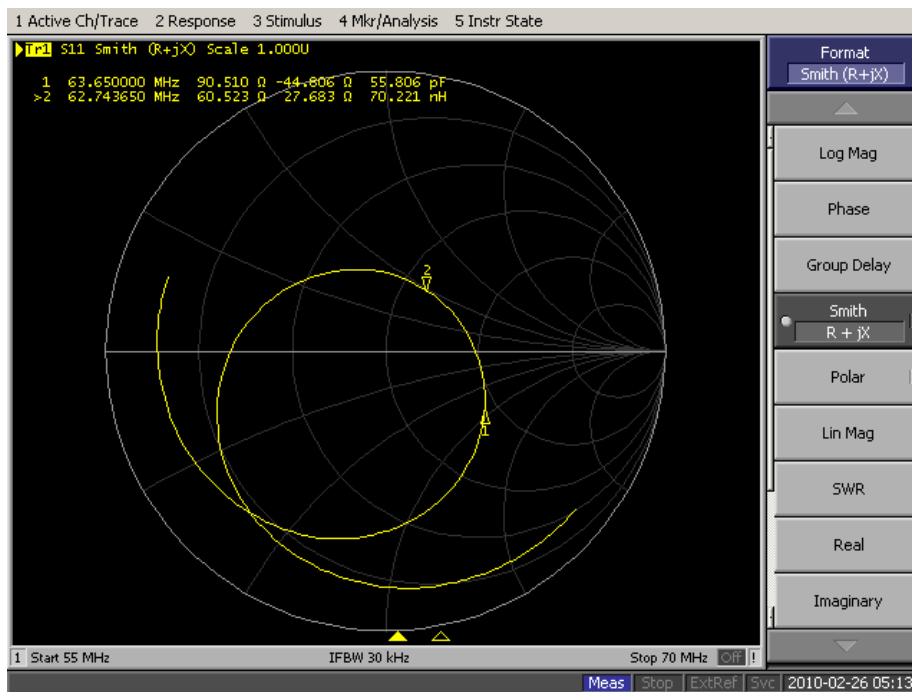


Loaded 19 Liters Smith Chart

Loaded 18 Liters

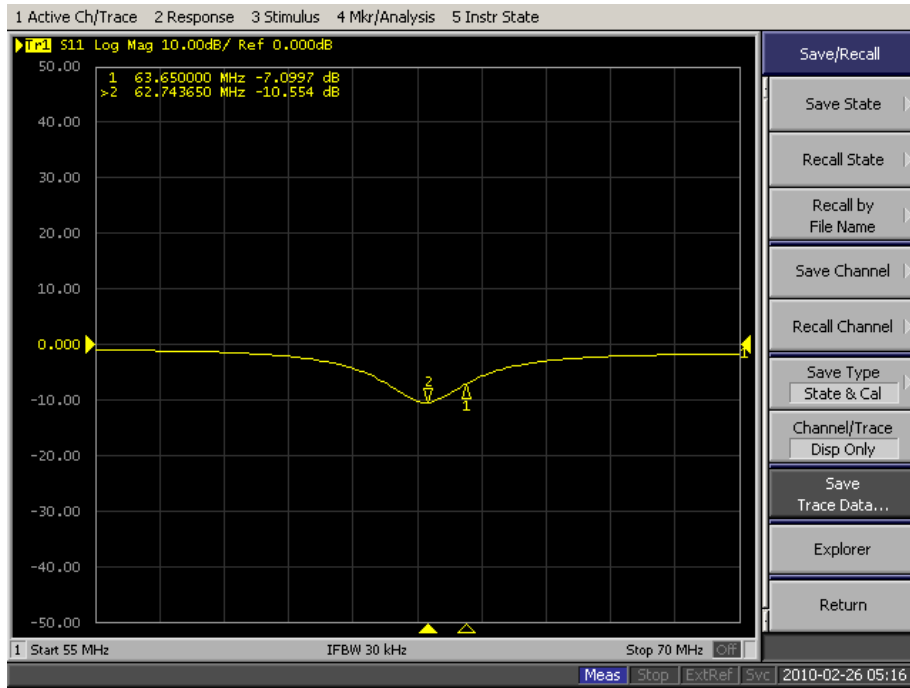


Loaded 18 Liters S11 Plot

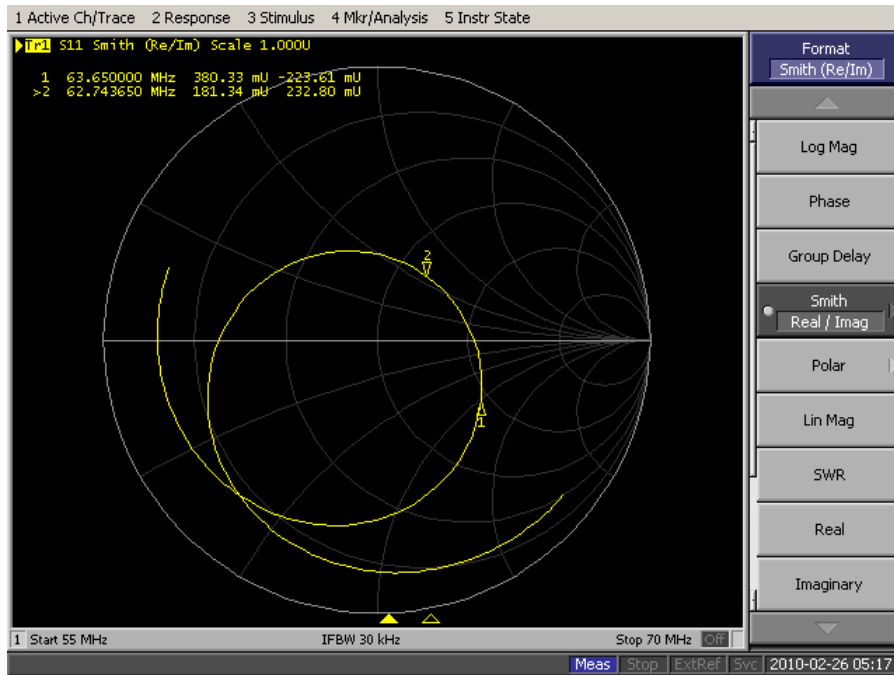


Loaded 18 Liters Smith Chart

Loaded 17 Liters

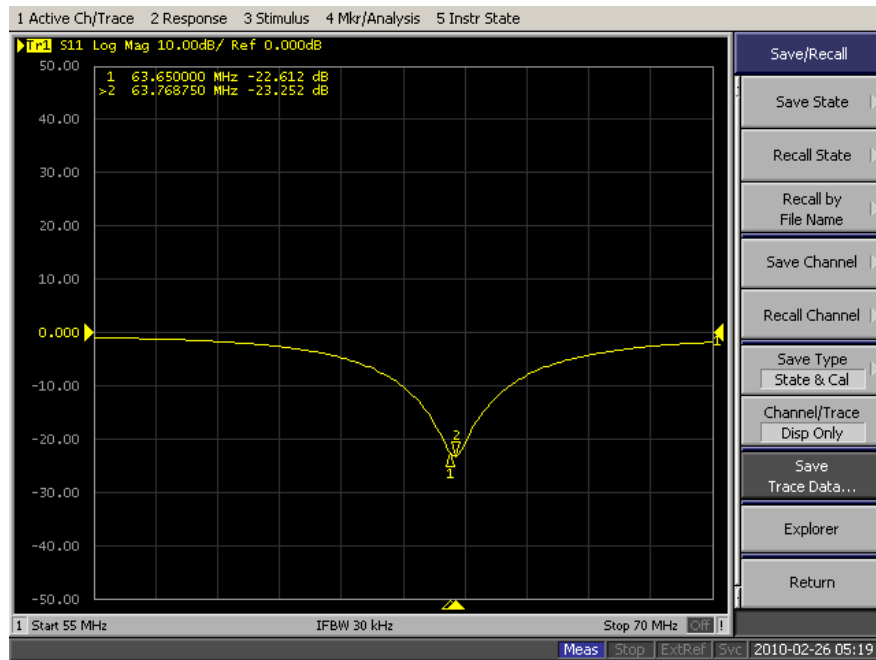


Loaded 17 Liters S11 Plot

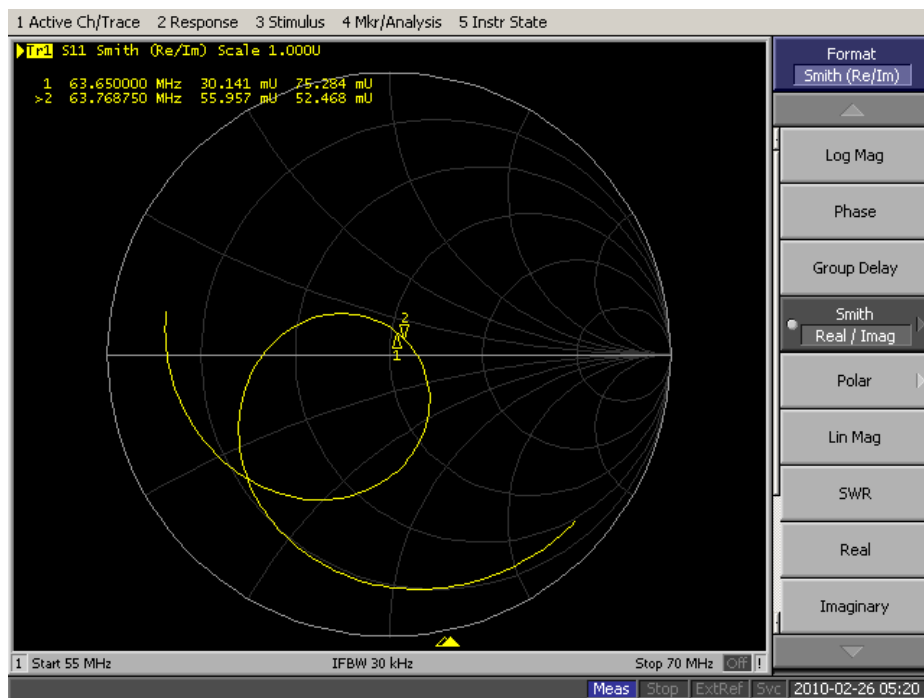


Loaded 17 Liters Smith Chart

Loaded 16 Liters

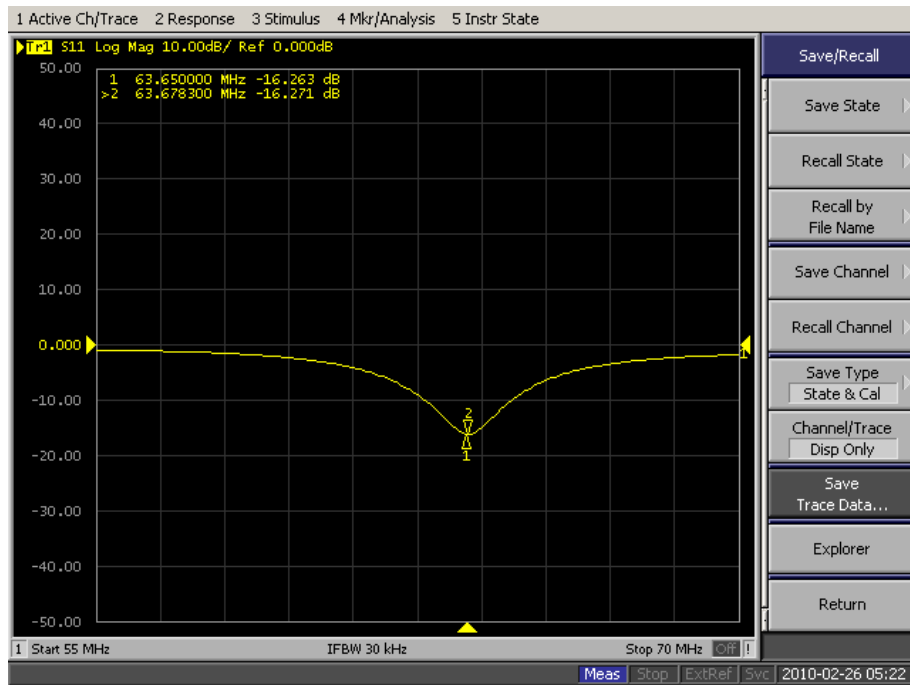


Loaded 16 Liters S11 Plot

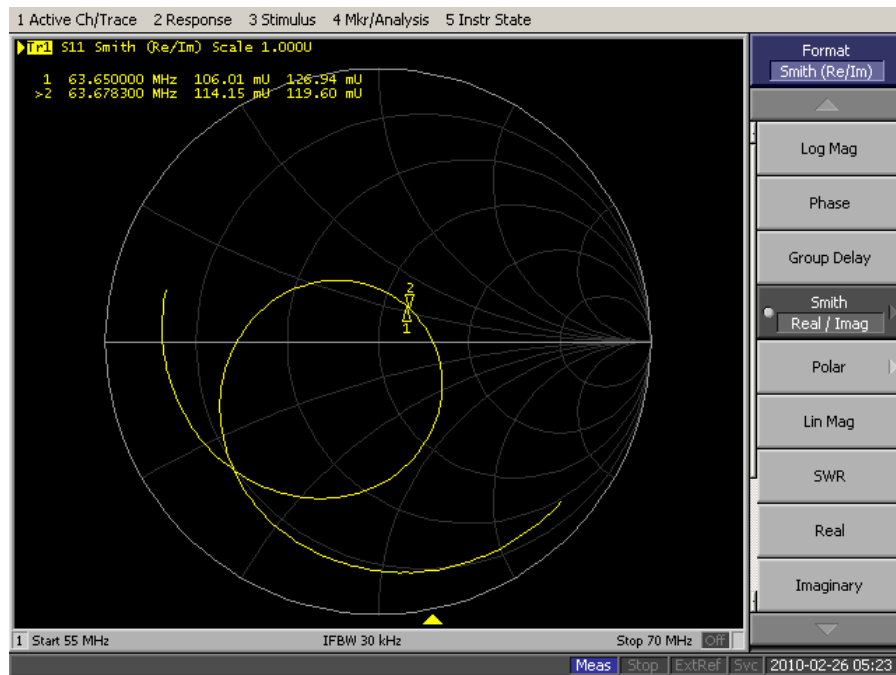


Loaded 16 Liters Smith Chart

Loaded 15 Liters

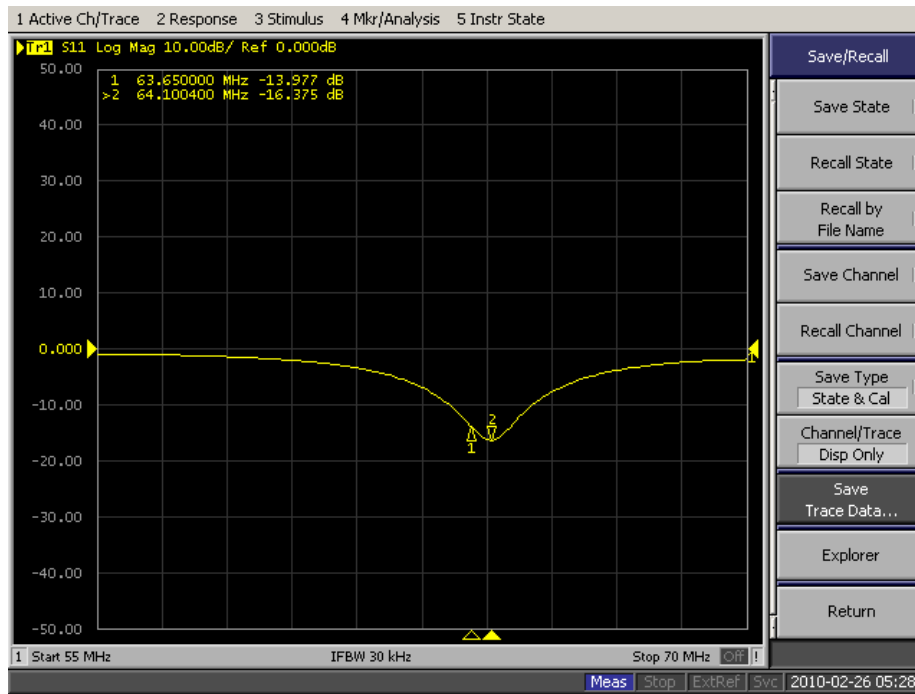


Loaded 15 Liters S11 Plot

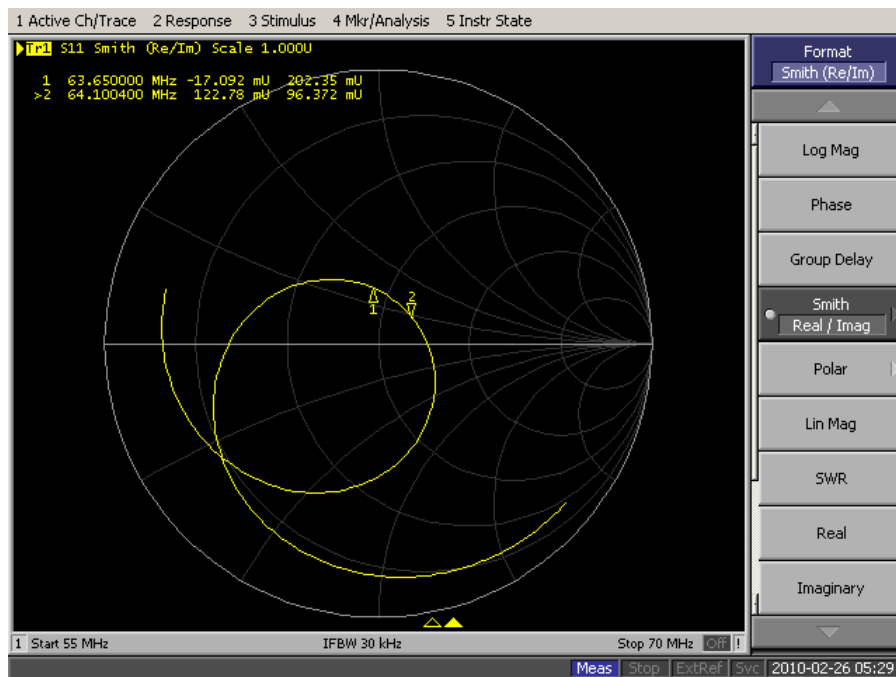


Loaded 15 Liters Smith Chart

Loaded 14 Liters

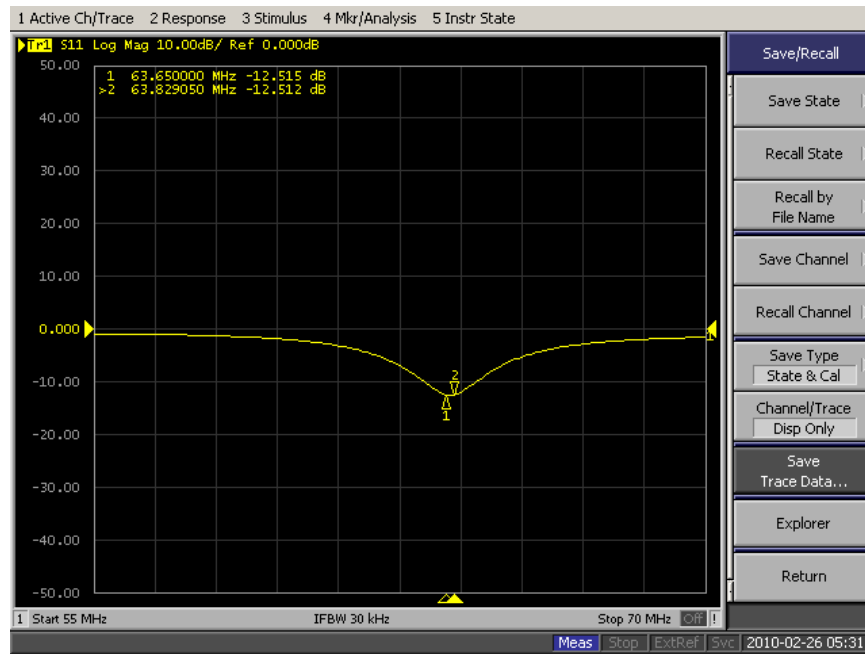


Loaded 14 Liters S11 Plot

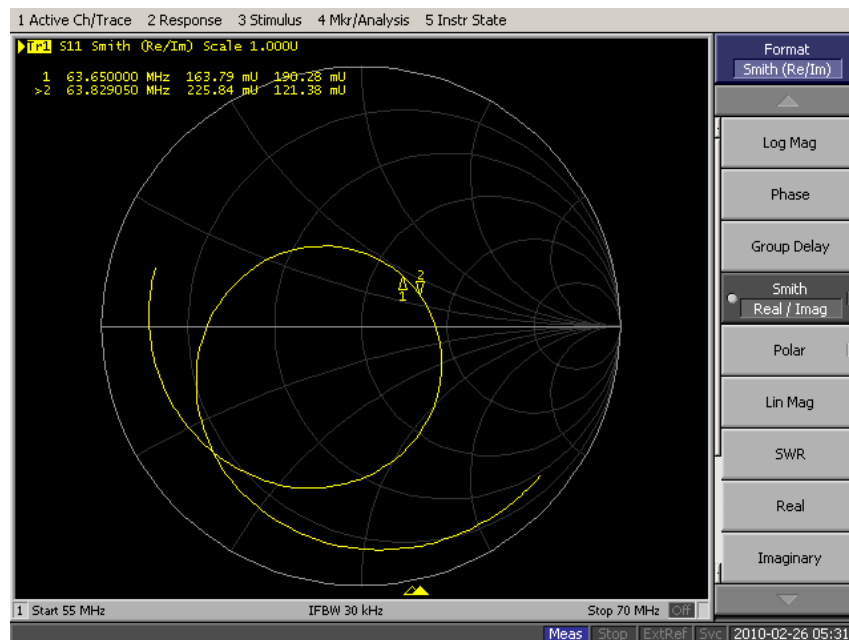


Loaded 14 Liters Smith Chart

Loaded 13 Liters

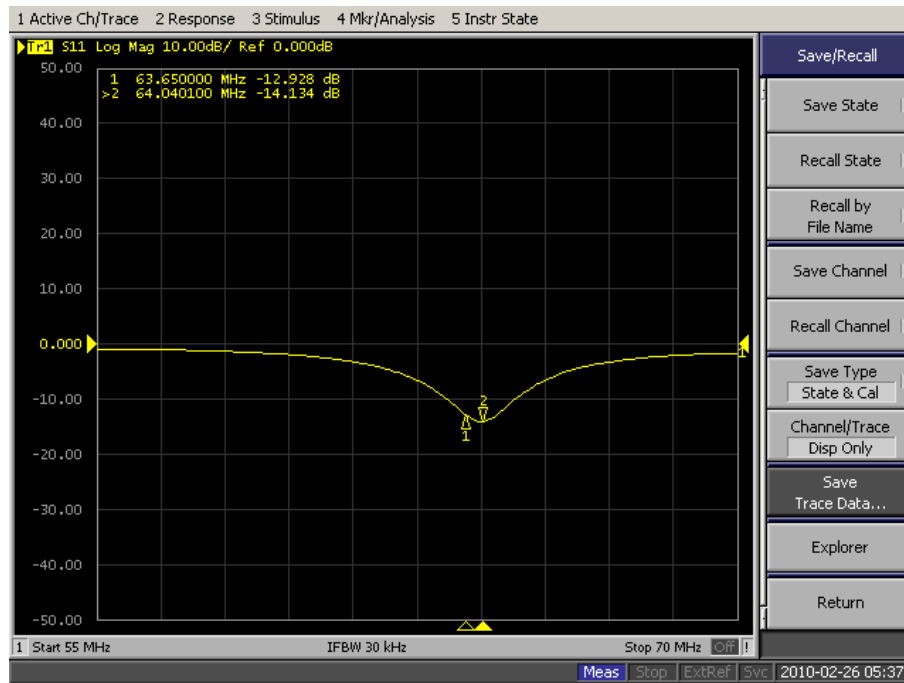


Loaded 13 Liters S11 Plot

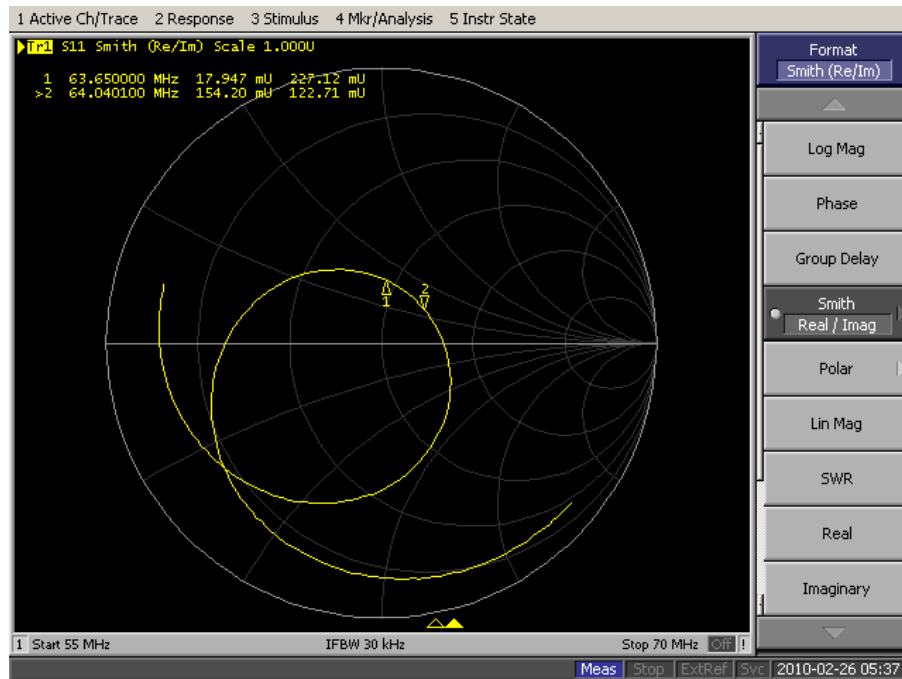


Loaded 13 Liters Smith Chart

Loaded 12 Liters

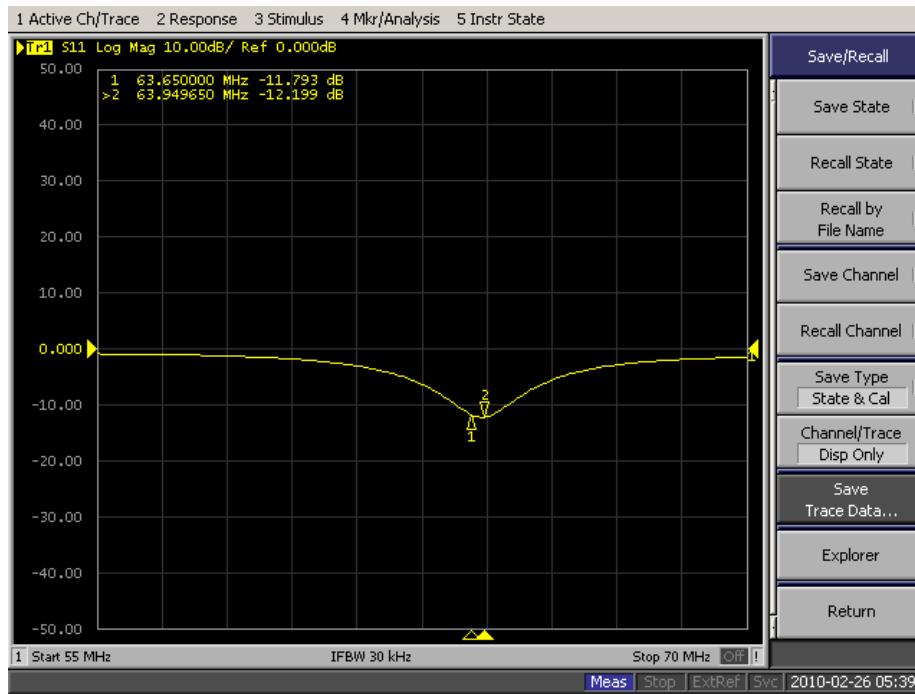


Loaded 12 Liters S11 Plot

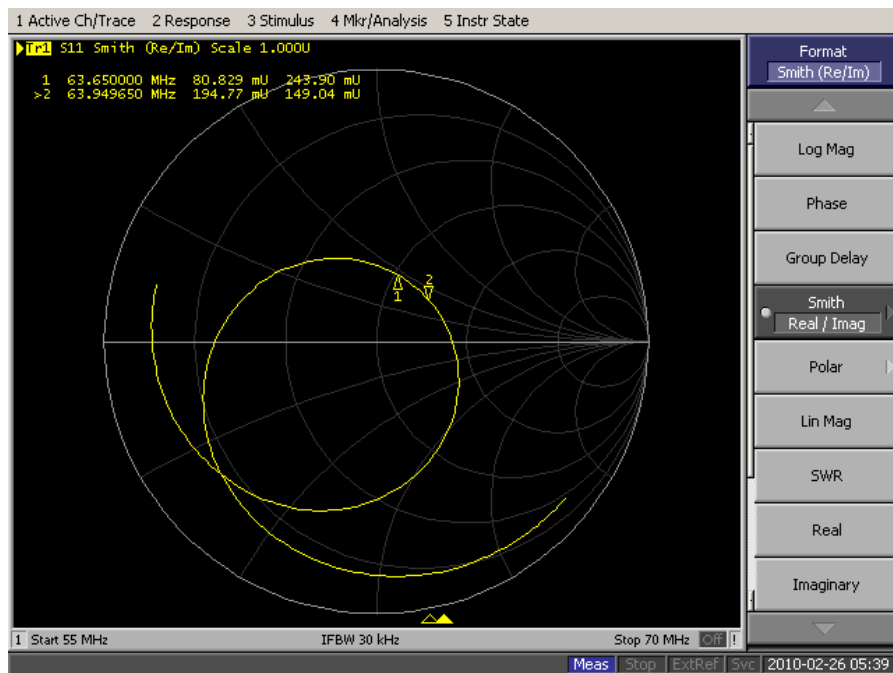


Loaded 12 Liters Smith Chart

Loaded 11 Liters

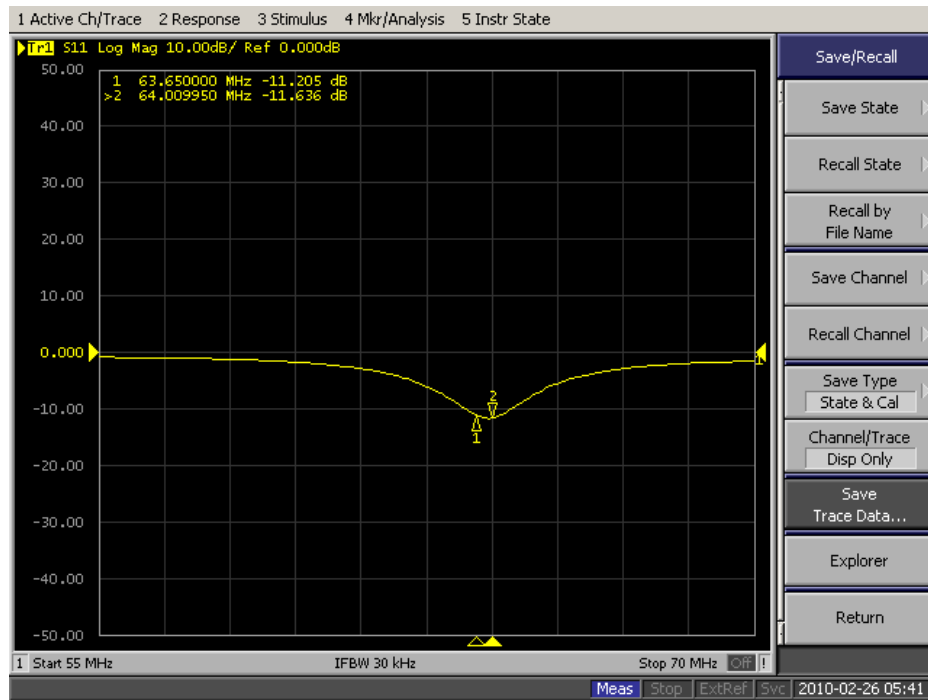


Loaded 11 Liters S11 Plot

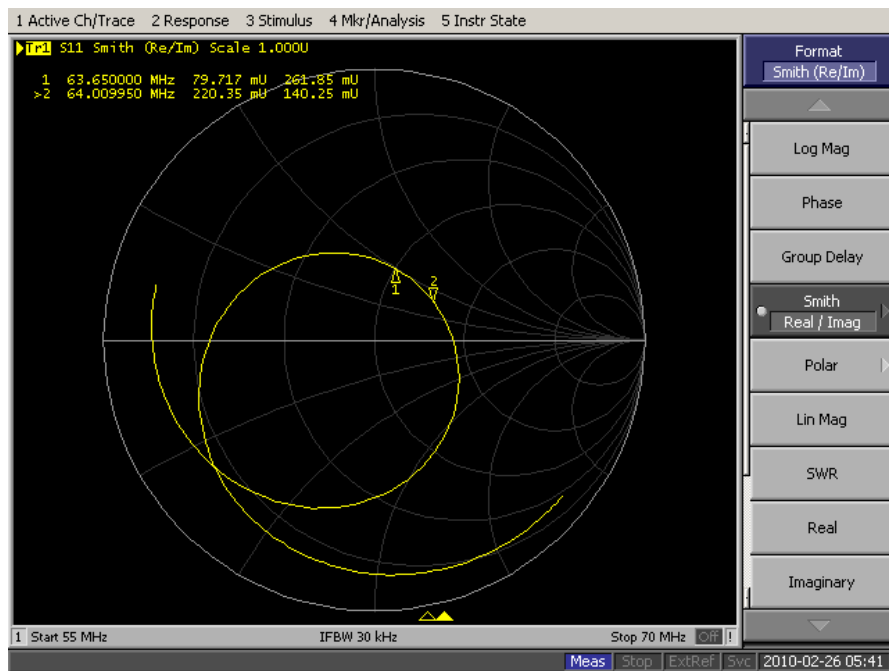


Loaded 11 Liters Smith Chart

Loaded 10 Liters

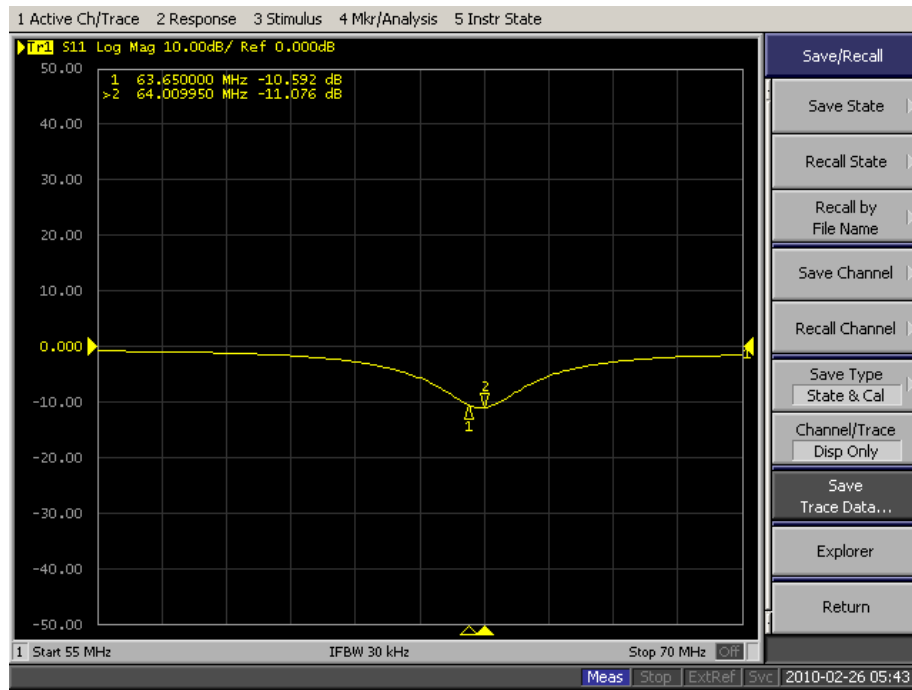


Loaded 10 Liters S11 Plot

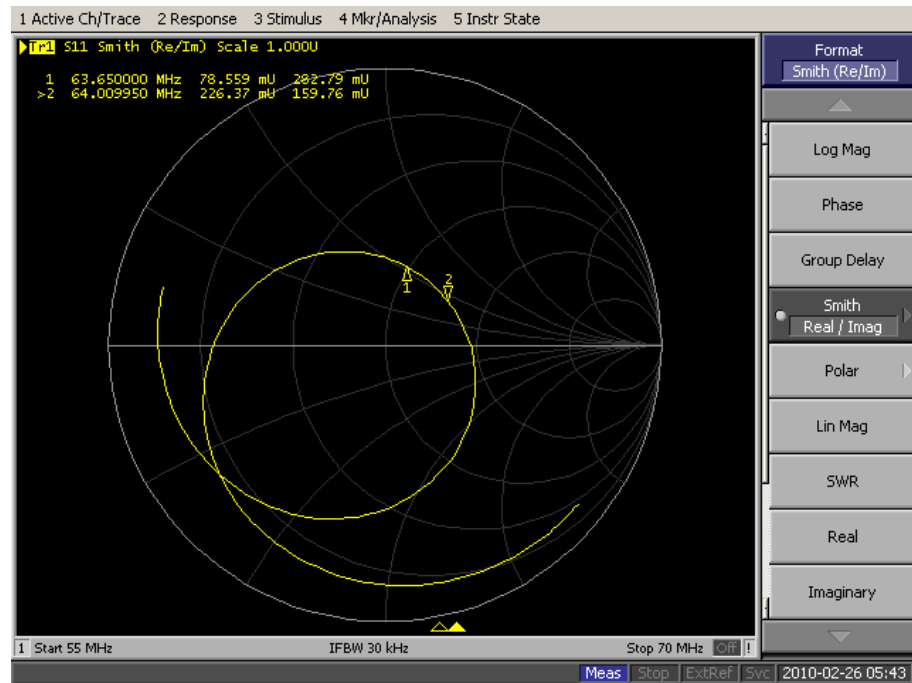


Loaded 10 Liters Smith Chart

Loaded 9 Liters

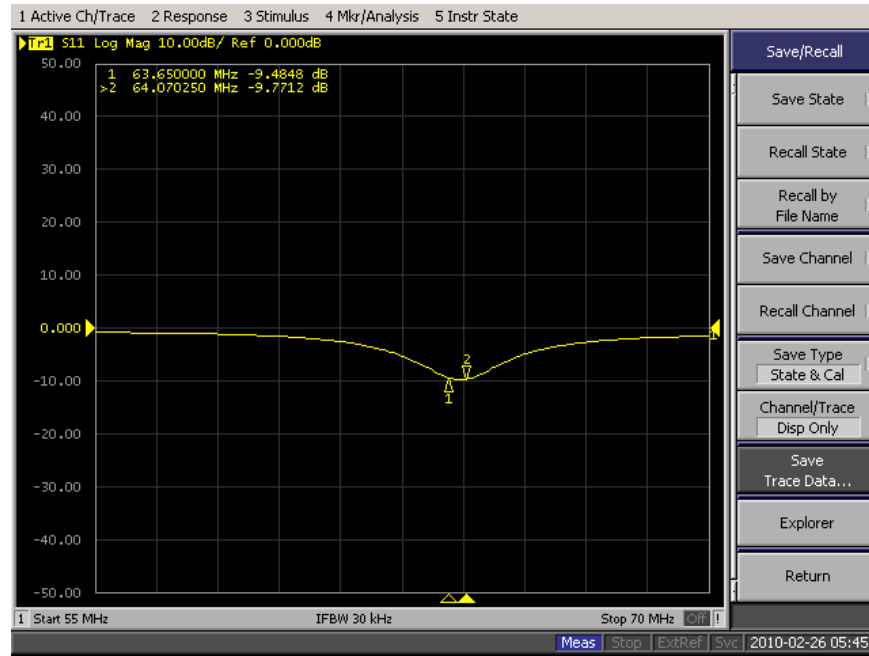


Loaded 9 Liters S11 Plot

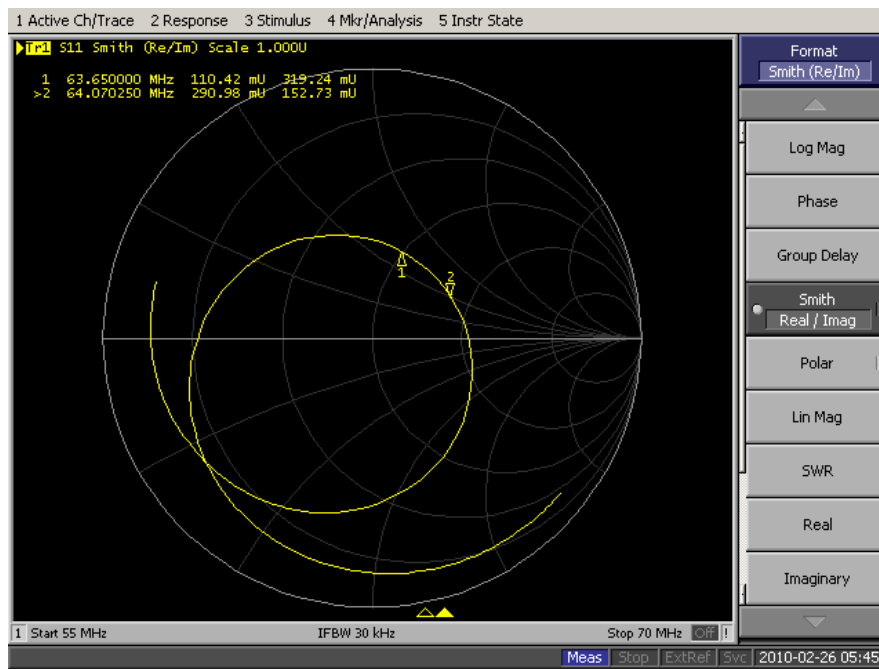


Loaded 9 Liters Smith Chart

Loaded 8 Liters

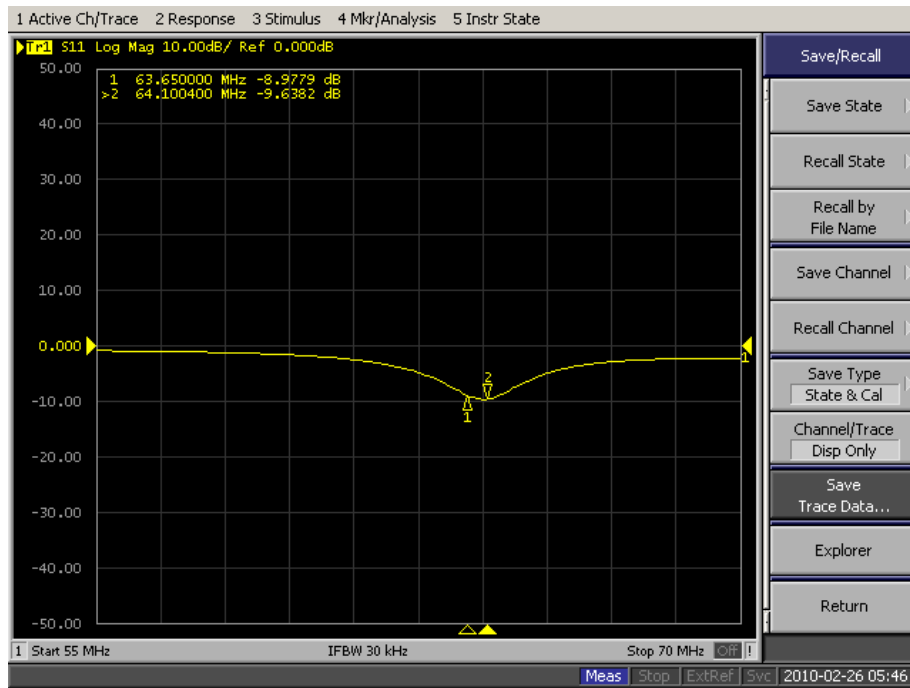


Loaded 8 Liters S11 Plot

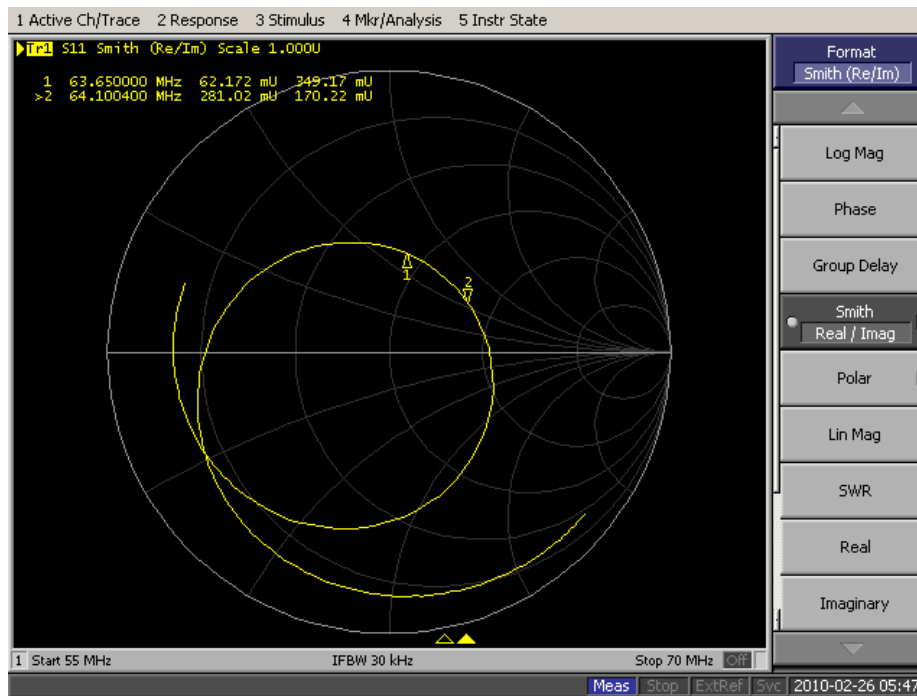


Loaded 8 Liters Smith Chart

Loaded 7 Liters

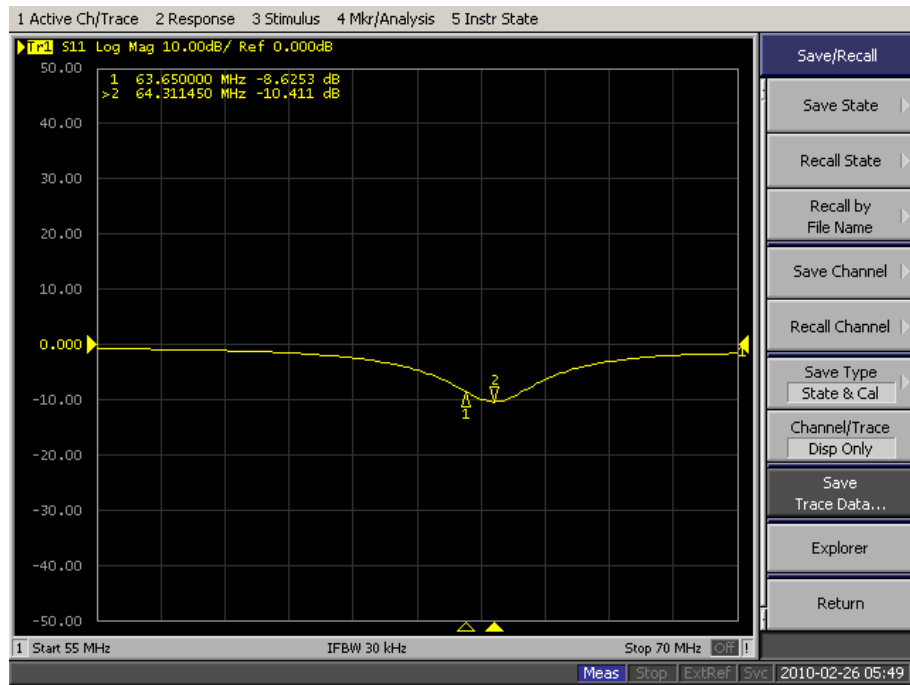


Loaded 7 Liters S11 Plot

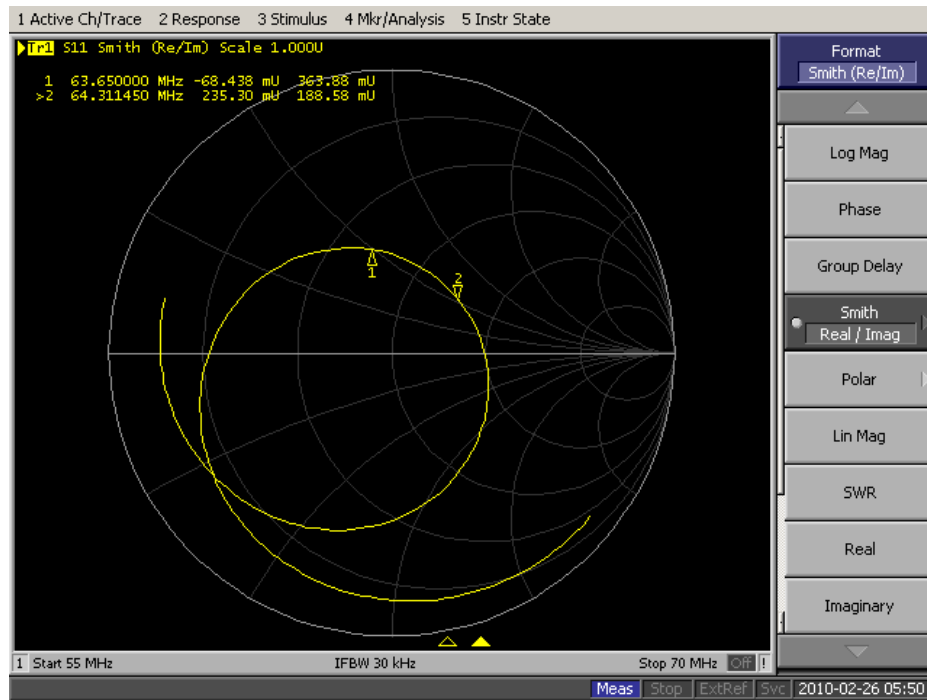


Loaded 7 Liters Smith Chart

Loaded 6 Liters

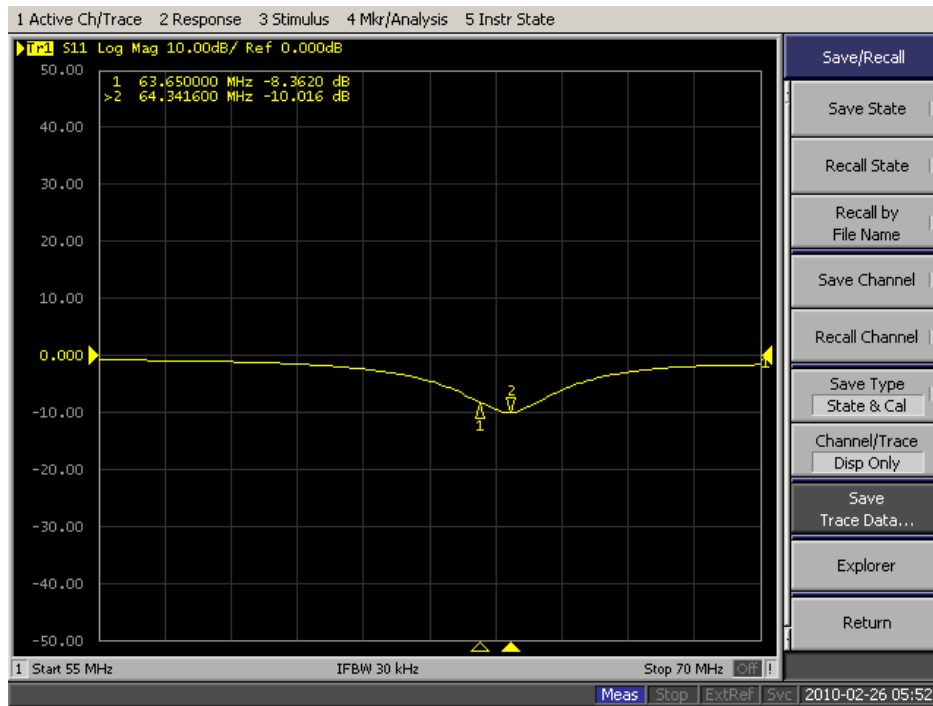


Loaded 6 Liters S11 Plot

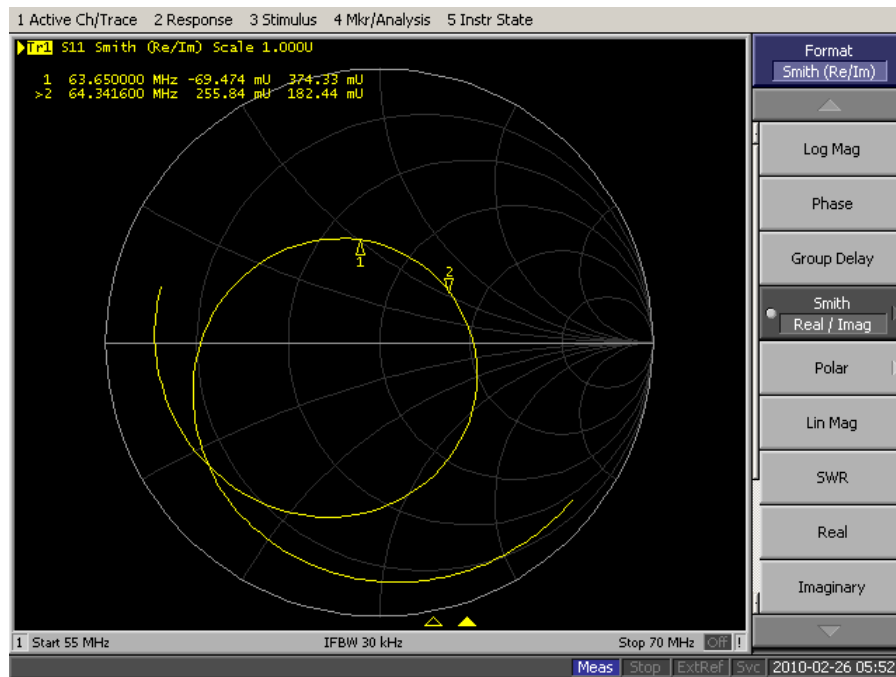


Loaded 6 Liters Smith Chart

Loaded 5 Liters



Loaded 5 Liters S11 Plot



Loaded 5 Liters Smith Chart

Instructions: Answer all questions. If you are asked to provide an explanation, please do so with adequate details. If needed, attach itemized replies. Any incomplete application will be returned.

1.) Purpose of Study: *(Please provide a concise statement of the background, nature and reasons for the proposed study. Insert below using non-technical language that can be understood by non-scientist members of the IRB.)*

The purpose of this study is to determine the behavior of our coil when loaded with a human subject.

2.) Study Protocol: *(Please attach sufficient information for effective review by non-scientist members of the IRB. Define all abbreviations and use simple words. Unless justification is provided this part of the application must not exceed 5 pages. Attaching sections of a grant application is not an acceptable substitute.)*

A.) For **biomedical, engineering and related research**, please provide an outline of the actual experiments to be performed. Where applicable, provide a detailed description of the experimental devices or procedures to be used, detailed information on the exact dosages of drugs or chemicals to be used, total quantity of blood samples to be used, and descriptions of special diets.

B.) For applications in the **social sciences, management and other non-biomedical disciplines** please provide a detailed description of your proposed study. Where applicable, include copies of any questionnaires or standardized tests you plan to incorporate into your study. If your study involves interviews please submit an outline indicating the types of questions you will include.

C.) If the study involves **investigational drugs or investigational medical devices**, and the PI is obtaining an Investigational New Drug (IND) number or Investigational Device Exemption (IDE) number from the FDA, please provide details.

D.) Please note if any **hazardous materials** are being used in this study.

E.) Please note if any **special diets** are being used in this study.

3.) Subject Information:

A.) Please provide the exact number of subjects you plan to enroll in this study and describe your subject population. *(eg. WPI students, WPI staff, UMASS Medical patient, other)*

Males: _____ Females: _____ Description: WPI Students, volunteers

B.) Will subjects who do not understand English be enrolled?

No Yes *(Please insert below the language(s) that will be translated on the consent form.)*

C.) Are there any circumstances under which your study population may feel coerced into participating in this study?

No Yes *(Please insert below a description of how you will assure your subjects do not feel coerced.)*

D.) Are the subjects at risk of harm if their participation in the study becomes known?

No Yes *(Please insert below a description of possible effects on your subjects.)*

E.) How will subjects be recruited for participation? (Check all that apply.)

- Referral: (By whom) Student Researchers
- Other: (Identify) _____
- Database: (Describe how database populated) _____
- Direct subject advertising, including: (Please provide a copy of the proposed ad. All direct subject advertising must be approved by the WPI IRB prior to use.)
- | | |
|-------------------------------------|---|
| <input type="checkbox"/> Newspaper | <input type="checkbox"/> Bulletin board |
| <input type="checkbox"/> Radio | <input type="checkbox"/> Flyers |
| <input type="checkbox"/> Television | <input type="checkbox"/> Letters |
| <input type="checkbox"/> Internet | <input type="checkbox"/> E-mail |

F.) Have the subjects in the database agreed to be contacted for research projects? No Yes N/A

G.) Are the subjects being paid for participating? (Consider all types of reimbursement, ex. stipend, parking, travel.)
No Yes (Check all that apply.) Cash Check Gift certificate Other: _____
Amount of compensation _____

4.) Informed Consent:

A.) Who will discuss the study with and obtain consent of prospective subjects? (Check all that apply.)

- Principal Investigator Co-Investigator(s) Student Investigator(s)

B.) Are you aware that subjects must read and sign and Informed Consent Form prior to conducting any study-related procedures and agree that all subjects will be consented prior to initiating study related procedures? No Yes

C.) Are you aware that you must consent subjects using only the IRB-approved Informed Consent Form? No Yes

D.) Will subjects be consented in a private room, not in a public space? No Yes

E.) Do you agree to spend as much time as needed to thoroughly explain and respond to any subject's questions about the study, and allow them as much time as needed to consider their decision prior to enrolling them as subjects? No Yes

F.) Do you agree that the person obtaining consent will explain the risks of the study, the subject's right to decide not to participate, and the subject's right to withdraw from the study at any time? No Yes

G.) Do you agree to either 1.) retain signed copies of all informed consent agreements in a secure location for at least three years or 2.) supply copies of all signed informed consent agreements in .pdf format for retention by the IRB in electronic form? No Yes

(If you answer No to any of the questions above, please provide an explanation.)

5.) Potential Risks: (A risk is a potential harm that a reasonable person would consider important in deciding whether to participate in research. Risks can be categorized as physical, psychological, sociological, economic and legal, and include pain, stress, invasion of privacy, embarrassment or exposure of sensitive or confidential data. All potential risks and discomforts must be minimized to the greatest extent possible by using e.g. appropriate monitoring, safety devices and withdrawal of a subject if there is evidence of a specific adverse event.)

A.) What are the risks / discomforts associated with each intervention or procedure in the study?

There as no health risks to the subjects. The students may feel uncomfortable in the coil.

B.) What procedures will be in place to prevent / minimize potential risks or discomfort?

Subjects will be asked to stay in the coil for a minimum period of time

6.) Potential Benefits:

A.) What potential benefits other than payment may subjects receive from participating in the study?

N/A

B.) What potential benefits can society expect from the study?

Further research into alternative methods for imaging the prostate

7.) Data Collection, Storage, and Confidentiality:

A.) How will data be collected?

The data will be collected by the network analyzer. Data of the receive coil will be saved on local storage devices without students names.

B.) Will a subject's voice, face or identifiable body features (eg. tattoo, scar) be recorded by audio or videotaping?

No Yes (Explain the recording procedures you plan to follow.)

C.) Will personal identifying information be recorded? No Yes (If yes, explain how the identifying information will be protected. How will personal identifying information be coded and how will the code key be kept confidential?)

D.) Where will the data be stored and how will it be secured?

The data will be stored on personal PCs of the researchers.

E.) What will happen to the data when the study is completed?

The data will be presented in the form of an MQP report, but the original data will be deleted.

F.) Can data acquired in the study adversely affect a subject's relationship with other individuals? (i.e. employee-supervisor, student-teacher, family relationships)

No.

G.) Do you plan to use or disclose identifiable information outside of the investigation personnel?

No Yes (Please explain.)

H.) Do you plan to use or disclose identifiable information outside of WPI including non-WPI investigators?

No Yes (Please explain.)

8.) Incidental findings: *In the conduct of information gathering, is it possible that the investigator will encounter any incidental findings? If so, how will these be handled? (An incidental finding is information discovered about a subject which should be of concern to the subject but is not the focus of the research. For example, a researcher monitoring heart rates during exercise could discover that a subject has an irregular heartbeat.)*

N/A

9.) Deception: *(Investigators must not exclude information from a subject that a reasonable person would want to know in deciding whether to participate in a study.)*

Will the information about the research purpose and design be withheld from the subjects?

No Yes *(Please explain.)*

10.) Adverse effects: *(Serious or unexpected adverse reactions or injuries must be reported to the WPI IRB within 48 hours. Other adverse events should be reported within 10 working days.)*

What follow-up efforts will be made to detect any harm to subjects and how will the WPI IRB be kept informed?

An email will be sent to consenting members whether the next day.

11.) Informed consent: *(Documented informed consent must be obtained from all participants in studies that involve human subjects. You must use the templates available on the WPI IRB web-site to prepare these forms. **Informed consent forms must be included with this application.** Under certain circumstances the WPI IRB may waive the requirement for informed consent.)*

Investigator's Assurance:

I certify the information provided in this application is complete and correct.

I understand that I have ultimate responsibility for the conduct of the study, the ethical performance of the project, the protection of the rights and welfare of human subjects, and strict adherence to any stipulations imposed by the WPI IRB.

I agree to comply with all WPI policies, as well all federal, state and local laws on the protection of human subjects in research, including:

- ensuring the satisfactory completion of human subjects training.
- performing the study in accordance with the WPI IRB approved protocol.
- implementing study changes only after WPI IRB approval.
- obtaining informed consent from subjects using only the WPI IRB approved consent form.
- promptly reporting significant adverse effects to the WPI IRB.

Signature of Principal Investigator _____ Date _____

Print Full Name and Title Professor Reinhold Ludwig

*Please return a signed hard copy of this application to the WPI IRB c/o Ruth McKeogh 2nd Floor Project Center
If you have any questions, please call (508) 831-6699.*

Research Procedure

- 1.) WPI Students will be informed of the following information by one of the student researchers.
 - The purpose of this MQP is to design a Helmholtz MRI Receive Coil for imaging the prostate. In an actual imaging setting, the patient will emit a signal that would be picked up by this coil.
 - For the scope of the project, we will not be imaging any patients.
 - We will be testing whether or not the coil behaves correctly outside of a magnet.
 - This coil has different RF behavior depending on the type of load placed inside of it. The size, weight, and electrical conductivity of the load can change the frequency which the coil resonates, as well as the quality of the resonance.
 - This experiment is designed to test our coil only
 - The student will be asked to empty his/her pockets and remove any belts
 - The student will be asked to sit in the coil as a patient would
 - While in the coil, the student will not be exposed to any dangerous electromagnetic radiation
 - The student will be exposed to less than 1 mW of radio waves centered around 63.65 MHz. This frequency and power level will have no effect on you.
 - The behavior of the coil will be recorded and saved independent of his/her name or any other personal information
 - The entire test will take less than 5 minutes.
- 2.) The students will be asked to sign the attached consent form.
- 3.) One of the student researchers will demonstrate how to sit in the coil.
- 4.) The students will be asked individually to sit in the coil.
- 5.) A RF frequency sweep from 55 to 70 MHz will be used on the network analyzer. The data for the S11 parameter for the patient will be dumped into a .CSV file, which will be saved as Patient followed by a number.
- 6.) A Smith chart display will be saved from the network analyzer for the same frequency range.
- 7.) The patient will then be allowed to leave.

Informed Consent Agreement for Participation in a Research Study

Investigator: Professor Reinhold Ludwig
Contact Information: ludwig@wpi.edu

Student Investigators:
Nathan Climer (nclimer@wpi.edu)
Deepa Krishnaswamy (deepa_k@wpi.edu)
Ben Holmes (ben.holmes@wpi.edu)

Title of Research Study: External Helmholtz coil for Prostate MR Imaging

Sponsor: N/A

You are being asked to participate in a research study. Before you agree, however, you must be fully informed about the purpose of the study, the procedures to be followed, and any benefits, risks or discomfort that you may experience as a result of your participation. This form presents information about the study so that you may make a fully informed decision regarding your participation.

Purpose of the study: To determine the RF behavior of the prototype Helmholtz coil for different biological loads

Procedures to be followed:

- The student will be asked to empty his/her pockets and remove any belts
- The student will be asked to sit in the coil as a patient would
- The behavior of the coil will be recorded and saved independent of his/her name or any other personal information
- The entire test will take less than 5 minutes.

Risks to study participants: There are no risks associated with this procedure. Subjects may be exposed to less than 1 mWatt of radio waves centered around 63.65 MHz. This radiation is very small and at safe levels.

Benefits to research participants and others: There are no benefits to participating in this study.

Record keeping and confidentiality: All data will be stored on student researchers persal PCs. The data will be stored independent of all subject personal information. The data will be stored in file names "Student" followed by a number. These files will be deleted at the end of the project.

The data collected may be shown in the final MQP report, but contains no personal information.

Compensation or treatment in the event of injury: You do not give up any of your legal rights by signing this statement.

For more information about this research or about the rights of research participants, or in case of research-related injury, contact:

Principle Investigator

Professor Reinhold Ludwin, Tel. 1-508-831-5315, E-Mail Address: Ludwig@wpi.edu)

Student Investigators:

Nathan Climer, E-Mail Address: nclimer@wpi.edu

Deepa Krishnaswamy, E-Mail Address: deepa_k@wpi.edu

Ben Holmes, E-Mail Address: ben.holmes@wpi.edu

IRB Chair

Professor Kent Rissmiller, Tel. 508-831-5019, Email: kjr@wpi.edu)

University Compliance Officer

Michael J. Curley, Tel. 508-831-6919, Email: mjcurley@wpi.edu)

Your participation in this research is voluntary. Your refusal to participate will not result in any penalty to you or any loss of benefits to which you may otherwise be entitled. You may decide to stop participating in the research at any time without penalty or loss of other benefits. The project investigators retain the right to cancel or postpone the experimental procedures at any time they see fit.

By signing below, you acknowledge that you have been informed about and consent to be a participant in the study described above. Make sure that your questions are answered to your satisfaction before signing. You are entitled to retain a copy of this consent agreement.

Study Participant Signature

Date: _____

Study Participant Name (Please print)

Approved by WPI IRB
From: 3/1/2010
To: 2/28/2011

Signature of Person who explained this study

Date: _____



100 Institute Road
Worcester, MA 01609-2280, USA
508-831-5000, Fax: 508-831-6090
www.wpi.edu

**Worcester Polytechnic Institute IRB #1
IRB 00007374**

1 March 2010
File: 10-041

Worcester Polytechnic Institute
100 Institute Road
Worcester, MA 01609

Re: IRB Expedited Review Approval: #10-041, "Helmholtz Coil for Prostate Imaging"

Dear Prof. Ludwig,

The WPI Institutional Review Committee (IRB) approves the above-referenced research activity, having conducted an expedited review according to the Code of Federal Regulations 46.

Consistent with CFR 46.116 regarding the general requirements for informed consent, we remind you to only use the **attached stamped approved consent form** and to give a copy of the signed consent form to your subjects. You are also required to store the signed consent forms in a secure location and retain them for a period of at least three years following the conclusion of your study. You may also convert the completed consent forms into electronic documents (.pdf format) and forward them to the IRB Secretary for electronic storage.

The period covered by this approval is 1 March 2010 until 28 February 2011, unless terminated sooner (in writing) by yourself or the WPI IRB. This approval becomes immediately null and void if this project receives any federal sponsorship. Amendments or changes to the research that might alter this specific approval must be submitted to the WPI IRB for review and may require a full IRB application in order for the research to continue.

Please contact the undersigned if you have any questions about the terms of this approval.

Sincerely,

Kent Rissmiller
WPI IRB Chair

Appendix G Biological Load Test of Tuning and Matching

This section summarizes the results collected under the protocol outlined in Appendix F.

This section contains the raw data used in testing the S11 parameter for the MRI phantom load. The results are summarized below in Table G-1.

Table G-1: Summary of Biological Load Testing

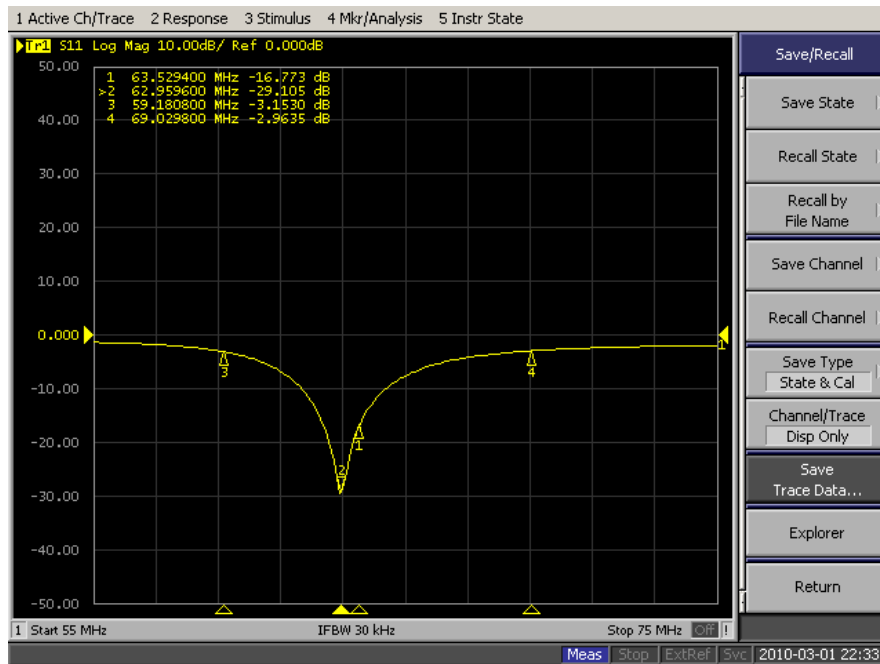
Subject	Operating Frequency (MHz)	Absolute Shift from 63.65 MHz	Fractional Shift from 63.65 MHz	Lower Cutoff (MHz)	Upper Cutoff (MHz)	Bandwidth (MHz)	Q	Lowest point (dB)
1	62.9596	0.6904	1.0847%	59	69	10	6.29596	-9.540456157
2	63.1606	0.4894	0.7689%	59.8	68.5	8.7	7.25983908	-9.613644872
3	63.241	0.409	0.6426%	59.9	68.2	8.3	7.61939759	-9.951886773
4	63.1636	0.4864	0.7642%	59.5	68.2	8.7	7.260183908	-9.769904916
5	62.7536	0.8964	1.4083%	59.2	68.2	9	6.972622222	-9.853182892
6	63.0832	0.5668	0.8905%	59	69.1	10.1	6.245861386	-9.99343202
7	63.2812	0.3688	0.5794%	59.8	69.5	9.7	6.523835052	-9.591705702
8	62.7032	0.9468	1.4875%	59.1	66.7	7.6	8.250421053	-9.974233343
9	62.9748	0.6752	1.0608%	59.5	67	7.5	8.39664	-9.721958419
10	62.8238	0.8262	1.2980%	58.8	67.8	9	6.980422222	-9.981531608
11	63.043	0.607	0.9537%	59.6	68.9	9.3	6.778817204	-9.658509225
Mean	63.01705455	0.632945455	0.009944155	59.38181818	68.28181818	8.9	7.143999974	-9.786404175
Standard Deviation	0.194267961	0.194267961	0.003052128	0.378993883	0.865815433	0.8694826	0.71736397	0.172361604
Fractional Deviation	0.003082784	0.30692686	0.30692686	0.006382322	0.012680029	0.09769467	0.10041489	-0.017612353

For each subject, the -3 dB cutoff was used to find the bandwidth of the coil. The lowest point in the dip was used to find the resonance frequency of each coil. The quality factor Q for each coil was found from

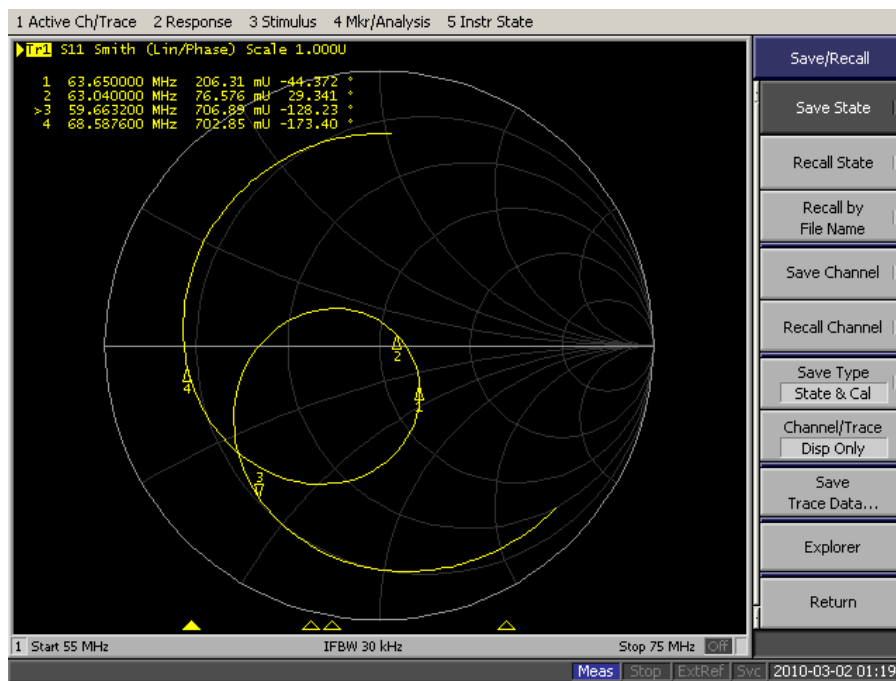
$$Q = \frac{\text{Resonance Frequency}}{\text{Bandwidth}}$$

Where the bandwidth is the -3dB cutoff of the S11 parameter.

Subject 1

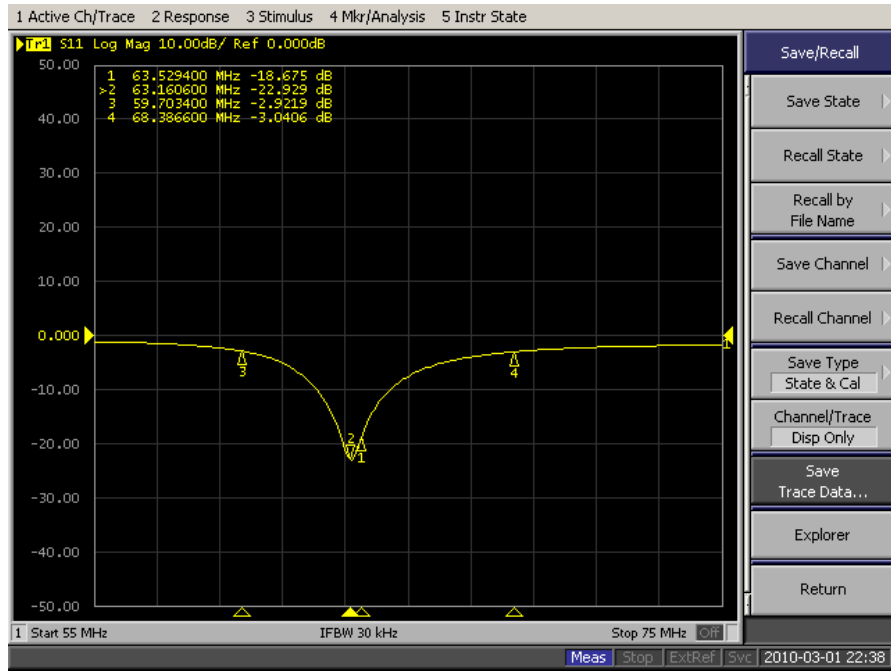


Subject 1 S11 Plot

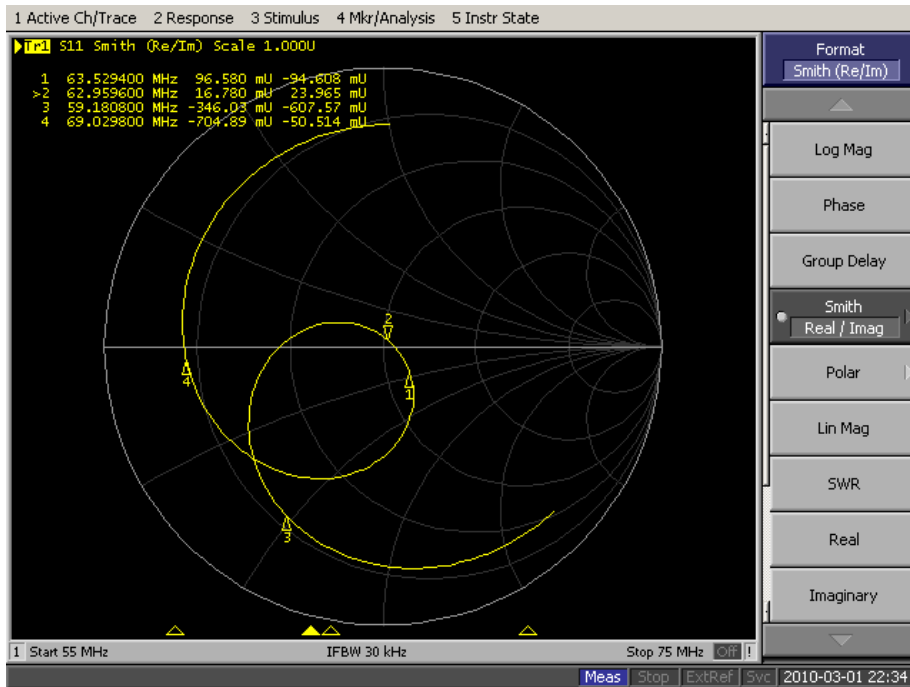


Subject 1 Smith Chart

Subject 2

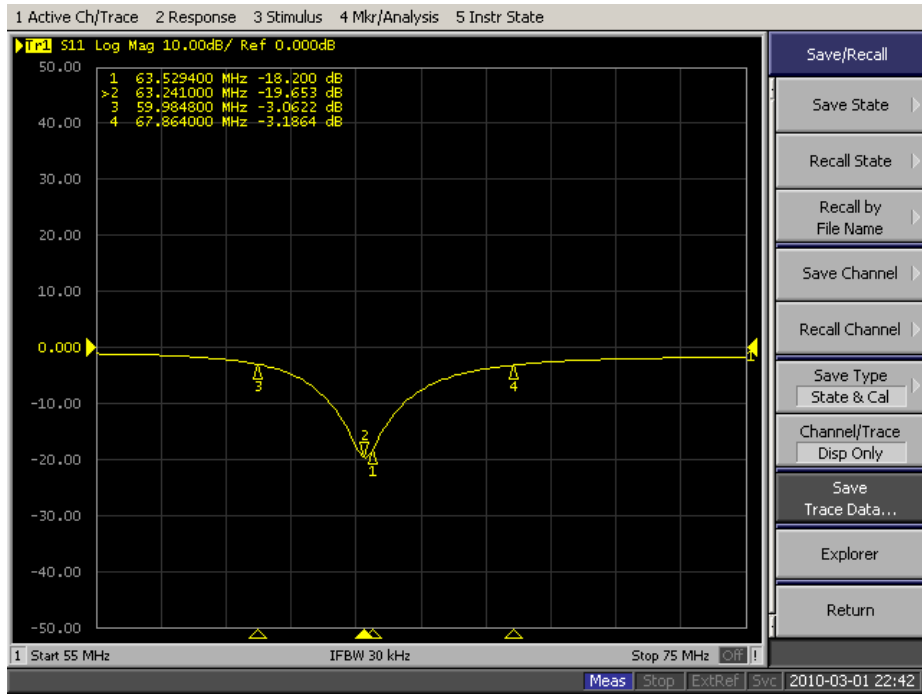


Subject 2 S11 Plot

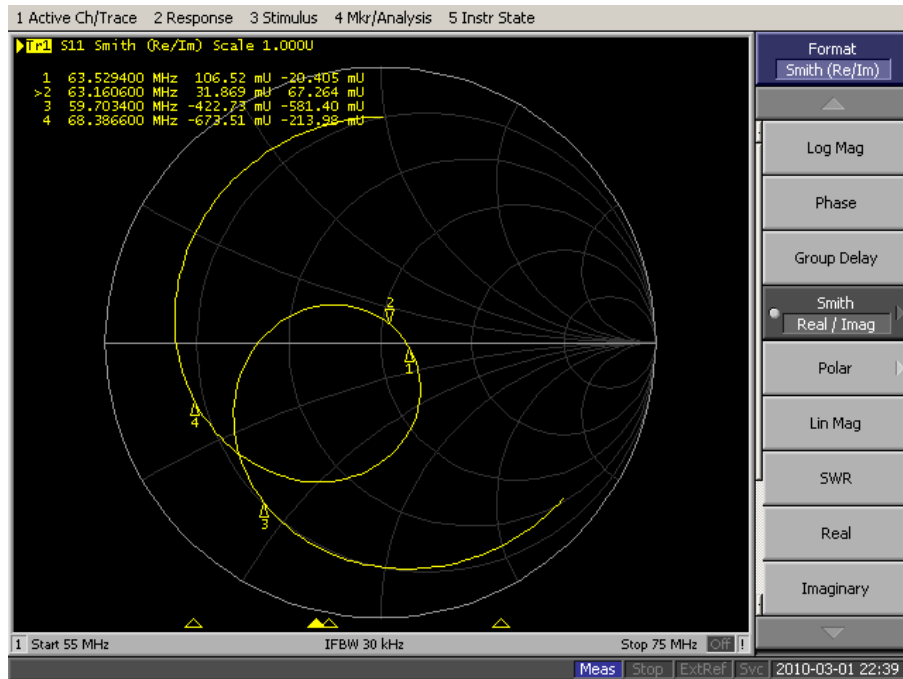


Subject 2 Smith Chart

Subject 3

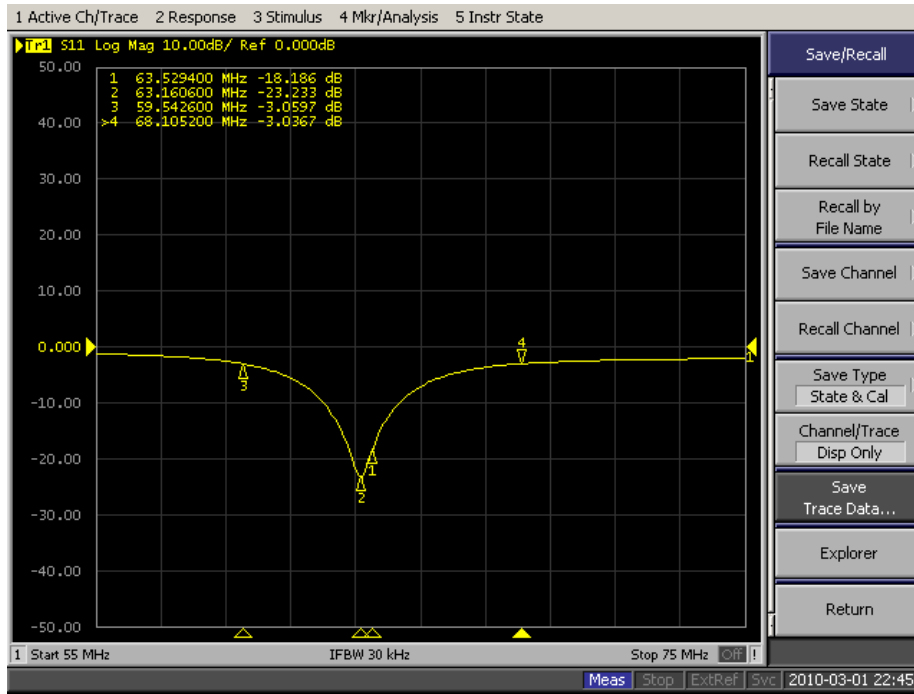


Subject 3 S11 Plot

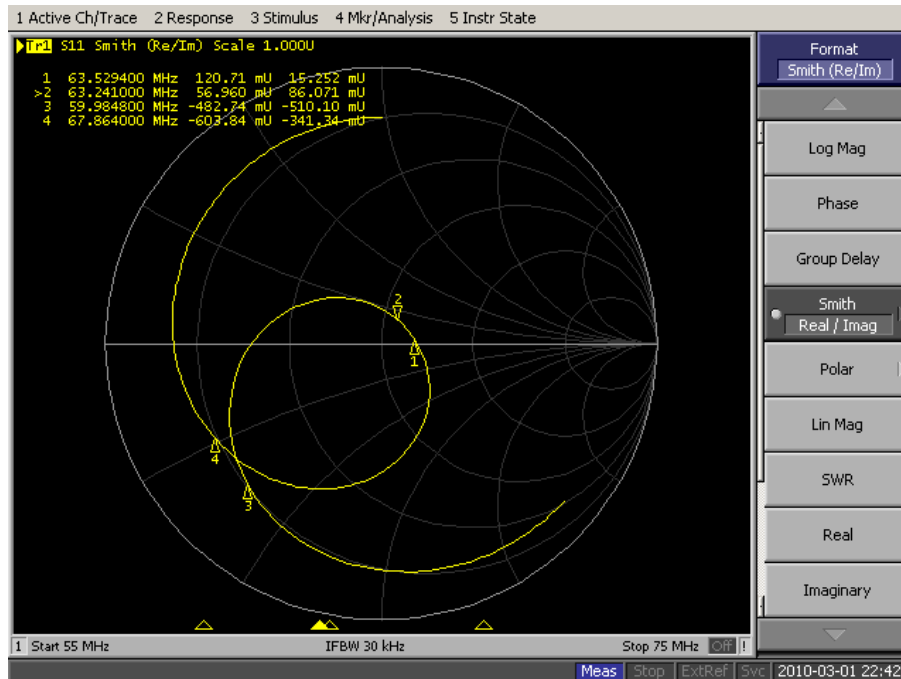


Subject 3 Smith Chart

Subject 4

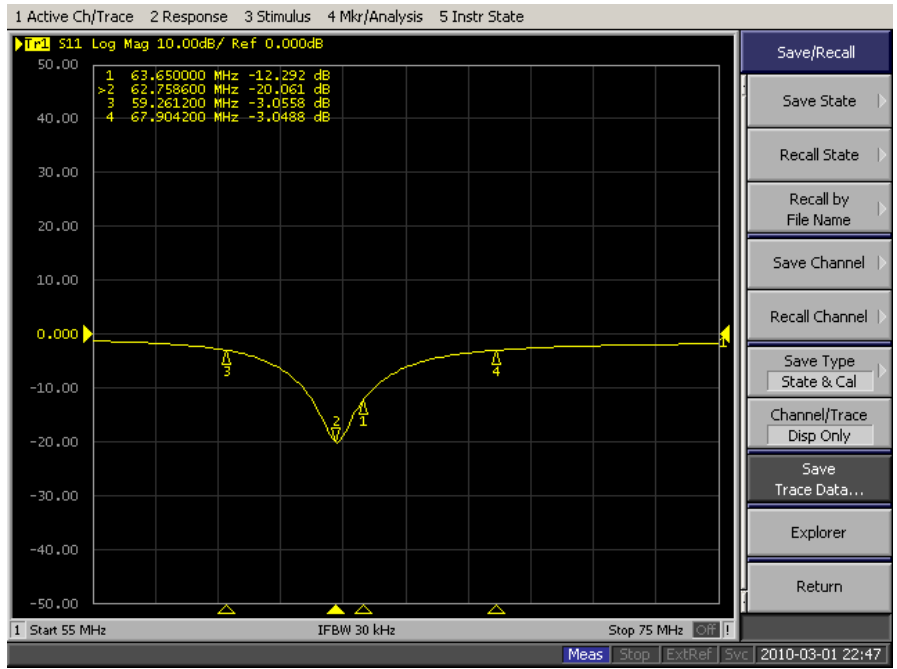


Subject 4 S11 Plot

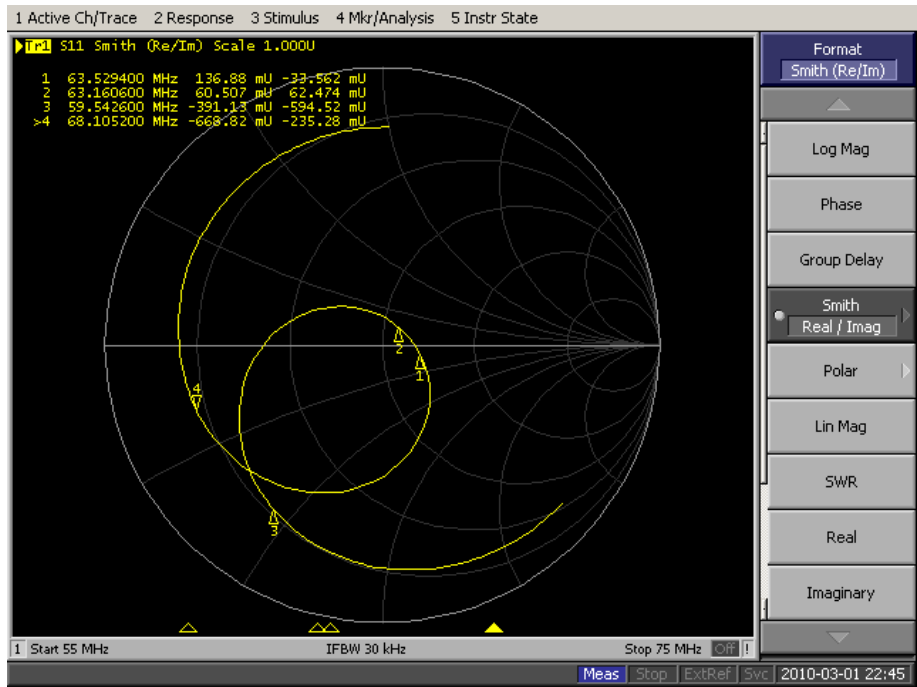


Subject 4 Smith Chart

Subject 5

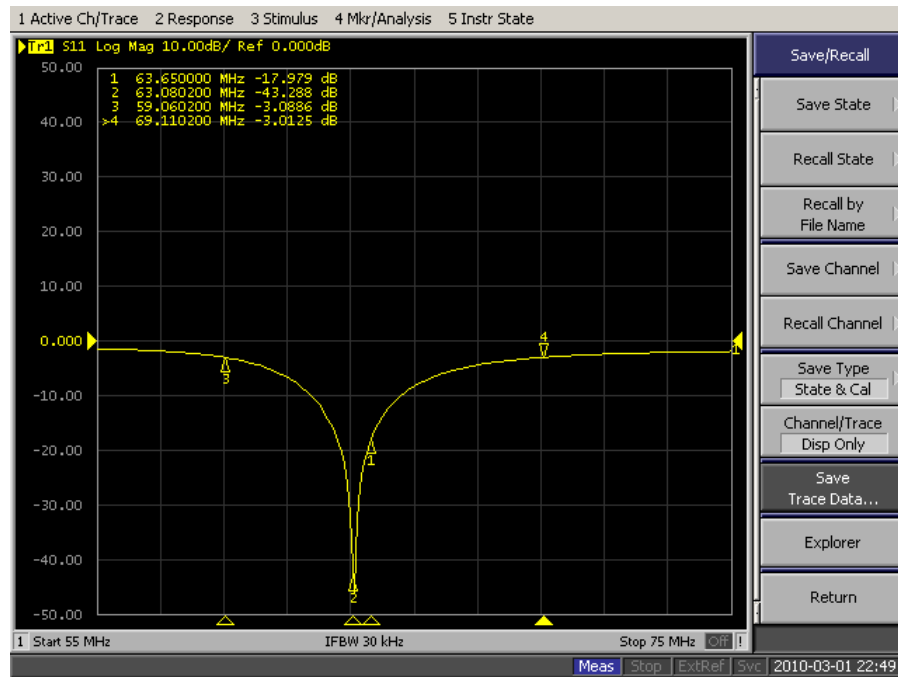


Subject 5 S11 Plot

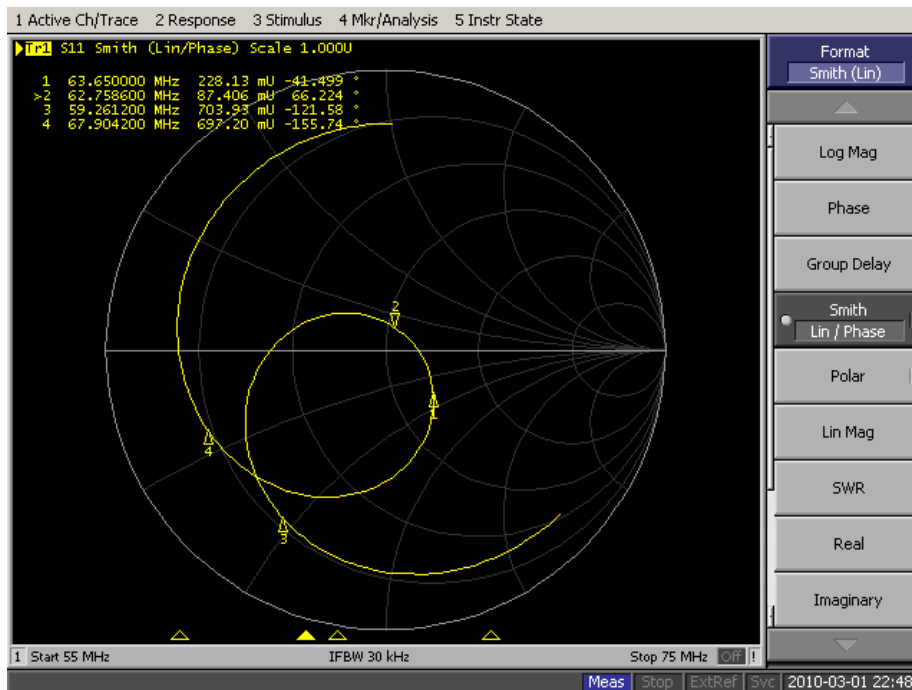


Subject 5 Smith Chart

Subject 6

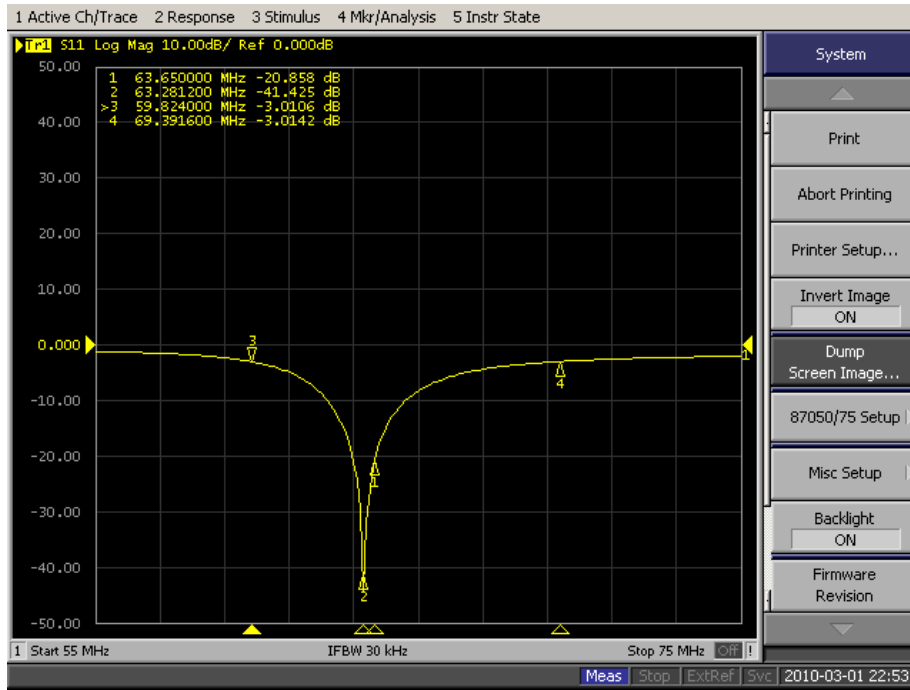


Subject 6 S11 Plot

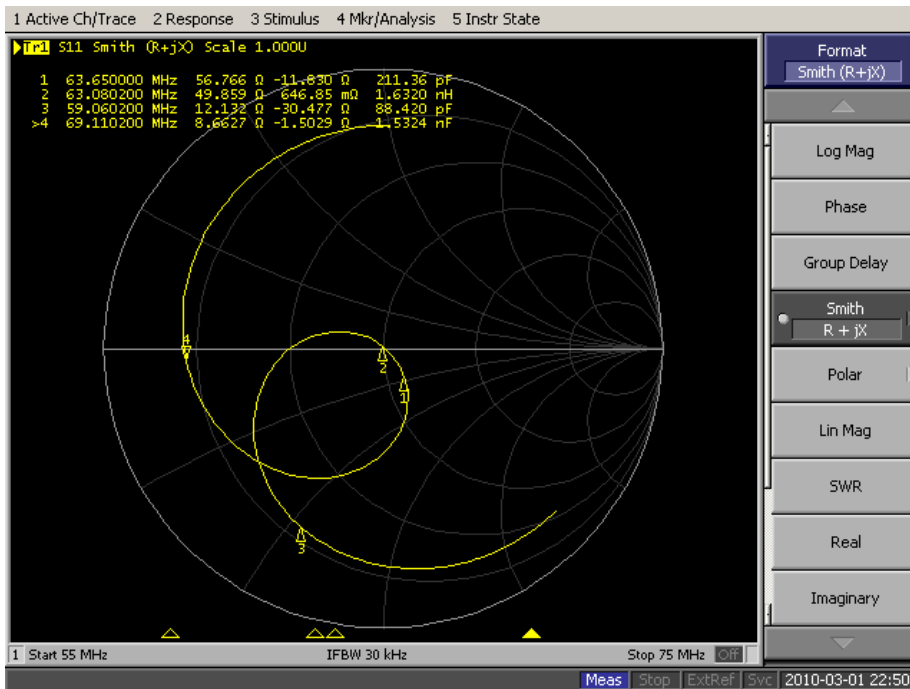


Subject 6 Smith Chart

Subject 7

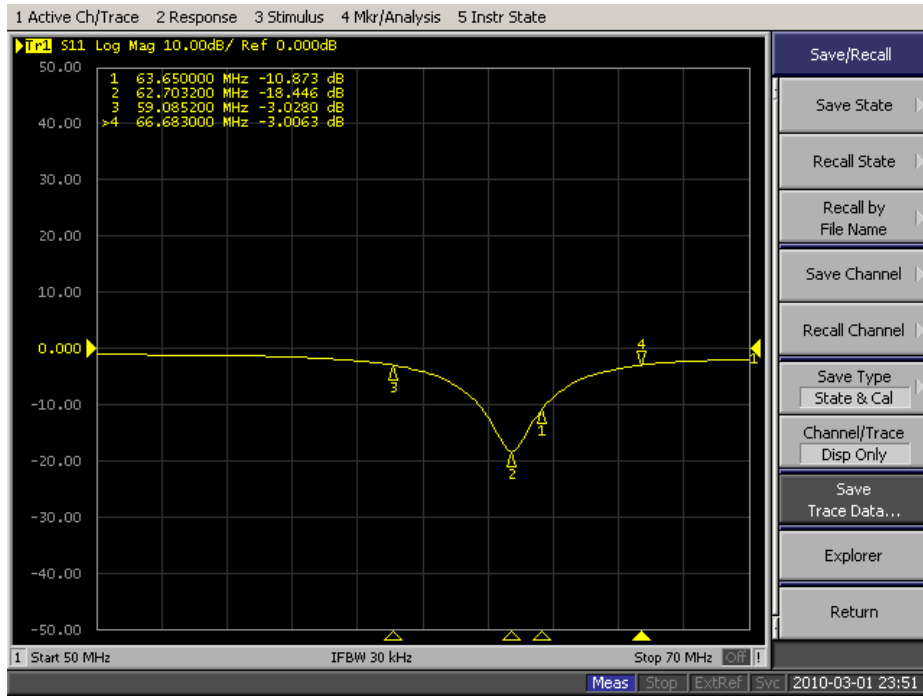


Subject 7 S11 Plot

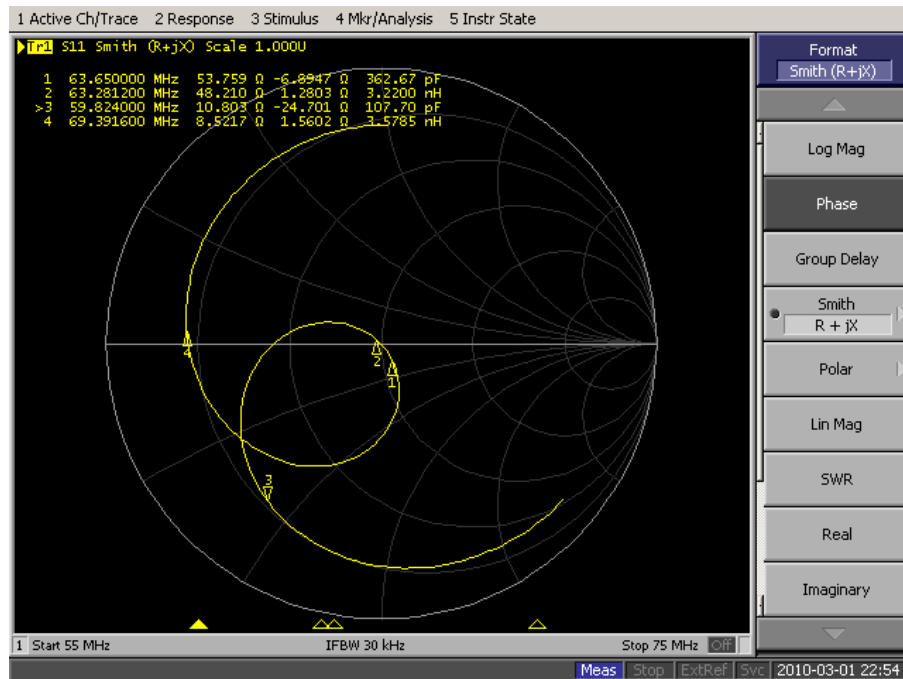


Subject 7 Smith Chart

Subject 8

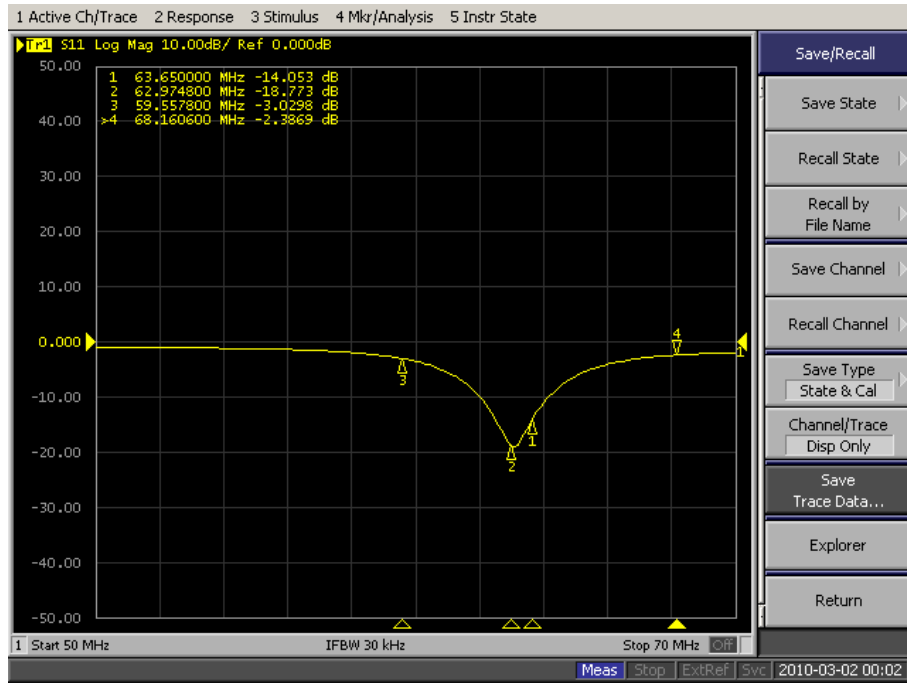


Subject 8 S11 Plot

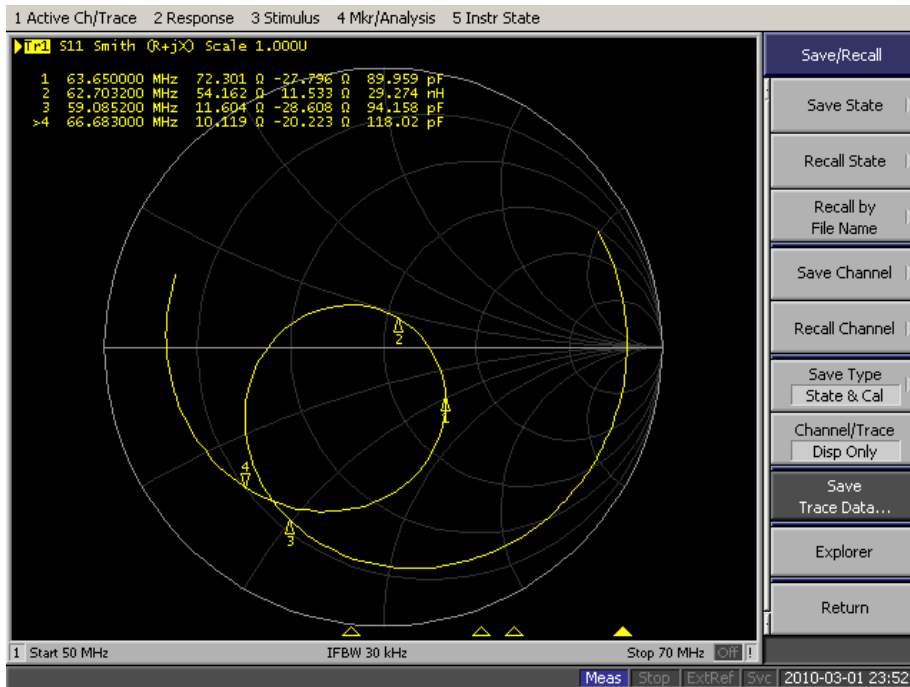


Subject 8 Smith Chart

Subject 9

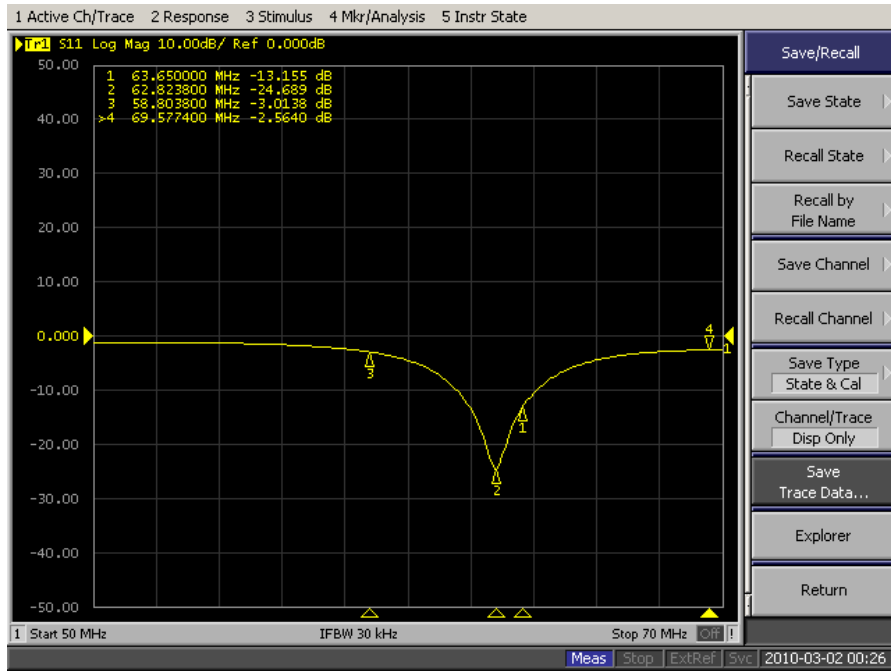


Subject 9 S11 Plot

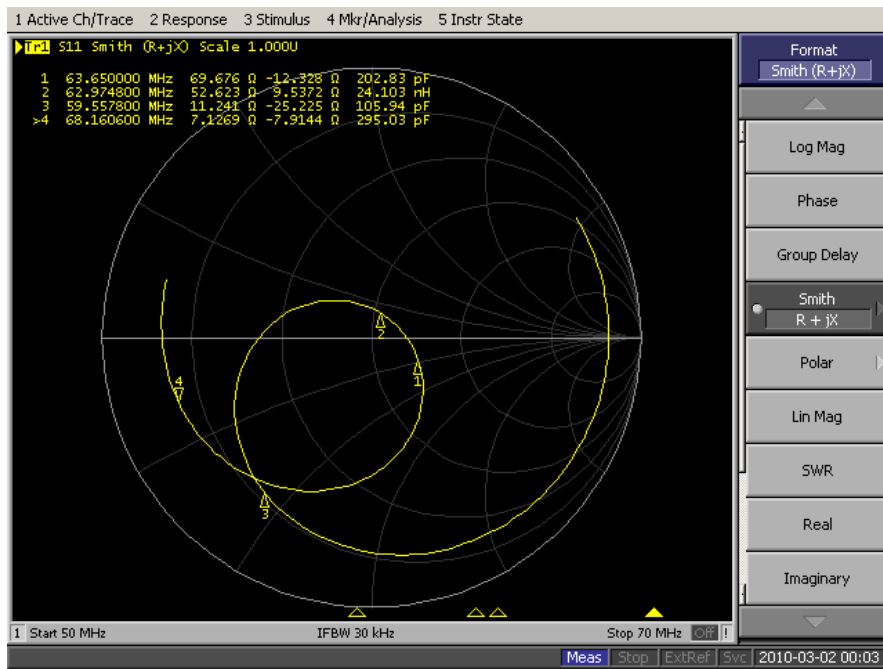


Subject 9 Smith Chart

Subject 10

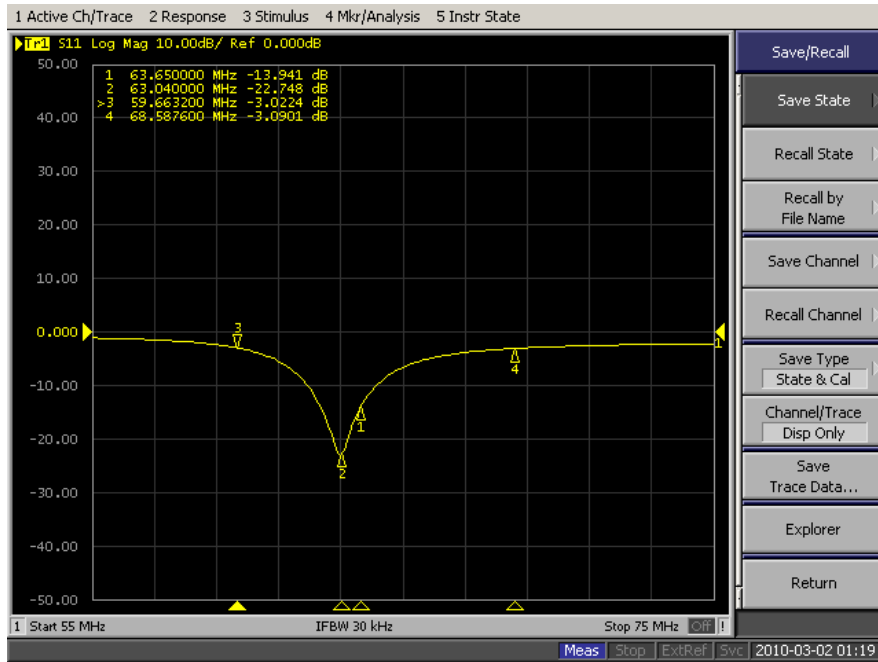


Subject 10 S11 Plot

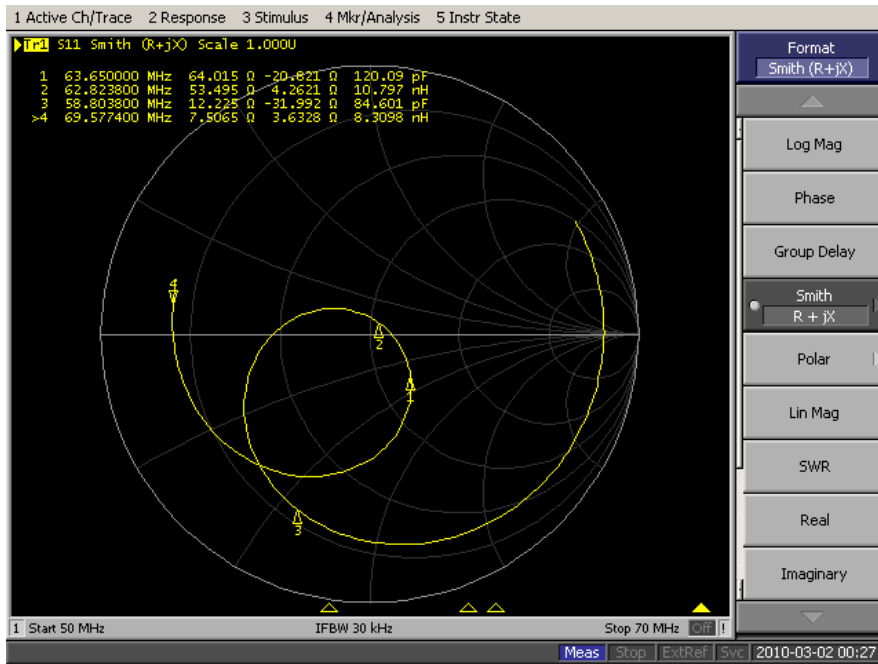


Subject 10 Smith Chart

Subject 11



Subject 11 S11 Plot



Subject 11 Smith Chart

Appendix H Raw Data for Magnetic Field Uniformity Testing

Position (cm)	S21 Parameter				
	Unloaded Vertical	Unloaded Side to Side	Loaded Side to Side	Unloaded Back to Front	Loaded Back to Front
0	-35.5	-44.6	-42.6	-44.6	-46
1	-35.3	-43.5	-41.6	-43.7	-44.9
2	-35.4	-42.7	-41	-43	-44.8
3	-37.6	-42	-40.15	-42.1	-41.6
4	-36.3	-41.3	-39.4	-41.6	-40.5
5	-36.8	-40.8	-38.8	-40.9	-39.6
6	-37.4	-40.3	-38.2	-40.5	-38.8
7	-37.7	-39.9	-37.8	-40	-38.3
8	-37.9	-39.7	-37.5	-39.7	-38.1
9	-37.5	-39.5	-37.3	-39.4	-37.4
10	-38.4	-39.2	-37.1	-38.9	-37.1
11	-38.5	-39	-37	-39.1	-37
12	-38.9	-38.9	-37	-38.9	-37.1
13	-38.9	-38.8	-36.9	-38.9	-37.5
14	-38.9	-38.8	-37	-38.9	-38
15	-38.8	-38.7	-37.2	-38.9	-39.5
16	-38.6	-38.8	-37.4	-39	-39.9
17	-38.5	-38.8	-37.9	-39.1	-39.3
18	-38	-39	-39.4	-39.2	-40.2
19	-37.7	-39.2	-40.2	-39.5	-40.5
20	-37.5	-39.5	-41.5	-39.7	-41.1
21	-37.2	-39.7	-42.4	-40	
22	-37	-40.1	-44	-40.3	
23	-36	-40.5	-36.9	-40.6	
24	-36.1	-41.1		-41.1	
25	-36.4	-41.7		-41.6	
26	-35.9	-42.2		-42.4	
27	-35.7	-42.9		-42.9	
28	-35.5	-43.9		-42.6	
29	-35.3	-45.1		-43.9	
30	-35	-46.1		-45.1	
31	-34.8				
32	-34.7				

Each axis was normalized to the theoretical center value. In the case of the vertical direction, this is the lowest S21 point. In the case of the other axis, this is the highest S21 parameter. This data is shown below:

Normalized S21 Parameter					
Unloaded Vertical	Unloaded Side to Side	Loaded Side to Side	Unloaded Back to Front	Loaded Back to Front	
3.4	-5.9	-5.7	-5.7	-9	
3.6	-4.8	-4.7	-4.8	-7.9	
3.5	-4	-4.1	-4.1	-7.8	
1.3	-3.3	-3.25	-3.2	-4.6	
2.6	-2.6	-2.5	-2.7	-3.5	
2.1	-2.1	-1.9	-2	-2.6	
1.5	-1.6	-1.3	-1.6	-1.8	
1.2	-1.2	-0.9	-1.1	-1.3	
1	-1	-0.6	-0.8	-1.1	
1.4	-0.8	-0.4	-0.5	-0.4	
0.5	-0.5	-0.2	0	-0.1	
0.4	-0.3	-0.1	-0.2	0	
0	-0.2	-0.1	0	-0.1	
0	-0.1	0	0	-0.5	
0	-0.1	-0.1	0	-1	
0.1	0	-0.3	0	-2.5	
0.3	-0.1	-0.5	-0.1	-2.9	
0.4	-0.1	-1	-0.2	-2.3	
0.9	-0.3	-2.5	-0.3	-3.2	
1.2	-0.5	-3.3	-0.6	-3.5	
1.4	-0.8	-4.6	-0.8	-4.1	
1.7	-1	-5.5	-1.1		
1.9	-1.4	-7.1	-1.4		
2.9	-1.8	0	-1.7		
2.8	-2.4		-2.2		
2.5	-3		-2.7		
3	-3.5		-3.5		
3.2	-4.2		-4		
3.4	-5.2		-3.7		
3.6	-6.4		-5		
3.9	-7.4		-6.2		
4.1					
4.2					

The point of the normalized S21 parameter equal to zero was the considered a point of calibration between the different methods of measuring the axis. This allowed the different measurements to be compared. The data was thus shifted until the two lined up, shown below:

S21 Parameter				
Unloaded Vertical	Unloaded Side to Side	Loaded Side to Side	Unloaded Back to Front	Loaded Back to Front
3.4	-5.9		-5.7	
3.6	-4.8		-4.8	
3.5	-4	-5.7	-4.1	-4.1
1.3	-3.3	-4.7	-3.2	-3.5
2.6	-2.6	-4.1	-2.7	-3.2
2.1	-2.1	-3.25	-2	-2.3
1.5	-1.6	-2.5	-1.6	-2.9
1.2	-1.2	-1.9	-1.1	-2.5
1	-1	-1.3	-0.8	-1
1.4	-0.8	-0.9	-0.5	-0.5
0.5	-0.5	-0.6	0	-0.1
0.4	-0.3	-0.4	-0.2	0
0	-0.2	-0.2	0	-0.1
0	-0.1	-0.1	0	-0.4
0	-0.1	-0.1	0	-1.1
0.1	0	0	0	-1.3
0.3	-0.1	-0.1	-0.1	-1.8
0.4	-0.1	-0.3	-0.2	-2.6
0.9	-0.3	-0.5	-0.3	-3.5
1.2	-0.5	-1	-0.6	-4.6
1.4	-0.8	-2.5	-0.8	-7.8
1.7	-1	-3.3	-1.1	-7.9
1.9	-1.4	-4.6	-1.4	-9
2.9	-1.8	-5.5	-1.7	
2.8	-2.4	-7.1	-2.2	
2.5	-3	0	-2.7	
3	-3.5		-3.5	
3.2	-4.2		-4	
3.4	-5.2		-3.7	
3.6	-6.4		-5	
3.9	-7.4		-6.2	
4.1				
4.2				

